Structuration, selective dispersion and compatibilizing effect of (nano)fillers in polymer blends

Aurélie Taguet, Philippe Cassagnau, José-Marie Lopez-Cuesta

Structuration, selective dispersion and compatibilizing effect of (nano)fillers in polymer blends

A. Taguet [a,*], P. Cassagnau [b], J.-M. Lopez-Cuesta [a]

[a] Centre des Matériaux C2MA, Ecole des mines d'Alès, 6 avenue de Clavières, F-30319 Alès Cedex, France
[b] Université Lyon 1, CNRS, UMR5223, Ingénierie des Matériaux Polymères, F-69622 Lyon, France

A B S T R A C T

Hybrid ternary blends comprising two polymers and one mineral (nano)filler are increas-ingly studied because they are starting to be widely used to respond to industrial issues. The objective of this review is to gather information on these particular systems. Concerning first thermodynamic effects of fillers on the phase separation of an immiscible polymer blend, Flory–Huggins theory demonstrate stabilization. This theory was particularly taken up and developed for the case of two polymers and one filler by Lipatov and Nesterov in the 90s. More recently, Ginzburg generalized this theory to the case of unfavorable enthalpic interactions between a particle and the two polymers. They showed that the amount of particles had to attain a certain threshold to stabilize the system and the lower the particle radius, the higher the stable zone area. Generally speaking, all the phenomena regarding the morphology of polymer blends are governed by thermodynamics and/or kinetic effects, as well as the localization of nanoparticles. The main discussed thermodynamically con-trolling parameter of the localization is the wetting parameter ω_{AB}. However, because of the viscosity of the system, the equilibrium dictated by ω_{AB} may never be reached. Hence, concerning the kinetic effects, the final localization of fillers in a polymer pair is guided by the sequence of mixing of the components, the viscosity ratio, the composition, the temper-ature, the shear rate and the time of mixing. When the particles are placed at the interface between two polymers, coalescence can be suppressed or/and interfacial tension can be reduced. In that case, particles are known to play the role of a compatibilizer. In a ternary system, (i) the shape of the particle (spheres, rods or "onions-shape"), (ii) the particle radius (R_p) *versus* the radius of gyration of the polymers (R_g) and (iii) the surface chemistry of the particles affect the final localization of the particles (thus, the compatibilizing effect) and the final properties of the material, such as mechanical, conductive, magnetic and ther-mal properties. This review details recent works for which those four above mentioned properties are improved by incorporating different kind of fillers in polymer blends.

Keywords:
Polymer blends
Nanoparticles
Compatibilization
Thermodynamics effects
Kinetics effects
Wettability

Contents

* Corresponding author. Tel.: +33 4 66 78 56 87; fax: +33 4 66 78 53 65.
E-mail addresses: aurelie.taguet@mines-ales.fr (A. Taguet), philippe.cassagnau@univ-lyon1.fr (P. Cassagnau), jose-marie.lopez-cuesta@mines-ales.fr (J.-M. Lopez-Cuesta).

1. Introduction

The incompatibility between polymers in polymer blends has led the researchers and the industry to develop strategies to improve the adhesion between the phases. The first patent mentioning the improvement of compatibility between two polymers dates from the 50s. Ten years after, the scientific community started to take an interest in improving the compatibility of targeted systems of two polymers (PVC/polyolefin and PVC/elastomer from Monsanto Chemical [1,2], PVC/polybutadiene [3], PVDF/PMMA [4], PS/PVME [5] and PE/PP). The first reviews on the interface and compatibility in polymer blends dated from the 75s with the works of Yu [6], Gaylord [7], Lipatov [8] and Paul [9,10].

Nowadays there are many books, articles and reviews dealing with the compatibilization of polymer blends. The key routes are (i) addition of tailored block or graft copolymer, (ii) addition of reactive polymers [11], (iii) addition of multi-functionnal copolymer as impact modifier, (iv) addition of co-solvent [12], (v) by ionic interaction [12], and (vi) by γ-irradiation or electron beam (combined with or without a co-agent) [13]. However, most recently, a new approach has attracted interest: compatibilization by addition of targeted fillers. The adsorption of polymeric components on the solid surface was shown to change the thermodynamic state of the blends [14]. In the past ten years, the number of publications on fillers as compatibilizers for polymer blends raised dramatically. Most of them pointed out the necessary conditions on fillers to be efficient as compatibilizers. One necessary but not sufficient condition is their size: the particle radius (R_p) must be of the same order of magnitude as the gyration radius (R_g) of the polymer. Indeed, the stabilizing energy gain is particularly efficient when the inorganic phase has a larger surface area per unit weight. Nanoparticles (NPs) have been used as modifiers to polymeric materials for many years, especially to improve elastic, barrier, thermal and fire properties [15–18]. Achieving a good NPs dispersion or exfoliation (for clays) in the polymer matrix was shown to be a key factor to obtain convenient ultimate performances. Nowadays, the issues of the NPs dispersion as well as the properties of the resulting composite are fairly well understood.

Very recently, an interesting book chapter [19] describes recent developments on theoretical and modeling approaches to predict the equilibrium phase behavior and morphologies of polymer/NPs systems. Especially, interesting aspects on the theory of thermodynamics of polymer grafted NPs in polymer matrix and NPs in polymer blends were investigated.

However, there is a lack of clear information on the influence of important factors, such as for instance: the nature of the NPs, the parameter of process on the effect of the NPs (structuring, compatibilizing) in polymer blends. Hence, to overcome this lack of information the objective of the present article is to collect information to see if the localization and the compatibilization role of NPs can be predicted by investigating different aspects (thermodynamic, wettability, dynamic processes and nature of the NPs) of ternary systems. For the rest of the article, "ternary systems" will consist in two polymers in blends with one filler. Moreover, it is necessary to define what is meant by "compatibilization by nanoparticles". A definition was supplied by Utracki in 2002: NPs can act as compatibilizers if they ensure a strong interfacial adhesion between two incompatible polymers [20]. Section 2 deals with the thermodynamic theory on phase separation for ternary systems. The works summarize in this section is derived from Lipatov's and more recently Ginzburg's research teams. These works based on Flory–Huggins theory permitted to predict the influence of the addition of fillers on the phase diagram of binary blends. Section 3 points out the role of wettability in the prediction of particle localization, whereas Section 4 deals with the influence of the dynamic parameters (during the process) on the morphological predictions (where will be located the particle when considering the processing conditions?). In Section 5, the compatibilizing effect of fillers in polymer

Nomenclature

ABS acrylonitrile butadiene styrene
a-PA amorphous polyamide
APP ammonium polyphosphate
ATH aluminum trihydroxide
CB carbon black
CTBN carboxyl-terminated (butadiene-*co*-acrylonitrile)
dPMMA deuterated poly(methyl methacrylate)
EAA ethylene-*co*-acrylic acid copolymer
EBuAMA ethylene-butyl acrylate-maleic anhydride
EGMA ethylene-*co*-glycidyl methacrylate copolymer
EMA ethylene methacrylate copolymer
EMG terpolymer a compatibilizer based on ethylene/methyl acrylate
EnBACO-MAH ethylene-n butyl acrylate-carbon monoxide-maleic anhydride
ENR epoxidized natural rubber
EOR ethylene-1-octene copolymer elastomer
EPDM ethylene–propylene–diene terpolymer
EPR poly(ethylene-*ran*-propylene)
EVA ethylene vinyl acetate copolymer
FMWCNTs functionalized multi-walled carbon nanotubes
FPS terminal maleic anhydride functionalized PS
FR fire retardant
HDAA HDPE-*g*-acrylic acid
HDPE high density polyethylene
HNBR hydrogenated acrylonitrile butadiene rubber
HRR heat release rate
LCST lower critical solubility transition
LDH layered double hydroxide
LDPE low density polyethylene
LLDPE linear low density polyethylene
MA maleic anhydride
MH magnesium oxide
MMT montmorillonite
N6 Nylon6
NPs nanoparticles
NR natural rubber
O-MMT organo-modified montmorillonite
PA12 polyamide12
PB polybutadiene
PBO 2,2′-(1,3-phenylene)-bis(2-oxazoline)
PBT poly(butylene terephthalate)
PC polycarbonate
PDMS poly(dimethylsiloxane)
PE polyethylene
PEG polyethylene glycol
PEMA poly(ethyl methacrylate)
PEO poly(ethylene oxide)
PET poly(ethylene terephtalate)
PIB poly(isobytylene)
PLLA poly(L-lactic acid)
PLS plasticized starch
PMMA poly(methyl methacrylate)
POEs ethylene-α-olefin copolymer-based polyolefin elastomers
PP polypropylene
PPB propylene block copolymer
PPE poly(2,6-dimethyl-1,4-phenylene ether)
PPR propylene random copolymer
PS polystyrene
PTPA polytriphenylamine
PTT poly(trimethyl terephthalate)
PVA poly(vinyl acetate)
PVC poly(vinyl chloride)
PVDF poly(vinylidene fluoride)
PVME poly(vinyl methyl ether)
R_g gyration radius
R_p particle radius
SAN poly(styrene-*co*-acrylonitrile)
SBM polystyrene-*block*-polybutadiene-*block*-poly(methyl methacrylate) triblock terpolymer
SBS styrene–butadiene–styrene
SEBS poly(styrene-*b*-ethylene butylene-*b*-styrene)
SEM Scanning Electron Microscope
TEM Transmission Electron Microscope
TPS thermoplastic starch (plasticized from glycerol and water)

Organic modifier of commonly used montmorillonite
Cloisite® 30B (C30B) methyl, tallow, bis-2-hydroxyethyl quaternary ammonium
Cloisite® 20A (C20A) dimethyl, ditallow quaternary ammonium
Cloisite® 25A(C25A) dimethyl, tallow, 2-ethylhexyl quaternary ammonium
Cloisite® 15A (C15A) dimethyl, ditallow quaternary ammonium
Cloisite® 6A (C6A) dimethyl, ditallow quaternary ammonium
Cloisite® 93A (C93A) methyl ditallow quaternary ammonium
Nanofil 15A distearyl, dimethyl quaternary ammonium
Nanofil 919 stearyl, benzyl, dimethyl ammonium
Nanofil 2 stearyl, benzyl, dimethyl ammonium
Nanomer® I.44 dimethyl, dialkyl quaternary ammonium
Nanomer® I.44PA dimethyl, dialkyl quaternary ammonium
Nanomer® I.30TC octadecyl, trimethyl quaternay ammonium

blends is highlighted. A large part of this section is devoted to the effect of the nature of the filler (shape, size and surface chemistry) on its localization and its compatibilizing ability in polymer blends. Finally, the main ultimate properties and applications are emphasized (Section 6) and especially how do structuration and morphology of ternary systems determine the macroscopic properties of the final material?

2. Fillers in polymer blends: the thermodynamic theories on phase separation

The effect of fillers on the phase behavior of polymer pairs has been studied until the 90s by Lipatov and Nesterov, well before the first investigation on the behavior (thermal, mechanical, rheological) of such materials was performed.

2.1. Lipatov and Nesterov thermodynamic theory on phase separation

Lipatov and Nesterov [21] were the first to really utilize the Flory–Huggins thermodynamic theory of mixing to explain the phase separation behavior of ternary systems comprising two immiscible homopolymers A and B and one unmodified inorganic solid filler S. As for Flory–Huggins theory for polymer blends, the Gibbs free energy change of the system including the 3 components was described by Nesterov as:

$$\Delta G_{mix} = RTV(\chi_{AB}\varphi_A\varphi_B + \chi_{AS}\varphi_A\varphi_S + \chi_{BS}\varphi_B\varphi_S)$$
$$= RTV\chi_{A+B+S} = \Delta G_{AB} + \Delta G_{AS} + \Delta G_{BS} \quad (1)$$

where V is the mixture volume, χ_{ij} is the interaction parameter between components i and j and φ_i is the volume fraction of component i.

The equation giving the free energy of mixing, postulates that for polymer mixtures, the combinatorial entropy contribution may be neglected because of the high molecular weight of the polymers. Hence, their miscibility is driven by enthalpic forces.

Nesterov et al. considered a negative change of enthalpy by adsorption of a polymer onto solid. Hence, if both polymer components of the blend are strongly adsorbed onto the filler surface we may accept that the interaction parameters of polymers A and B with the functional groups on surface S are negative (χ_{AS} and $\chi_{BS} < 0$). For immiscible polymers, $\chi_{AB} > 0$ and the introduction of a filler will decrease the value of χ_{A+B+S} and improve the thermodynamic stability of the system. The sign of χ_{A+B+S} and then that of ΔG_{mix} is given by:

- $|\Delta G_{SA} + \Delta G_{SB}| < \Delta G_{AB} \Rightarrow \Delta G_{mix} > 0$
- $|\Delta G_{SA} + \Delta G_{SB}| > \Delta G_{AB} \Rightarrow \Delta G_{mix} < 0$ and the blend is more thermodynamically stable

In their article [21], they simulated the variation in χ_{A+B+S} when keeping χ_{AS} and χ_{BS} constant (and negative) and changing χ_{AB} from negative to positive values (Fig. 1). Fig. 1 shows that even for incompatible polymer pairs, the introduction of a filler may lead to improve the compatibility of the system. They concluded that the filler can then play the role of a compatibilizer for binary polymer mixture, and increasing filler content would enhance the compatibilizing effect.

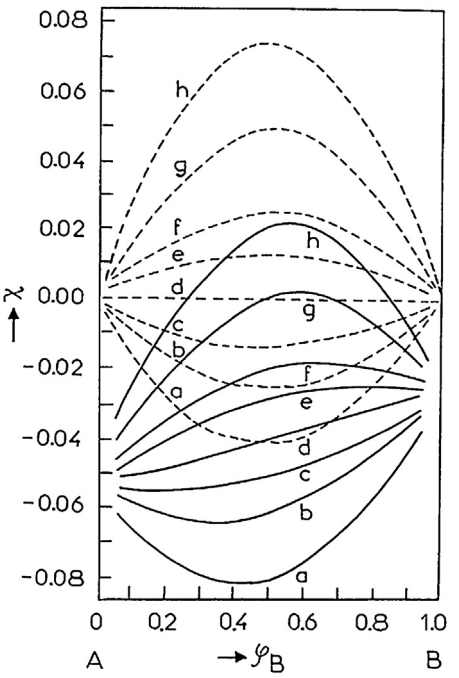

Fig. 1. Parameter of thermodynamic interaction χ *versus* the concentration in polymer B for a binary mixture polymer A + polymer B in dotted lines (χ_{AB}) and for a ternary system polymer A + polymer B + filler surface S in solid lines (χ_{A+B+S}) at various χ_{AB}: (a) −0.2, (b) −0.1, (c) −0.05, (d) 0, (e) +0.05, (f) 0.1, (g) 0.2, and (h) 0.3. χ_{A+B+S} was calculated using $\chi_{AS} = -0.6$, $\chi_{BS} = -0.3$, $\varphi_s = 0.1$.
[21], Copyright 1999. Reproduced with permission from Elsevier Ltd.

This result was limited by hypothesis postulated implicitly, *i.e.* the ideal system comprises a mineral filler with:

- spherical shape
- radius much higher than polymer radius of gyration R_g (*i.e.* $R_p \gg 50$ nm)
- no aggregates formation
- an equivalent affinity with either A or B polymer: both polymeric components of the blend are strongly adsorbed
- no particle–particle interactions

Nesterov et al. based their theory on previous observations on phase separation diagram from the introduction of a fumed silica within two polymers: poly(methyl methacrylate) (PMMA) and poly(vinyl acetate) (PVA) [22,23]. PMMA and PVA have close chemical nature and the same adsorption propensity at the surface of the filler. They observed changes in temperature of the phase separation and shape of the cloud point curve. But, they observed either a decrease or an increase of the phase separation temperature with the filler content at component ratio 30/70 or 20/80 (PVA/PMMA), respectively. To explain these variations, they postulated a selective adsorption of one of the components at the filler interface. Hence, the selective adsorption of one component at the interface changes the

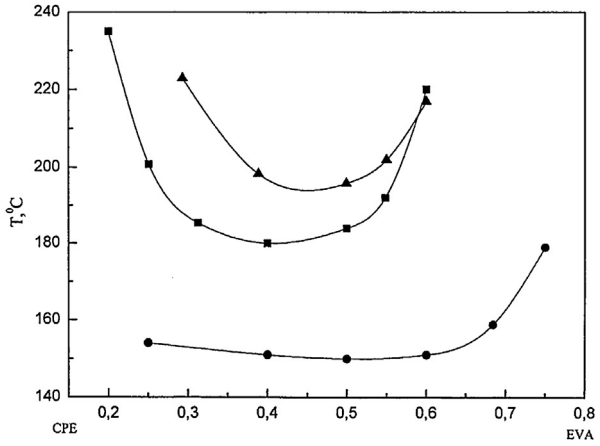

Fig. 2. Curves of cloud points for unfilled (■), filled with 10% (▲) and filled with 5% (●) fumed silica.
[25], Copyright 2002. Reproduced with permission from Elsevier Ltd.

ratio of this component both in the border layer and in the matrix bulk, and this would change the thermodynamic compatibility.

Later, a further study on the same system (PMMA/PVA/fumed silica) [24] confirmed the compatibilizing effect of the filler. Indeed, they used the glass transition temperatures values to calculate the component ratios of PVA-enriched phase and PMMA-enriched phase and further calculated $(\chi_{AB})_{filled}$ and $(\chi_{AB})_{unfilled}$ .They clearly established that $(\chi_{AB})_{filled} < (\chi_{AB})_{unfilled}$ and then proved the compatibilizing effect of the filler.

Finally, to describe a more realistic system, Lipatov and Nesterov [25] investigated a ternary system in which the polymers have different chemical natures and therefore different affinities to the solid surface of a fumed silica (chlorinated polyethylene and ethylene-vinyl acetate copolymer). Hence, χ_{AS} and χ_{BS} are different. Carbonyl groups of vinyl acetate can form hydrogen bonds with the silanol of fumed silica whereas other hydrogen bonds can be formed between chlorinated polyethylene and carbonyl groups of vinyl acetate. This system presents a lower critical solubility transition (LCST) and the introduction of the fumed silica (at 5 and 10%) dramatically changes the temperature of phase separation and the shape of the cloud point curve (Fig. 2). They noted that the thermodynamic stability of the filled blend may increase or decrease with 10 or 5% of filler, respectively. According to the authors, these variations may be ascribed to a border layer formed at the surface of the filler in which the composition differs from the initial one (as already mentioned previously in [23]). Changing the interaction of the macromolecules at the interface with the filler would change the parameter of thermodynamic interaction between the two polymers (χ_{AB}) [14]. Hence, for 10% of fumed silica, the thickness of the layer between two particles is low enough that both components transit into the state of border layer and both polymer chains are fully under the influence of the surface field forces. In that case, the variation of shape and position of the binodal curve of the phase diagram, when introducing the filler, is only due to the variation of free energy of the ternary system and the filler has a compatibilizing effect. Hence, the phase separation temperature would increase. For 5% of filler, the ternary system must be divided into two sections: one for the border layer and the other for the bulk, both with proper compositions. Considering the border layer, as the polymers used are very polydispersed, a fraction of lower molecular mass polymer chains are preferentially adsorbed at the surface and the volume fraction of the blend will be enriched with macromolecules comprising higher molecular masses. Hence, the phase separation temperature will decrease. The phase separation temperature of the bulk was not observed experimentally.

More recently, Nesterov and Lipatov [24,26] proposed a new expression of the thermodynamic interaction parameter between the two polymeric components. In that new expression (2), they considered independently the contribution of the interaction between polymers A and B near the surface filler and in the bulk:

$$(\chi_{AB})_{exp} = \chi_{AB}(1 - f_i) + (\chi_{AB})_i f_i \quad (2)$$

where $(\chi_{AB})_{exp}$ is the experimental value of the interaction parameter for the filled mixture, χ_{AB} is the interaction parameter for the matrix, f_i represents the volume fraction of interphase layer and $(\chi_{AB})_i$ is the interaction parameter for the interphase layer.

Lipatov not only considered the effect of filler on the shape of the phase diagram but also on the kinetics of phase separation [26]. Arising from the consideration of two main regions in the polymer volume (bulk and surface layer), he explained that in all filled systems the filler exerted a retarding action on all kinetic processes, leading to a non-equilibrium state. Indeed, as molecular chains are adsorbed at the interface, it restricts both their mobility in the surface layer, and their number of conformational rearrangements. Hence, if the interactions with the surface are symmetric ($\chi_{SA} = \chi_{SB}$), the phase separation is not simultaneous in the whole system (slower at the surface layer than in the bulk) and heterogeneity of structure in the phase-separated system will be observed. If the interactions are asymmetric, phase separation is initiated by the filler surface but is retarded.

Lipatov and Nesterov's theory has limitations because the assumptions on which it rests are no longer valid if either the particle radius (R_p) is small, and particularly if R_p is smaller than the polymer radius of gyration R_g, or if the particle has a better affinity for one of the two polymers. This theory was largely taken up by Ginzburg et al.

2.2. Ginzburg thermodynamic theory

In the same way, Ginzburg formulated a more complete theory to predict how nanoparticles can influence the phase separation behavior of blends. He expressed the free energy per unit volume of a binary mixture of two homopolymers A and B with spherical nanoparticles (P) of radius R_p (coated by A-type ligands) and described how the addition of particles influenced the location of the spinodal compared to the pure polymer blend [27]. In their expression of the free energy of the ternary system, they took into account polymer, particle and polymer–particle interactions, taking as hypothesis that $\chi_{AB} = \chi_{BP}$ and $\chi_{AP} = 0$. By

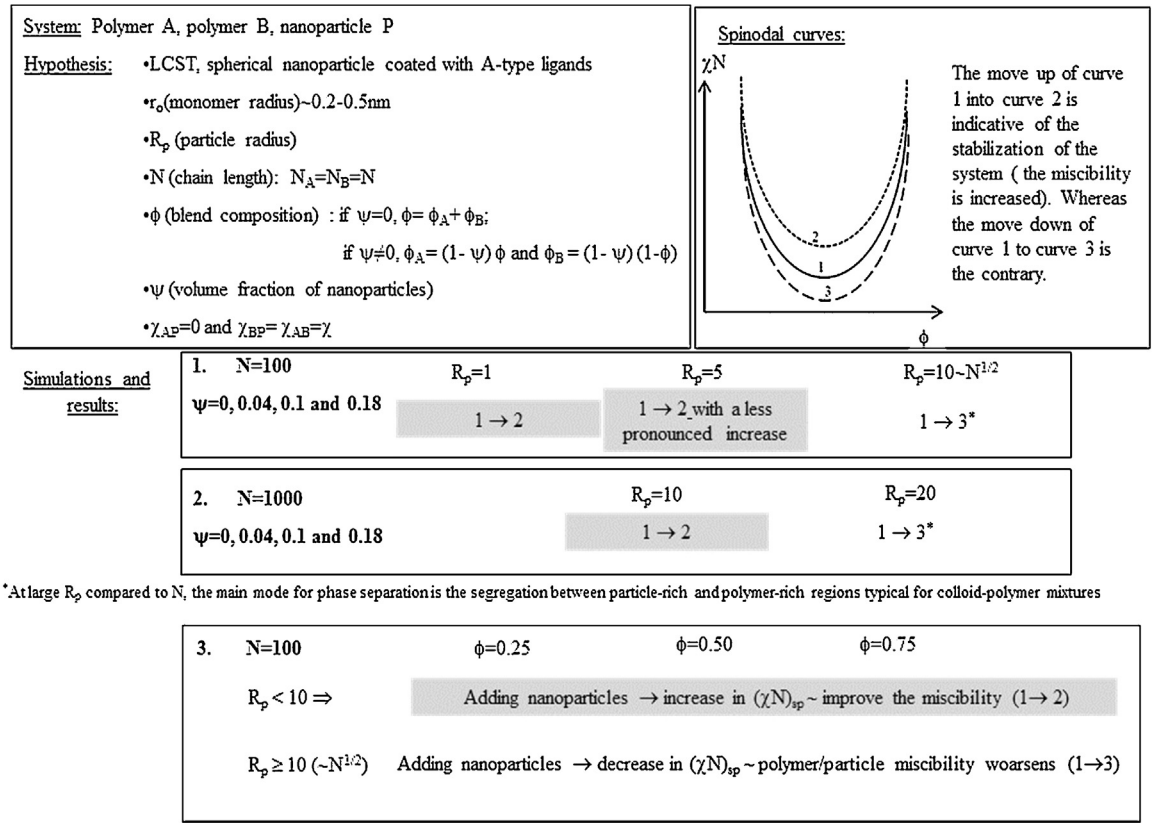

Fig. 3. Schematic summary of the work simulation performed by Ginzburg in [27]. In the top left box, hypothesis of the model are recalled; in the top right box, a scheme draws the evolution of the spinodal curve in phase diagram to account for the evolution of the miscibility; the three bottom boxes show the evolution of the spinodal curve when input parameters of the model are modified. In gray we highlight the modification that generates an improvement in the miscibility of the system.

plotting spinodal curves for various systems (χN *versus* ϕ), they evidenced that very small particles ($R_p < R_g$) act as compatibilizers, whereas with larger particles, the spinodal is determined by the polymer–nanoparticle phase separation. Their different simulations of calculations are schematically summarized in Fig. 3. They explained that if R_p is similar to R_g (typically 15 nm), the particles begin to influence the configurational entropy of the chains. As particle radius is increased, the role of entropic surface tension become stronger finally when R_p is much higher than R_g, the particle-rich phase would segregate from the polymer at very low particle concentrations regardless of the polymer composition. Hence, for very large R_p, the main mode for the phase separation would be the segregation between particle-rich and polymer-rich regions, typical for colloid–polymer mixtures.

For example, Ginzburg calculated that for a binary blend with a critical temperature of 400 K, the addition of 10 vol% of nanoparticles can reduce this critical temperature up to 40 K if R_p = 15 nm (considering r_o(monomer radius) = 0.5 nm and N(polymer degree of polymerization) = 1000). Moreover, Ginzburg predictions were in good agreement with Lipatov experimental results concerning a PVA/PMMA blends filled with fumed silica [23] that are exposed in Section 2.1. Particularly with the experimental results showing that at low PMMA content, the particles would decrease the phase separation temperature and hence decrease the compatibility, whereas at high PMMA content, they can compatibilize the two polymers by increasing the phase separation temperature.

In a more recent article, He et al. [28] conducted the same works on theoretical predictions, but considering a most general case where all three enthalpic interaction parameters (χ_{AB}, χ_{AP} and χ_{BP}) are independent variables. However, they choose to depict the particular case where particles could have an enthalpic unfavorable interaction with the respective A and B homopolymers (χ_{AP} and $\chi_{BP} \geq 0$). Hence, they were able to establish the influence of the chemical nature of the particle on the stability region in the particle–polymer interaction space of the system by plotting the curves which function is given in Eq. (3):

$$\frac{\chi_{AP} - \chi_{BP}}{2} = f(\phi\chi_{AP} + (1-\phi)\chi_{BP}), \quad (3)$$

where the ordinate represents a measure of the relative affinity between the particles and the different homopolymers ($y < 0$, the particles prefer the A phase, whereas, $y > 0$, the particles prefer phase B). The abscissa represents a measure of the average enthalpic field acting on the particles, due to the homopolymers. All the predictions concerning

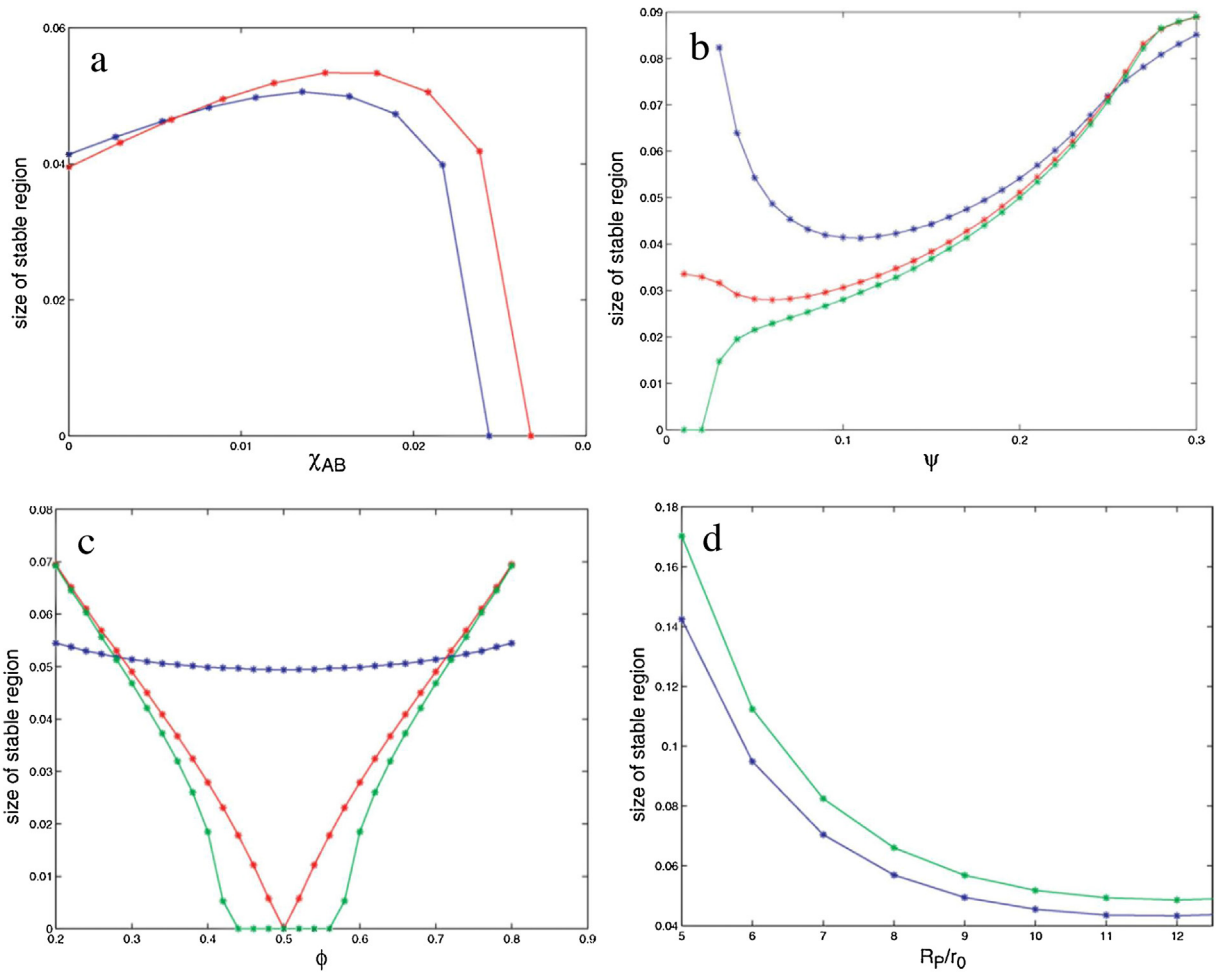

Fig. 4. Size (area) of the stable region in the first quadrant (χ_{AP},χ_{BP}) plane as a function of χ_{AB} (a), ψ (b), ϕ (c) and R_p/r_o (d). For (a): $R_p/r_o = 10$, $\psi = 0.18$, $N = 100$ and the blue and red curves correspond to $\phi = 0.5$ and 0.35, respectively. For (b): $R_p/r_o = 10$, $N = 100$, $\phi = 0.5$ and blue, red and green curves correspond to $\chi_{AB} = 0.01$, 0.02 and 0.0205, respectively. For (c): $R_p/r_o = 10$, $\psi = 0.18$, $N = 100$, and blue, red and green curves correspond to $\chi_{AB} = 0.01$, 0.0244 and 0.025, respectively. For (d): $\chi_{AB} = 0.02$, $\psi = 0.18$, $N = 100$ and blue and green curves correspond to $\phi = 0.5$ and 0.35, respectively. (For interpretation of the references to color in this figure legend, the reader is referred to the web version of the article.)
[28], Copyright 2006. Reproduced with permission from John Wiley and Sons.

the increase or decrease of the stability region of the system, when varying successively χ_{AB} (enthalpic interaction parameter), ψ (volume fraction of nanoparticle), ϕ (blend composition), R_p (particle radius) and N (chain length) are exposed in Fig. 4. Concerning the influence of the amount of nanoparticles, ψ must be above a minimum amount to stabilize the system. Concerning the blend composition, there is a difficulty of creating stable systems with symmetric mixtures of homopolymers ($\phi = 0.5$). Concerning the size of the particles, decreasing R_p helps in broadening the stability region for a given set of χ_{AB} parameters.

Here again, and even if Ginzburg's model presented above is a very general one, it has some limitations and particularly concerning the coating of the nanoparticles. The model presented above does not take into account the chain-like characteristics of a polymer coating. Hence, if the grafted chains are relatively short, the model is correct but if they are relatively long, configurational entropy of these chains must be taken into account in the total free energy expression of the system.

2.3. Phase separation in PMMA/SAN and PS/PVME blends filled with NPs

The phase separation from an homogeneous to an heterogeneous system was particularly studied in the case of two partially immiscible polymer blends characterized by a LCST: poly(methyl methacrylate)/poly(styrene-*co*-acrylonitrile) (PMMA/SAN) and polystyrene/poly(vinyl methyl ether) (PS/PVME) blends filled with spherical (silica) and non spherical (clay) nanoparticles. In most cases, the phase transition temperatures were compared using rheological methods, optical microscopy and thermodynamic theories.

Huang et al. [29] filled poly(methyl methacrylate)/poly(styrene-*co*-acrylonitrile) (70/30) blends with silica and

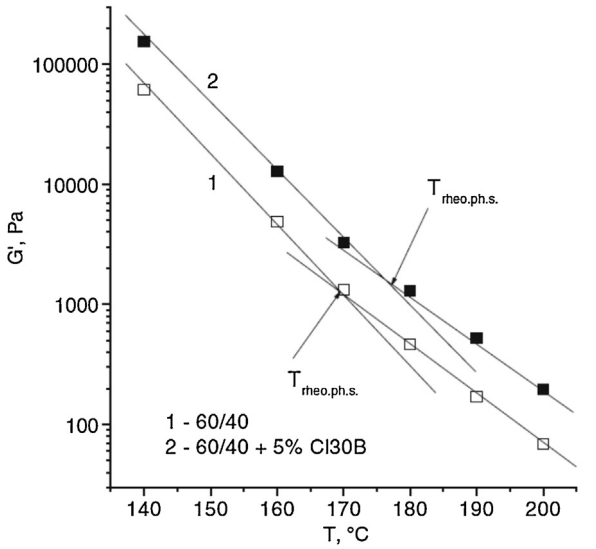

Fig. 5. Determination of the phase separation temperature by rheological method.
[31], Copyright 2010. Reproduced with permission from Springer.

showed by dynamic shear rheology that the phase separation temperature was increased and the thermodynamic interaction parameter decreased when introducing silica. The selective absorption of PMMA on the surface of SiO_2 results in the difference between the composition of surface layer and that of polymer matrix, especially for 30/70 PMMA/SAN filled with 5 wt% SiO_2 [30]. Hence, the effect of SiO_2 on the phase separation behavior of PMMA/SAN blend obviously depends on the composition of the blend matrix. More recently, Shumsky et al. [31] investigated the viscoelastic characteristics of the blends of PMMA/SAN blends at various temperatures below, near, and above the phase separation temperature. The presence of non spherical nanofillers (natural montmorillonite Cloisite®Na^+ (ClNa), montmorillonite Cloisite®30B (C30B) modified with triple ammonium salt) in the blend results in the change of the interactions between the components at the interphase that promote the change of the free mixing energy. As a result, the phase separation occurs at a higher temperature ($\Delta T = 6\,^{\circ}C$), as shown in Fig. 5. At the isothermal conditions, the phase separation begins earlier and proceeds with a higher rate as compared with the same blend without filler. This result was lately confirmed by Gao et al. [32] using spherical fillers. These authors studied the determination of the phase separation temperature of PMMA/SAN blends with or without the silica nanoparticles. They found that the incorporation of silica nanoparticles significantly shift the PMMA/SAN blend's phase diagram, increasing the phase separation temperature especially for blends with PMMA as minor phase. Actually, note that the authors developed a new original method called gel-like method. This method was successfully introduced to obtain the binodal temperature of PMMA/SAN blends' critical components. Very recently, authors also investigated the phase separation of PMMA/SAN blends with controlled distribution of silica [33]. This is the case of Huang et al. [34] and Chung et al. [35]. As the silica used was modified by polystyrene and poly(methyl methacrylate) chains at the surface, respectively, these articles are detailed in Section 5.3.4.

NPs filled polystyrene (PS)/poly(vinyl methyl ether) (PVME) blends were studied until the 2000s. Krishnamoorti's team [36,37] were the first to investigate the influence of layered silicates on the phase-separated morphology of near-critical PS/PVME blends.

The influence of hydrophilic SiO_2 nanoparticles on the morphology of polystyrene (PS)/poly(vinyl methyl ether) (PVME) blends in an unstable region has been investigated by Gharachorlou and Goharpey [38] for 80/20, 60/40, 40/60 and 20/80 compositions and more recently by Xia et al. [39] for 10/90 compositions. The addition of hydrophilic SiO_2 nanoparticles leads to an unexpected morphological transition in near-critical PS/PVME (10/90) blends, from a typical network structure to a droplet structure. This behavior was ascribed to the selective affinity of SiO_2 nanoparticles for PVME phase.

Finally, the final properties of nanocomposites are widely determined by the localization of the particles in one of the two polymer phase or at the interface. This localization is established during the step of mixing and more generally during the processing. To estimate the localization of a particle in an immiscible polymer blend, authors first tried to calculate the wettability parameter (Section 3). However, this was shown to be largely insufficient to predict the final morphology because the thermodynamics of wetting determined the localization of particles only when thermodynamic equilibrium is attained. Hence processing conditions and kinetics effects must be emphasized (Section 4).

3. The role of wetting parameters on particle localization

The localization of nanoparticles in polymer blends was predicted by estimating the interactions between all three components (two polymers and one filler). The balance of interaction energies can be predicted by calculating the wetting parameter ω_{AB} presented in Fig. 6, where θ represents the contact angle, and γ_{S-B}, γ_{S-A} and γ_{AB} represent the interfacial tension between the particle and polymer B, the particle and polymer A and the two polymers A and B, respectively.

As described by Sumita et al. [40] and afterwards by Fenouillot et al. [41], if $\omega_{AB} > 1$, the particles are present only in polymer A; if $\omega_{AB} < -1$, the particles are present only in polymer B and if $-1 < \omega_{AB} < 1$, the particles are situated at the interface between the two polymers. The interfacial tensions between polymers are relatively easy to get by using different equations: Wu [42,43], Owens–Wendt [44], and Girifalco–Good [45,46]. Those equations (not presented here) are based on the measurement of surface tension of each component that could also be determined by different techniques [47]. Those techniques were summarized by Bousmina et al. [48]. They determined interfacial tension for a PS/PA6 blend using the breaking thread method (BTM), the imbedded fiber retraction method (IFRM), the retraction of deformed drop method

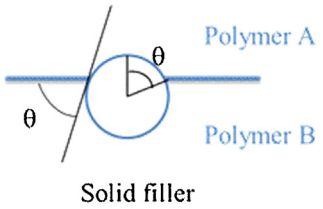

$$\omega_{AB} = cos\theta = \frac{\gamma_{S-B} - \gamma_{S-A}}{\gamma_{AB}}$$

Fig. 6. Schematic representation of the interface between polymer A, polymer B and solid filler and equation giving the wetting parameter ω_{AB}.

(DDPM), the pendant drop method (PDM) and a rheological method based on linear viscoelastic measurements (RM). A 20% difference between the values of interfacial tension was obtained, that is acceptable. Moreover, even if each method has its advantages and limitations, the experimental error increased in the following order: equilibrium method < dynamic method < rheological method. However, things get more complicated when determining the surface tension of filler and the interfacial tension between polymer and filler. Contact angle between liquids or molten polymers subsequently cooled on different carbon fibers (graphite fibers, nanofibrils and multiwalled carbon nanotubes) can be measured by electron microscopy [49] or by coupling AFM tip and Wilhelmy balance [50]. However, as mentioned by Fenouillot et al. [41], it is difficult to obtain reliable values of interfacial tensions between polymer and filler because measurements are disturbed by the filler surface structure. Kamal et al. [47] studied the surface roughness of clay tablets because surface roughness has a considerable influence on the measurement of contact angles of liquid drop when it is larger than 0.5 μm [51]. Whereas it was shown that contact angles are independent of surface roughness when average roughness is lower than 0.15–0.1 μm [52,53].

Moreover, almost all interfacial tensions between polymer and filler are measured at room temperature and in the solid state while the establishing of the morphology due to interfacial tension is performed in the molten state. There are few articles measuring the interfacial tension at the processing temperature. For instance, Elias et al. [54] present a corrected value of the interfacial tension between PP, PS and both hydrophilic and hydrophobic silica at 200 °C using Guggenheim's equation. Indeed, in the case where the liquids are organic solvent, it is possible to theoretically calculate the surface tension at any temperature using Eqs. (4) and (5) [55–57]:

$$\frac{-d\gamma}{dT} = \frac{11}{9}\frac{\gamma_0}{T_c}\left(1 - \frac{T}{T_c}\right)^{2/9} \quad (4)$$

$$\gamma = \gamma_0\left(1 - \frac{T}{T_c}\right)^{11/9} \quad (5)$$

where γ_0 is the surface tension at 0 K, T_c is the critical temperature and T is the temperature of the polymer.

Dharaiya and Jana [58] proved that the surface free energy and surface polarity of organically modified montmorillonite clay change when exposed to elevated temperatures. For example, the surface polarity (γ^p/γ) decreased from 0.36 for the as received organoclay to 0.070 after 7 min at 220 °C followed by 17 min at 250 °C. The surface polarity of the organoclay is therefore closer – at high temperature – to the polarity of PP (0) than to the polarity of PA6 (0.373). Hence, exposure to heat at the mixing temperature increased the value of interfacial tension between clay and PA6, while that between clay and PP decreased substantially, rendering the dispersion of clay platelets in the PP phase possible.

Kamal et al. [47] evaluated the surface tension of organoclays and the interfacial tension between organoclays and PS or PE. They took into account the thermal stability of resins and organoclays, the calculation of surface tension of resins in the melt state, the study of surface roughness of organoclays and the measurement of contact angles at high temperatures of sessile drops of the polymer melts on the organoclay surface. It must be noticed that organically modified nanofillers, and especially those with intercalated molecules such as organoclays are more sensitive to a temperature increase than covalently modified or pristine nanofillers.

Nevertheless, in many articles, the prediction of localization of the filler by the interfacial tension measurement coincides with real morphology observed by microscope [59].

Table 1 lists the surface energies of common polymers and fillers of some blends. A large dispersion in surface energy values can be noted, especially for fillers. This is mainly due to the different surface chemistries. For same filler, surface chemistry can be varied by adopting different chemical treatment.

Hence, to realize the selective distribution of filler in a polymer blend, interfacial tension can be varied by applying an appropriate surface modification. For example, Chen et al. [72] modified pristine CNTs (leading to FMWCNTs) to achieve a selective distribution of the nanotubes at the interface of a polymer blends. They were acidified by strong acid and grafted by maleic anhydride for PLLA/EVA blends [73], whereas they were only acidified for HDPE/PA6 blends [72]. Du et al. [68] varied the localization of MWCNTs in a SAN/PPE blend by functionalizing the nanotubes with random copolymers of methyl methacrylate and styrene (P(MMA-*co*-S)). The P(MMA-*co*-S) copolymers were grafted onto MWCNT *via* atom transfer radical polymerization (ATRP).

Finally, it is clear that the estimation of the wettability of the components of the system is very restrictive to evaluate the final morphology because in the molten state, the thermodynamic equilibrium may be difficult to attain and hence the processing conditions and kinetics effects must be taken into account.

Table 1
Surface energies, dispersive and polar components of some common polymers and fillers.

	Trade name	γ	γ^d (mN/m)	γ^p (mN/m)	Ref.
Polymers					
HDPE	Sholex F5012M from Showa Denko	25.9[a]	25.9	0	[40,57]
LDPE	0020 from Bandar Imam Petrochemical	22.59[b]	22.59	0	[60]
LDPE	2100TN00W from SABIC	17.9[c]	17.9	0	[55]
PP	Shoaromer MA2010 from Showa Denko	20.2[a]	19.8	0.4	[40,57]
PP	PPH 7060 from Atofina	30.1[d]	30.1	0	[54]
PP	51S30V from Equistar Chemicals	28.3[e]	28.3	0	[58]
PP	T30S from Lanzhou Petrochemical	30.1[d]	30.1	0	[61]
PP	Moplen HP400H from LyondellBasell	15.7[c]	15.7	0	[62]
PS	GP5250 from Taihua Plastic	40.7[d]	34.5	6.1	[61]
PS	Lacqrene Cristal PS 1960N from Arkema	40.7[d]	30.5	6.1	[54]
PMMA	MF from Mitsubishi Rayon	28.1[a]	20.2	7.9	[40,57]
PMMA	VH001 from Diapolyacrylate	26.62[b]	19.14	7.48	[60]
PA6	Zytel®7301 NC010 from DuPont Eng. Polym.	41.7[e]	15.6	26.1	[58]
PA6	Durethan B40F from Bayer	37.7[f]	27.2	10.6	[63]
PA6/12 (copolyamide 6/12)	Grilon CF6S from EMS Grivory	52.0[g]	34.1	17.9	[64]
PA12	Vestamid L2101F from Evonik Degussa AG	26.4[f]	23.2	3.2	[63]
EVA28 (28%VA)	From Arkema	35.9[d]	33.4	2.5	[65]
EVA39 (39% VA)	From Tosoh Co. Japan	25.9[g]	23.1	2.8	[66]
EMA (26–30% of methyl acrylate)	Lotryl 28MA07 from Arkema	26.9[g]	25.0	1.9	[64]
PC	Makrolon 2858 from Bayer	46.80[d]	45.45	1.35	[67]
		37.2[h]	36.12	1.07	
PBT	Tecodur PB 70 NL from Eurotec	49.10[d]	43.53	5.58	[67]
		33.5[h]	29.69	3.8	
PET	skyPET BL8050 from SK Eurochem	28.3[c]	22.0	6.3	[62]
PET	SG04 from OCTAL	20.4[c]	15.9	4.5	[55]
SAN	Luran®358N from BASF	29.5[h]	22.4	7.1	[68]
PPE	PX100F from Mitsubishi Eng. Plast. Eur.	28.4[h]	22.2	6.2	[68]
PLA	2002D from NatureWorks	51.1[d]	34.9	16.1	[69]
		42.1[i]	28.8	13.3	
PLLA	From Toyota Motor Co. Japan.	34.8[g]	17.5	17.3	[66]
TPS	Wheat starch and glycerol from ADM and Labmat, respectively	33.01[d]	25.4	7.61	[70]
PCL	CAPA6500 from Solvay	52.3[d]	42.0	10.2	[69,70]
		43.1[i]	34.8	8.3	
Fillers					
Carbon black	NC7000 from Nanocyl	55[a]	51–49	4–6	[40,57]
Carbon black	From Denki-kagaku Co. Japan	108.8[g]	108.1	0.7	[66]
Carbon black	Printex XE 2B from Degussa	42[b]	3–5	37–39	[60]
Silica	Aerosil A200 from Degussa	80[d]	29.4	50.6	[54]
Silica	Aerosil R974 from Degussa	81.7[d]	72.3	9.4	[61]
Silica	Aerosil R805 From Degussa	32[d]	30	2	[54]
Montmorillonite	Cloisite®30B from Rockwood additives	48.35[d]	34.6	14.75	[67]
		24.35[h]	17.42	6.92	
Montmorillonite	Cloisite®30B from Rockwood additives	35.0[d]	22.4	12.6	[69,71]
Montmorillonite	Cloisite®20A from Rockwood additives	42.08[d]	31.81	10.27	[67]
		18.08[h]	13.66	4.41	
Montmorillonite	Cloisite®15A from Rockwood additives	42.54[d]	31.47	11.06	[67]
		18.54[h]	13.72	4.82	
Montmorillonite	D2K from Zhejiang Fenghong Clay	45.2[d]	33.4	11.8	[69]
CNT	NT7000 from Nanocyl	27.8[c]	17.6	10.2	[55,69]
(Carboxylic)CNT	From Chengdu Organic Chemistry Institute	27.8[d]	17.6	10.2	[50,69]
MWCNT	Nanocyl-7000 from Nanocyl	27.8[f,g]	17.6	10.2	[63,64]
(Pristine)MWCNT	From FutureCarbon GmbH	27.8[h]	17.6	10.2	[68]
MWCNT	From Nanolab (USA)	45.3[d]	18.4	26.9	[49,69]
(Amine)MWCNT	From FutureCarbon GmbH	45.3[h]	18.4	26.7	[68]
MWCNT	NC3101 from Nanocyl	45.3[j]	18.4	26.9	[70]

[a] At 190 °C.
[b] At 210 °C.
[c] At 270 °C.
[d] At 25 °C.
[e] Not mentioned.
[f] At 240 °C.
[g] At 180 °C.
[h] At 260 °C.
[i] At 170 °C.
[j] At 145 °C.

4. Influence of dynamic processes on ternary nanocomposites morphology

4.1. Influence of processing (mixing sequences)

The final localization of a filler in a polymer pair can be directed by varying the sequence of mixing of the components [74]. Generally speaking, it must be pointed out that the particle diffusivity is controlled by the Brownian forces ($\sim k_B T$, k_B is the Boltzmann constant) in the suspending liquid matrix (viscosity η_s), which exerts the Stokes friction ($\sim 6\pi\eta_s R$) on the particle (radius of the particle R). The diffusion coefficient is expressed as $D_0 = k_B T/6\pi\eta_s R$. Due to the high viscosity of a molten polymer matrix, the diffusion coefficient D_0 of the filler in viscous media is extremely low so that the inorganic particles movements are not Brownian. Consequently the equilibrium dictated by the wetting parameter may never be reached even after reasonable time of mixing. Actually, for example, Elias et al. [75] have selected different sequences of addition for a PP/EVA/hydrophilic silica 80/20/3 system. In a first procedure of compounding, the three components were loaded simultaneously to the mixing chamber (200 °C, 5 min) of a microcompounder and in the second compounding procedure, the silica was pre-compounded with PP (200 °C, 5 min) and then the PP/silica was blended with the EVA during a second extrusion step. SEM and TEM micrographs showed that in the first case (first compounding procedure) the hydrophilic silica was essentially dispersed in the EVA droplets, whereas in the second case, silica particles appeared to be located in the EVA phase but close to the interface.

Other authors studied the final morphology of ternary systems by verifying the processing conditions, but also either by considering the conditions of mixing [76] or the affinity between the filler and the matrix [62,77]. Indeed, Médéric et al. [76] investigated the effect of processing procedures on the morphologies of PE/PA12/nanoclay systems. They showed that in a 80PE/20PA12/1C30B system (1 wt% of C30B based on the amount of PA12), a sequenced processing procedure – in which nanoclays were first melt-mixed with PA12 and PE was further added – gave lower PA12-nodules diameters ($d_n = 1.43\,\mu m$) than that obtained with a simultaneous procedure ($d_n = 2.24\,\mu m$). They explained this growth in the size of PA12 dispersed phase by the increase of the contact time between PE and PA12 with simultaneous procedure. A higher contact time would increase the coalescence phenomenon between the polymeric phases due to a weak interfacial coverage (discontinuous) of the interface by the nanoclay platelets. In the same article, the authors varied the processing conditions to change the morphology of the final systems. They showed that increasing the average shear rate (and hence the mixing energy) during the internal mixing procedure led to a better exfoliation of the platelets. This tended to limit the PA12-nodules break-up, leading to larger sizes. Concerning other process parameters, it is known that longer mixing time and higher rotation speed resulted in better dispersion of fillers [78]. On the other hand, Li et al. [62] prepared PET/PP/TiO_2 and PET/PP/PP-*g*-MA/TiO_2 composites with different blending procedures. They studied the influence of the mixing sequences, the interfacial tension ($\gamma_{TiO_2\text{-PP}}$ and $\gamma_{TiO_2\text{-PET}}$) and the possible interaction of maleic anhydride with TiO_2 and with PET. In procedure 1, TiO_2 was firstly melt mixed with PP, and PET (with or without PP-*g*-MA) was further added; in procedure 2, all components were added simultaneously; in procedure 3, TiO_2 was firstly added to PET, and PP (with or without PP-*g*-MA) was further added; and in procedure 4, PET, PP (with or without PP-*g*-Ma) were firstly melt mixed and TiO_2 was further added. The calculation of interfacial tensions (at 270 °C) between TiO_2 and both polymers showed that $\gamma_{TiO_2\text{-PP}} > \gamma_{TiO_2\text{-PET}}$, predicting then a thermodynamically preferential dispersion of TiO_2 in PET dispersed phases or at the PET/PP interface. This predicted distribution was obtained for all PET/PP/TiO_2 systems (whatever the procedure), but was only obtained for procedures 3 and 4 for PET/PP/PP-*g*-MA/TiO_2 systems. For procedures 1 and 2 of these last systems, TiO_2 was dispersed in the PP matrix, because PP-*g*-MA macromolecules could be absorbed onto TiO_2 surface by electronic donation and then nanoparticles were compatible with the PP phase. Finally, for PET/PP/TiO_2 systems (that do not contain any maleic anhydride), the localization of TiO_2 is governed by thermodynamic forces, whereas for PET/PP/PP-*g*-MA/TiO_2 systems (that contain maleic anhydride), the localization of TiO_2 is also governed by the mixing sequences. The compatibilization role of TiO_2 was explained in another article [77], and is reused in Section 5.1 of the present article.

Some authors have varied the sequence of mixing of their polymer pairs with fillers and have seen a strong effect of the order of addition on the final properties of the system [79–86]. For example, Zaikin et al. [87,88] have varied the sequence of mixing of their polymer pairs with carbon black (CB) showing different values of electrical conductivity due to different localization of the CB particles. Gubbels et al. [89] performed a co-continuous PE/PS 45/55 system containing carbon black at the interface by using two different melt blending process. In the first process, PE and PS were mixed and CB was added. The localization of CB at the interface was then controlled by thermodynamics. In the second process the CB was first added to the molten polymer with which it has the lowest affinity and afterwards the other polymer was added to the previous system. In that last case, the kinetic control of the thermodynamically driven transfer of the filler from the less preferred phase to the most preferred one allows one to stop the melt blending process when most of the CB particles have accumulated at the interface. This implies that the melt mixing time should be controlled to maintain the CB at the interface and optimize the conductivity (minimize the resistivity) as shown in Fig. 7. The kinetics of this transfer depends on the shear forces involved and the rheology of each polymer phase under the processing conditions.

More recently, some authors [79,85] studied the effect of ternary blend morphologies on mechanical properties. Martins [85] prepared ternary nanocomposites of PP(+PP-*g*-acrylic acid)/EVA/organoclay (60/40/5) by different blending procedures. He showed different localization of the platelets, depending on the procedure and on the organo-modifier of the clay. Different localizations lead to different mechanical properties. In the case of Cloisite® 20A

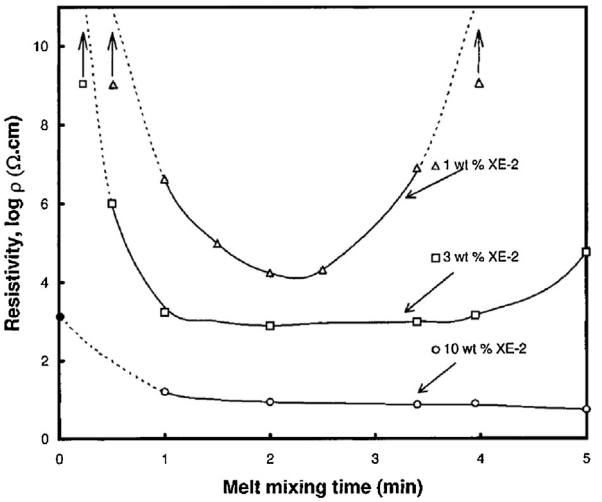

Fig. 7. Influence of the melt mixing time on the resistivity for 45/55 PE/PS blends loaded with 1 (□), 3 (△) and 10 (○) wt% of CB. ● refers to PS loaded with 10 wt% of CB.
[89], Copyright 1998. Reproduced with permission from the American Chemical Society.

(the organic modifier is non-polar and bears two long alkyl groups), whatever the mixing procedure, all the clay platelets are located in the EVA dispersed phase and impact strength is increased compared to that of neat PP/EVA blend. Contrarily, in the case of Cloisite®30B (the organic modifier is polar and bears one long alkyl group), clay platelets are either located at the interface (procedure M1 and M2) or in the EVA phase (procedure M3). Consequently, for this system, the authors showed a disadvantageous influence of the localization of platelets at the interface on the impact strength (that decreases compared to the neat blend). More recently, Borah et al. [79] used three different processing sequences to perform different morphologies for LLDPE/EMA/organoclay (Cloisite®20A and Cloisite®30B). They studied the influence of the dispersion of clay platelets and their localization in the binary blend on the molecular motion and mechanical properties. Unfortunately, to our knowledge, there are only very few publications studying not only the influence of processing procedures and conditions on the morphology of filled polymer blends systems, but also the influence on the final performances of the system (mainly mechanical, fire behavior and thermal).

4.2. Migration processes and evolution of morphology

As mentioned previously, Gubbels et al. [89] varied the sequence of mixing of PE, PS and CB components to localize CB particles at the interface. The kinetics of the transfer of the CB particles from the less preferred phase to the other can be used to allow the migration of the filler that will pass through the interface during the process of mixing creating a percolation system at low amount of CB. This was also performed by Sumita et al. [90] and Levon et al. [91] in order to investigate a multiple percolation system. Feng et al. [92] and Liebscher et al. [93] clearly proved that the rheology (viscosity ratio) of the polymers is a key factor for the determination of the final morphology. The morphologies of the three different systems investigated by Feng et al. are given in Fig. 8: CB can be dispersed in the PMMA phases (Fig. 8a) when the viscosity of PMMA is low (PMMA-1) or at the interface (Fig. 8b) when the viscosity of PMMA is intermediate (PMMA-2) or in the PP matrix (Fig. 8c) when the PMMA has the highest viscosity (PMMA-3).

Elias et al. [65] also showed the influence of the molecular weight (and hence of the zero shear viscosity) of two different EVA (EVA2803 and EVA28420) on the final morphology of 80PP/20EVA/hydrophilic silica and 80PP/20EVA/hydrophobic silica systems. The silica content of the blends was 3 wt% of the total material. The three components (PP, EVA and silica nanoparticles) were added simultaneously in the microcompounder, but the EVA melted before the PP (T_m(EVA) < T_m(PP)). The hydrophilic silica has more affinity with EVA, and as it initially placed in this EVA melted phase, the final morphology (given in Fig. 9a and b) is the most thermodynamically stable one. In the case of hydrophobic silica, it has better affinity with the PP matrix and their migration depended on the molecular weight of the EVA polymer (Fig. 9c and d). The migration of silica nanoparticles was easier with low viscosity EVA polymer (Fig. 9d).

Zhou et al. [94] studied the electrical properties of a LLDPE/EMA/CB system. The components were melt-mixed simultaneously and even if CB particles had higher interaction with EMA than LLDPE, they were selectively distributed in the non-polar LLDPE phase because of its lower viscosity compared to that of EMA. The authors concluded that the interfacial energy of particles/polymer would be of considerable importance just when the viscosities of the two polymers are comparable.

Finally, Persson and Bertilsson [95] studied aluminum borate whiskers dispersed in PE/PIB or PA/SAN polymer blends. The rheological (viscosity) and morphological (SEM) observations led them to conclude that the effects of viscosity ratio dominated the particle distribution when the interfacial tension between the two polymers was not too high. Otherwise, the thermodynamic interactions were predominant [96].

Fenouillot et al. [41] were the first to clearly identify and evaluate the mechanisms involved in the particle movement to or through the interface. They postulated that during mixing, shear forces are so high that they can shift the adsorption/desorption equilibrium by extracting the particles from the interface. Actually, the particle movement and localization are induced by particle migration in the molten state and under shear rate. Indeed, the transfer of nanoparticles between two phases of co-continuous immiscible blend is provided firstly by the contact between NPs and phase interface, and secondly by the transfer from one phase to the other. The transport toward the interface can be provided by a combination of particle diffusion and shear induced collisions of the particles with the blend interface. In the case of matrice/droplet morphology, same mechanisms are found when filler is initially located in the matrix phase. Whereas, when fillers are located in the dispersed phase, the transfer has to be provided by other mechanisms that Göldel et al. [56] acknowledge not to be known at that time.

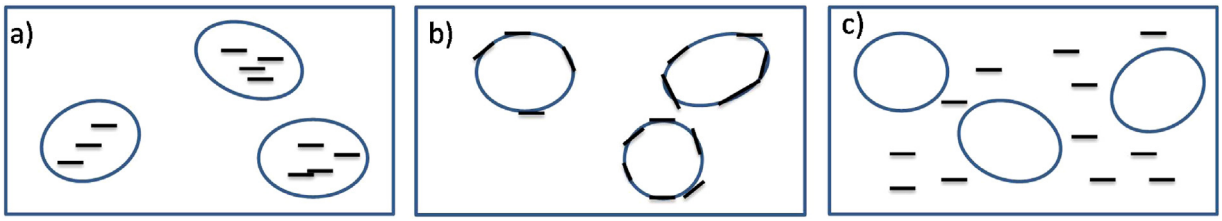

Fig. 8. Schematic morphology obtained by Feng et al. for a PP/PMMA-i/CB system where 10 wt% of CB were introduced and where PMMA-i was the dispersed phase with: (a) PMMA-1: the lowest viscosity (Mw = 25,000), (b) PMMA-2: the intermediate viscosity (Mw = 82,720) and (c) PMMA-3: the highest viscosity (Mw = 350,000). The viscosities of PMMA-1 and PP are comparable.

Göldel et al. [56,97] investigated the kinetics of transfer of CNT between immiscible co-continuous phases during melt mixing. They demonstrated that if complete transfer of MWCNTs from SAN to PC takes 5 min in a discontinuous microcompounder, it takes only 60–90 s in a continuous twin-screw extruder. The pre-mix of CNTs in one of the two polymer phases can be a determining factor for the final dispersion of CNTs in the blend. Moreover, the final morphology may be insconsistent with the thermodynamic predictions. Indeed, the first polymer that is in contact with the CNTs is thus adsorbed in a partially irreversible way as described by Baudouin et al. [63,64] and this adsorption can be responsible for the final blend morphology.

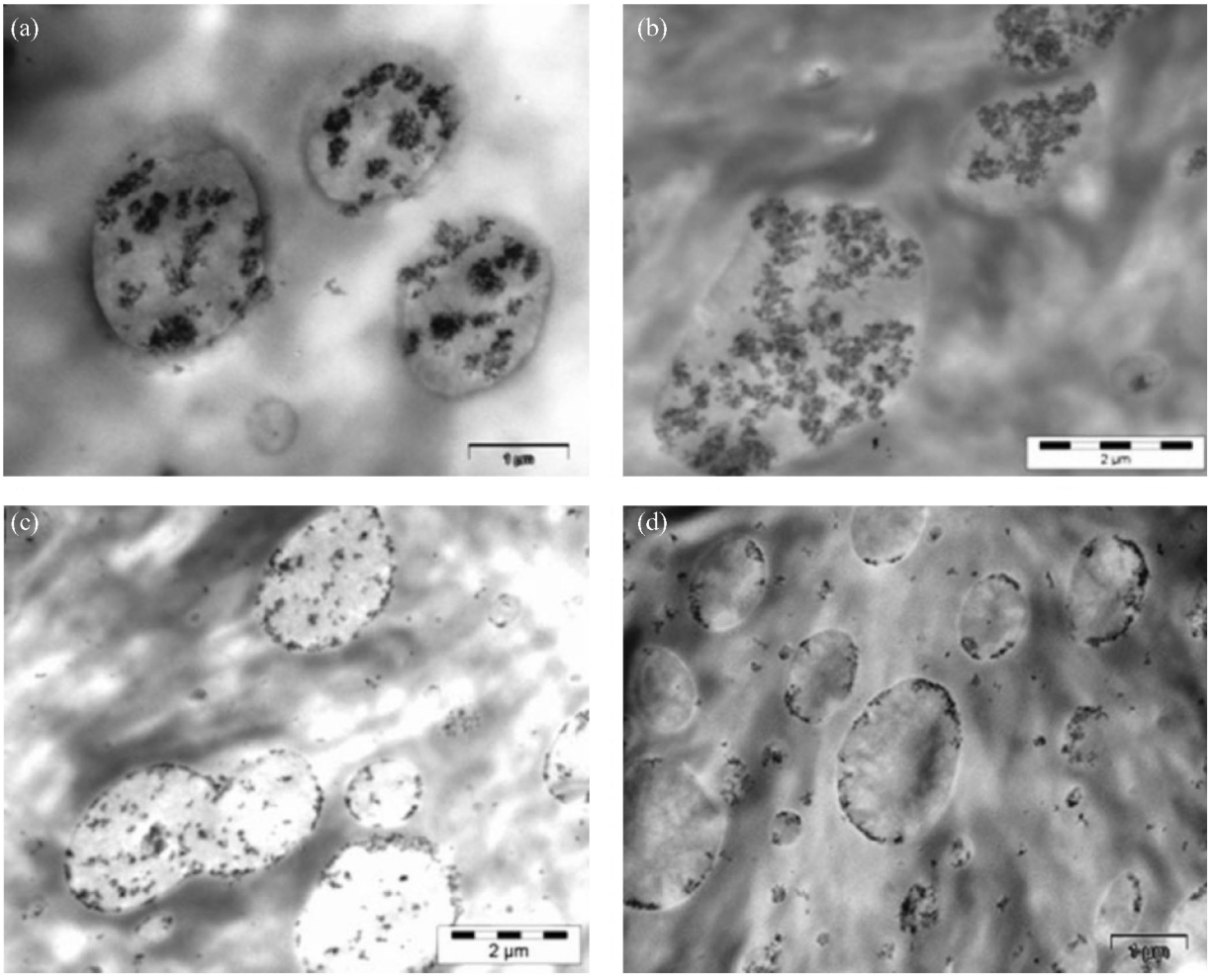

Fig. 9. TEM micrographs of PP/EVA/silica blends. All the components were added simultaneously in the extruder. (a) PP/EVA2803 (Mw = 53,500 g/mol)/hydrophilic silica. (b) PP/EVA28420 (Mw = 12,000 g/mol)/hydrophilic silica. (c) PP/EVA2803/hydrophobic silica. (d) PP/EVA28420/hydrophobic silica. [65], Copyright 2008. Reproduced with permission from John Wiley and Sons.

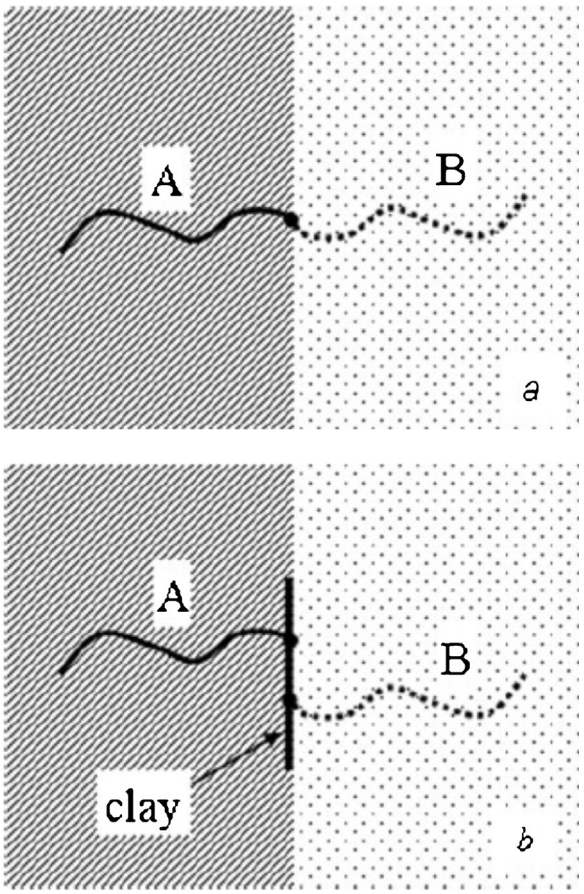

Fig. 10. Schematic representations comparing the compatibilizing mechanism of (a) a diblock copolymer and (b) a clay platelet.
[98], Copyright 2007. Reproduced with permission from John Wiley and Sons.

The shape dependance migration and localization of particles in polymer blends during mixing are described in Section 5.3.2.

5. Compatibilizing effect and interfacial rheology

5.1. Emulsification and coalescence in dispersed systems

When a compatibilizer is added to an immiscible polymer blend, it plays two major roles: (1) it lowers the interfacial tension, thus promoting breakup of droplets during processing (emulsification role) and (2) it helps prevent subsequent coalescence of the droplets, thus stabilizing the blend (coalescence suppressor role). Fang [98] compared – in a scheme reproduced in Fig. 10 – the role of diblock copolymer and clay platelet at the interface between two immiscible polymers. For a diblock copolymer, blocks A and B are compatible with phases A and B, respectively. In the case of organically modified clay, both A and B polymers have strong interactions with the exfoliated clay surface (located at the interface) and the clay plays the role of a coupling agent. Authors have often mentioned this surfactant role for nanoparticles, especially clay platelets. The objective of this paragraph is to explain the origin and the consequence of this compatibilizing effect.

Table 2
Number and volume average diameters of the different formulations containing PET, PP, PP-*g*-MA (MA) and TiO_2 (T).

Materials	PET droplets	
	Number average diameter (μm)	Volume average diameter (μm)
PET/PP	5.4	7.2
PET/PP/MA	3.4	5.1
PET/PP/2T	1.4	3.6
PET/PP/4T	1.1	3.0
PET/PP/3MA/2T	2.0	4.3
PET/PP/6MA/2T	3.8	5.5

[77], Copyright 2009. Reproduced with permission from John Wiley and Sons Inc.

From a history point of view, Gubbels et al. [89,99] were the first to observe the compatibilizing effect of nanofillers in polymer blends. They evaluated the coalescence suppression of a co-continuous 45/55 PE/PS filled with carbon black by performing static annealing (200 °C for a few hours). Carbon blacks are situated at the interface between the two polymer phases, in order to minimize the interfacial energy of the binary blend. In these systems, the coalescence and coarsening of both co-continuous immiscible phases depended on the weight fraction of CB (0, 1, 2 and 5 wt%). With only 1 wt% of CB, the stabilizing effect is moderate in contrast to 5 wt% of CB for which the average size of both PE and PS phase remain constant even after 24 h at 200 °C (Fig. 11).

As mentioned previously, Li et al. [77] compared different nanocomposites with PP as the matrix, PET the dispersed phase and TiO_2(T) that could play a compatibilizer role. The PP and polyalcohol treated TiO_2 were first melt mixed in a twin screw extruder. PET was then added in the presence of 0, 3 or 6 vol% of PP-*g*-MA (noted MA). The micrographs obtained by TEM showed that in both PET/PP/2T and PET/PP/4T systems, the TiO_2 nanoparticles migrated to the interface, and Table 2 shows a reduction in the PET droplet average diameter, indicating a compatibilizing effect of TiO_2.

In the case of PET/PP/3MA/2T, the nanoparticles were placed at the interface and in the PP (containing 3 vol% of PP-*g*-MA) matrix. Fig. 12 explains the two links occurring in the PP matrix (between MA and TiO_2) and PET dispersed phase (between PET and TiO_2). In the case of the PET/PP/6MA/2T system, there was enough maleic anhydride in order that all the hydroxyl groups of the treated TiO_2 reacted with the PP-*g*-MA and all nanoparticles were located in the PP matrix. Table 2 clearly shows that the most efficient compatibilizing systems are those where TiO_2 nanoparticles are present and localized at the interface between PP and PET. Indeed, in those PET/PP/2T and PET/PP/4T nanocomposites, nanoparticles at the interface prevent the coalescence of the dispersed PET droplets, thus yielding to a small droplet size.

Khatua [100] studied polyamide 6/poly(ethylene-*ran*-propylene)/nanoclay (Cloisite®20A) systems comprising either 80/20 or 20/80 N6/EPR with various rate of nanoclays. He observed that dispersed phase size can decrease

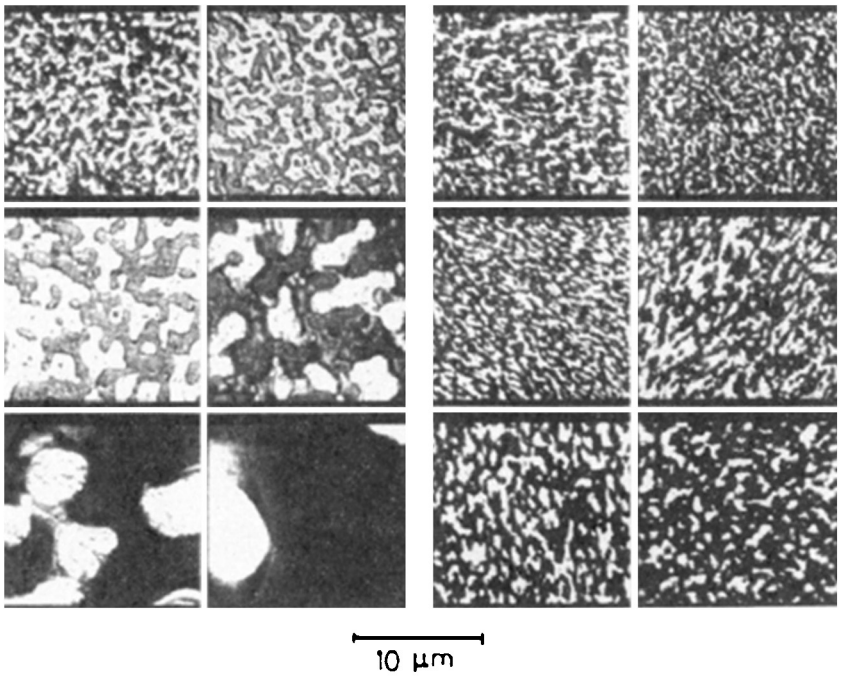

Fig. 11. Optical micrographs of co-continuous 45/55 PE/PS blends with 1 wt% CB (left) and with 5 wt% CB (right). Dark phase is the PE. Successive compression molding times at 200 °C are 0, 1, 10, 30, 300 and 1400 min.
[99], Copyright 1995. Reproduced with permission from the American Chemical Society

for both systems depending on the filler content. However, stabilization of morphologies against annealing permitted to differentiate the D_n decreasing mainly due to matrix viscosity rise (20/80 N6/EPR) or to a real compatibilizing effect (80/20 N6/EPR).

Coalescence suppression is one of the two main reasons for compatibilizing effect (interfacial tension reduction being the second one) [101]. When two immiscible polymers are blended, there are unfavorable interactions between molecular segments of the components, leading to large interfacial tension in the melt with low dispersion of both components in each other (giving coalescence). Hence, the interfacial modification of the system (classically performed by the addition of a block or grafted copolymer) would lead to morphological changing that are related to both a decrease in interfacial tension and/or a reduction of coalescence [11,102]. Consequently, this interfacial modification is accompanied by a droplet size

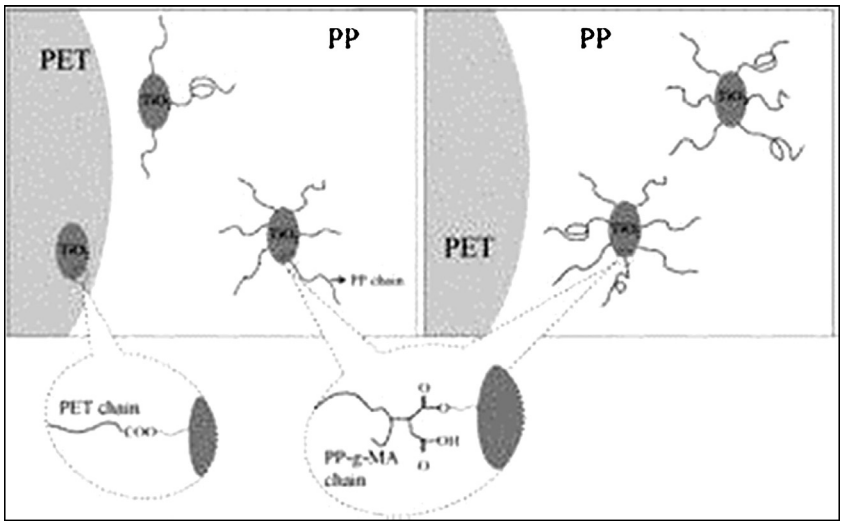

Fig. 12. Schematic representation of PP/PET/TiO_2 ternary system: (a) PET/PP/3MA/2T and (b) PET/PP/6MA/2T.
[77], Copyright 2009. Reproduced with permission from John Wiley and Sons.

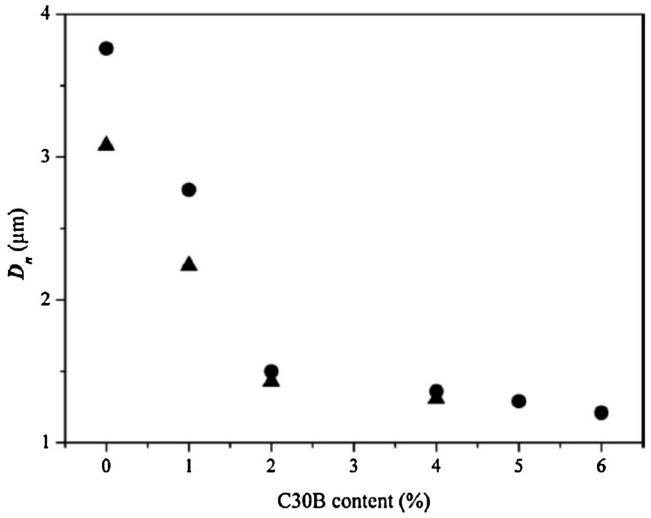

Fig. 13. Number average diameter as a function of Cloisite®30B weight fraction for (▲) 80/20 and (●) 20/80 LDPE/PA12 blends. The amount of C30B is relative to the PA content in the blend.
[103], Copyright 2009. Reproduced with permission from the Society of Rheology.

reduction and a narrowing of the droplet-size distribution of the dispersed phase. Some authors classically plotted the emulsification curve (*i.e.* the dispersed phase average diameter *versus* the wt% of nanoparticle) for a polymer A/polymer B/nanoparticle blend system [100,103], as in Fig. 13. The decreasing of the dispersed phase size when adding nanofiller (organo-modified MMT) is well known to be a proof of the emulsifying effect [100,104]. In the case where dispersed particles are not spherical – such as for instance for PP and ethylene-octene based elastomer filled with clay – authors adjusted the calculation of the dispersed phase diameter [105].

Actually, particle-size reduction in immiscible polymer blends containing nanoparticles is due to a complex process occurring during compounding (mainly extrusion and injection molding) in which the break-up mechanisms are opposed to coalescence [106]. Hence, different factors, especially local flow conditions (shear rate, residence time, and temperature) are engaged. Those processing conditions would modify properties such as viscosity ratio, elastic properties, interfacial tension [43,107]. Hence, attention must be paid on the factors leading to morphology changes in nanocomposite polymer blends. These factors were summarized and discussed by Fenouillot et al. [41] and comprised (i) a reduction of the interfacial energy, (ii) the inhibition of coalescence by the presence of a solid barrier around the minor droplet phase (iii) the viscosity ratio changing due to the presence of fillers in one of the two phases, (iv) the creation of a physical network of particles (when percolation threshold is reached) that inhibits the drops or matrix motion, and (v) the adsorption interaction of macromolecules at the surface of the solid particles. Huitric et al. [103] performed LDPE/PA12 systems containing from 1 to 6 wt% of MMT (Cloisite®30B). Morphological investigations and calculation (for example of the ratio between platelets situated in the matrix and at the interface) permitted to explain the origin of the reduction of the droplet size. When PE is the matrix (80PE/20PA), all the MMT platelets are situated at the interface and the size reduction results only from coalescence inhibition due to the solid-like barrier effect of MMT. In the 20PE/80PA system, platelets are localized both at the interface and in the PA matrix. Hence, the size reduction is due to both break-up mechanism and coalescence barrier effect. Indeed, the presence of platelets in the PA matrix increases the viscosity leading to break-up of PE nodules; moreover platelets at the interface inhibit coalescence. In the same manner, for a PBT/PE blend, Hong et al. [108,109] showed that a size reduction is obtained by the addition of organoclay having a specific preference for one of the two phases. Indeed, at low content, organoclays locate at the interface, suppressing the coalescence. And at higher contents, the rheological properties are being increased (due to a change in the viscosity ratio) leading also to a droplet size reduction.

Several authors tried to identify the origin of droplet size reduction by using different techniques. For example, Sinha Ray et al. [110] estimated the contribution of change in viscosity ratio on the droplet size reduction in a 30PC/70PMMA/Cloisite®20A (3 and 6%). They estimated the final particle size (R_e) by using Taylor equation:

$$R_e = \frac{0.5\Gamma}{\eta_m \dot{\gamma}} \times \frac{16p + 16}{19p + 16} \quad (6)$$

where η_m is the viscosity of matrix, p is the viscosity ratio, $\dot{\gamma}$ is the shear rate and Γ is the interfacial tension. They concluded that the important reduction in particles size due to C20A addition cannot be explained only by a change in viscosity ratio. Consequently, other possible mechanisms have been investigated at low concentration of filler, typically lower than 1 vol%. Developing Paliernes's model to polymer blends filled with nanofillers is another rheological way to understand the origin of the droplet size reduction. Palierne's rheological model was developed for incompressible spherical viscoelastic inclusions in an incompressible matrix [111]. The model is applied in the linear viscoelastic domain in order that the droplet

deformation remains small. The complex shear modulus is expressed as a function of the interfacial tension, volume average radius of the particles, the complex shear modulus of matrix and complex shear modulus of the inclusion. Palierne's model was adapted to ternary blends including immiscible polymers and mineral nanoparticles and permitted to express the complex shear modulus $G^*(\omega)$ through certain assumptions [54,112]. It can be used to evidence the origin of a droplet size reduction as demonstrated in 2007 for the first time by Hong et al. [108] and Elias et al. [54]. Hong et al. showed that for a 10/90 PBT/PE blend, the interfacial tension was reduced from 5.76 to 0.14 cN m^{-1} when 1 wt% of organoclay was added. In Elias et al. works [54], the presence of hydrophilic and hydrophobic silica in a 70/30 PP/PS blend can reduce 3.8 and 2.6 times the volume average diameter of the PS dispersed phase, respectively. By regarding the localization of either hydrophilic or hydrophobic silica in the PP/PS blend, the authors were not able to determine if – in their case – the reduction of the coalescence was due to a dense layer of solid particles at the interface (forming an interphase of almost 100 nm) or to the increase of viscosity of the continuous phase (that would make the drainage of the thin film separating two droplets more difficult). From the development of Palierne model to this blend system filled with 3 wt% of silica, they concluded that the stabilization mechanism of PP/PS blend by hydrophilic silica is due to the reduction in the apparent interfacial tension whereas hydrophobic silica acts as a rigid layer preventing the coalescence of PS droplets.

In another example, Vermant et al. [113] investigated the effect of hydrophobic nanometer sized silica on the flow-induced morphology of immiscible polymer blends (70PDMS/30PIB). Rheological measurements were performed following a particular flow protocol *versus* time including pre-shear conditions. The authors described the effect of particle concentration on the coalescence process by plotting the ratio of the volume average droplet radius over the interfacial tension of this polymeric emulsion. Fig. 14 used Palierne's model to plot the ratio between droplet average diameter and interfacial tension *versus* time and to show that the addition of 1% of nanoparticles completely slows down the coalescence of the dispersed droplets.

To conclude, it seems that the displacement of the nanoparticles in the melted polymer blends and their localization in the final binary blend influences the compatibilization effect especially because it influences the origin of the droplet size reduction. On the other hand, the understanding of the mechanisms responsible for the compatibilization has been improved by the last works of Vandebril et al. [114], Kong et al. [115], Filippone et al. [116] and Ville et al. [117]. Actually, Vandebril et al. [114] clearly shown using a rheological method that coalescence of the dispersed phase (30% PIB dispersed in PDMS) is slowed down or even totally suppressed when nanoparticles are present at the interface. Furthermore, the authors showed that anisotropic particles (ellipsoidal particles with an aspect ratio in the range of 2.5–4.0) significantly tend to stabilize blend more efficiently compared to spherical particles. On the other hand, Filippone et al. [116] found

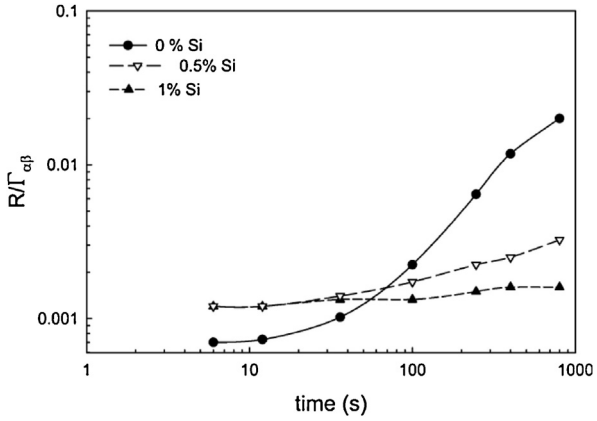

Fig. 14. Evolution of the $R/\Gamma_{\alpha\beta}$ ratio as a function of time for a 70/30 PDMS/PIB blend containing different amounts of silica at 20 °C. Silica is a Aerosil Rhodorsil R972, R is the volume average diameter of the PIB droplets, $\Gamma_{\alpha\beta}$ is the apparent interfacial tension of the system. [113], Copyright 2004. Reproduced with permission from Springer.

that poly(ethylene oxide) (PEO) phase droplet dispersed in HDPE is drastically reduced when particles (Cloisite®25A) are adsorbed at the HDPE/PEO interface and consequently susbstantially affect the interfacial rheology. More recently, Ville et al. [117] studied the structural and rheological characterization of PE/PA12 blends (80/20 or 20/80) filled with an organically modified clay having selective affinity toward PA phase. From XRD experiments combined with TEM microscopy, the authors evidenced numerous "interphase defects" such as irregular filler localization and stacking effect of nanofillers. Finally and from a compatibilization point of view, the droplet size reduction does not necessarily mean that nanofillers act as classical compatibilizers but as interfacial mobility modifiers. However, the modification of the phase viscosity in presence of filler at high concentration can be also in some examples at the origin of the dispersed phase size reduction [115,118].

As discussed previously, and as found in a large number of articles, compatibilization can be identified by (i) a decrease in interfacial tension between polymer pairs, (ii) a suppression of coalescence of dispersed nodules leading to a decrease of their size and (iii) an enhancement of interfacial adhesion between the two polymers. The first point is described in Section 2 using the thermodynamics theory and in the present section with Palierne's model. The second point is also largely described in the present section, whereas the last point is hard to describe as there is a lack of investigation in the literature because interfacial adhesion is difficult to evaluate directly. Mainly, an "indirect" method, such as the evaluation of the mechanical properties is used. However, interfacial adhesion can be evaluated by measuring the peel adhesion strength between polymer sheets. This test was performed by Chen et al. [72] on HDPE/PA6, HDPE-*g*-MA/PA6 and HDPE-*g*-MA + 1 wt%FMWCNTs/PA6. It consists in a tensile test carried out to separate two samples of polymers bonded to each other. Conclusions of on interfacial adhesion are given in Section 6.1.

5.2. Co-continuous morphologies of filled polymer blends

In polymer blends, the concentration range within which co-continuity is appearing is influenced by different parameters like blend composition, viscosity ratio and elastic properties of the polymers, also shear rates during mixing and mixing time [119]. Models were developed to predict the composition at the phase inversion point [120–124]. To stabilize co-continuous morphologies in polymer blends, several types of additives have been used, such as block or graft copolymers or more recently, nanoparticles.

Li et al. [125] obtained percolated nanoparticles network in PVME/PS co-continuous polymer networks, at relatively small particle volume fractions (1–2 vol% for nanorods, 2–3 vol% for nanospheres). Gubbels et al. [99] investigated the electrical properties of co-continuous PE/PS/CB systems. They measured the continuity fraction *versus* the wt% of PE without and with CB (Fig. 15). They observed that the selective localization of 4 wt% of CB in the PE phase was responsible for the extension of the dual phase morphology over a remarkably broader composition range; and the composition at which PE starts to be continuous dropped from 30 down to 5 wt% when filled with CB.

The same observation was investigated by Steinmann et al. [126] regarding a PMMA/PS/glass spheres system. The co-continuity of the polymer blend was obtained for 50PMMA/50PS without glass spheres, whereas in the case of the filled system (containing 30 vol% of glass spheres) the system remained co-continuous from 50 to 70 wt% of PMMA. Hence, the addition of fillers increased the stability of the co-continuous morphology [127]. This was partially explained by the slowdown of fibril break-up.

In the same manner, Wu et al. [128] proved that the addition of a second PA6 polymer (40 wt%) to an ABS matrix permitted to decrease the percolation threshold of a CB network from 8 to 2 phr. At this amount of CB in the polymer blend, a co-continuous network of polymers is formed. This is the double percolation effect [129–131]. And, an increase in CB loading (ϕ_{CB}) leads to a decrease in PA6 content (ϕ_{PA6}) needed to form a co-continuous network. Moreover, the authors showed that the product of ϕ_{CB} and ϕ_{PA6} is equal to a constant value noted n which is constant for a given system. This relation ($\phi_{CB}{}^{*}\phi_{PA6} = n$) can be applied for all immiscible polymer blends containing nanoparticles and can be used for designing and controlling co-continuous morphologies.

The morphology of PP/EPDM blends at different proportions, especially at the co-continuity of both phases was studied by Martin et al. [132]. More particularly, they studied the influence of both hydrophobic and hydrophilic silica particles on the co-continuity morphology. It was observed that hydrophilic silica particles tend to migrate within the elastomeric phase and form huge aggregates. On the other hand, hydrophobic particles are dispersed homogeneously and can be found both at the interface and within the EPDM phase. Surprisingly enough, the final co-continuous morphologies have not been altered too much as the presence of silica do not perturb the overall morphology. However, it must be pointed out that compared with usual thermoplastic blends, blends of ethylene–propylene–diene terpolymer (EPDM) and polypropylene (PP) possess a low interfacial tension of about 0.3 mN/m [133].

Lee et al. [134] showed that the addition of finely dispersed modified silica (fumed nanosilica grade Aerosil R805, surface modified with octylsilane, having a specific surface of 150 m^2/g) in co-continuous blends consisting of PP and ethylene-α-olefin copolymer-based polyolefin elastomers (POEs) resulted in a drop in the amount of continuity and a transformation to a finer morphology, consisting of elongated POEs domains inside the PP phase. Actually, this morphology transformation is associated to the presence of finely dispersed SiO_2 particles that are localized exclusively within the PP matrix. Actually, the viscosity ratio is altered when nano-silica are introduced in one phase and it is the most important factor influencing the phase inversion [135].

Zhang et al. [136] studied the role of hydrophilic silica to control the morphology of co-continuous polystyrene PS/PLLA blends. The influence of nanoparticle concentration on the co-continuity intervals and rheological properties of PS/PLLA blends were then examined. Actually, the incorporation of hydrophilic SiO_2 nanoparticles expanded the co-continuity of PS/PLLA blends and refined their pore size. The coarsening rate of co-continuous blends was decreased and the morphological stability of the blends under thermal annealing was improved. The increase of the viscosity of PLLA, due to the preferential location of the silica in the PLLA phase, was responsible for the phenomenon observed. On the other hand and as expected, it was observed that the suppression effect of SiO_2 nanoparticles on the coarsening rate of co-continuous PS/PLLA blends was more significant at lower PLLA content.

Filippone et al. [116] studied the impact of different types of nanoparticles (hydrophobic silica: Aerosil 150, hydrophobic silica: Aerosil R202 and clays: Cloisite®25A) on the morphology of blends of HDPE and PEO at different compositions. Wettability considerations supported by TEM analyses indicate that, depending on the mutual interactions among the phases, the filler unevenly distributes inside the blends, either selectively enriching the more affine of the polymer phases (hydrophilic silica A150 is located inside the PEO phase) or gathering at the polymer/polymer interface (Hydrophobic silica R202 and Cloisite®25A). Regarding co-continuity, they found that Cloisite®25A nanoparticles may unexpectedly alter the onset of phase co-continuity as shown in Fig. 16. Actually, such a phenomenon occurs when the filler locate at polymer/polymer interface and appreciably slows down the melt state relaxation dynamics of this interface.

Finally, Xiang et al. [137] investigated the effect of functionalized multiwall carbon nanotubes (FMWCNTs) on the phase morphology of immiscible high density polyethylene/polyamide 6 (HDPE/PA6, 50/50) blends. The unfilled 50/50 HDPE/PA6 blend exhibits a sea-island morphology, PA6 forming the continuous phase. The authors clearly observed, from electronic microscopy, that adding a small amount of FMWCNTs (<2.0 wt%) does not exert profound influence on the sea-island morphology of the nanocomposites. However, at moderate content of FMWCNTs (2.0 and 5.0 wt%), a typical co-continuous morphology

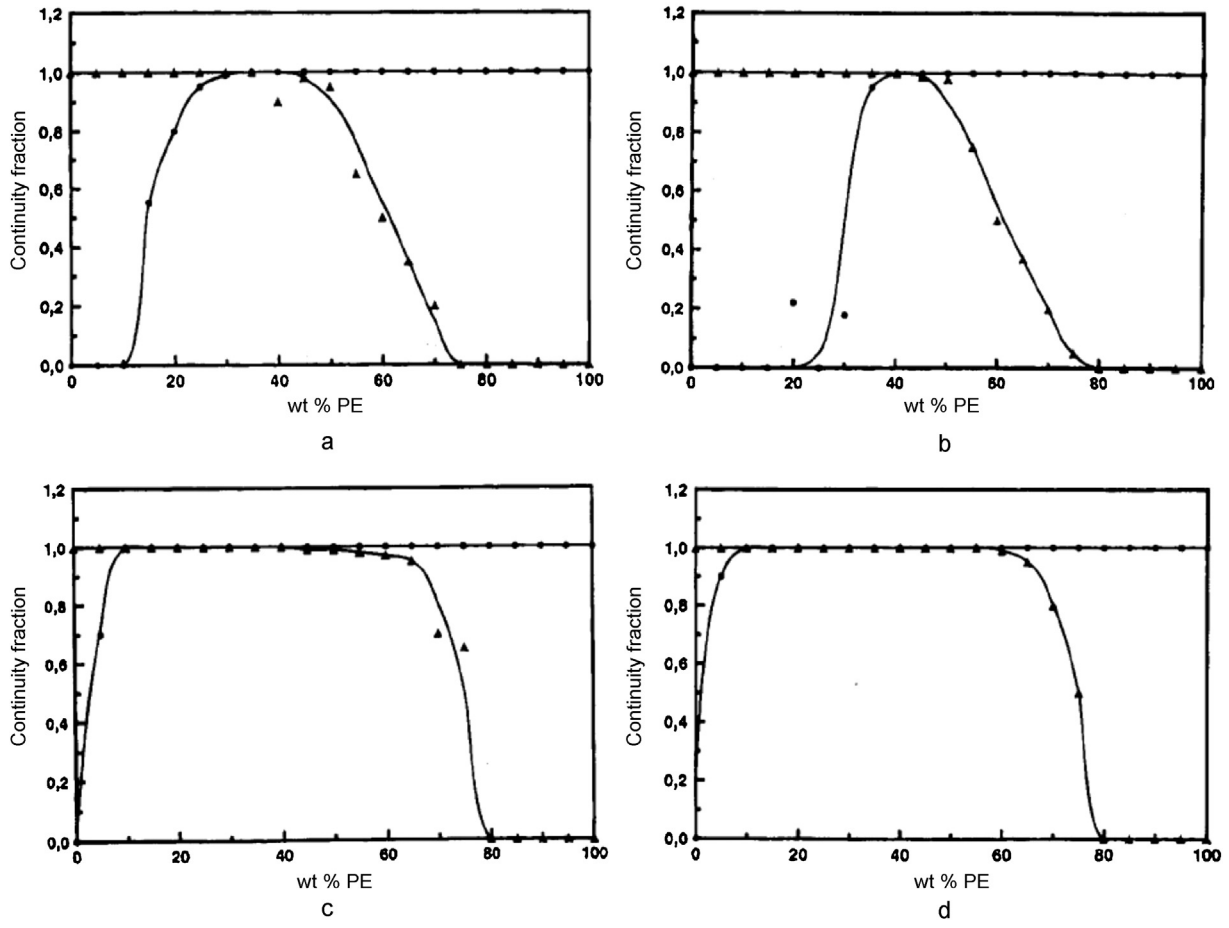

Fig. 15. Dependence of PE (●) and PS (▲) continuity on the PE/PS blend composition. (a) Without CB, (b) without CB, but compression molded at 200 °C for 10 min, (c) with 4 wt% of CB and (d) with 4 wt% of CB and compression molded at 200 °C for 10 min.
[99], Copyright 1995. Reproduced with permission from the American Chemical Society.

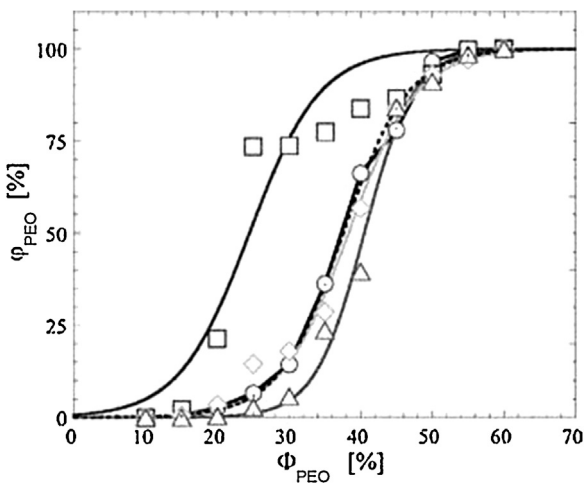

Fig. 16. Degree of phase continuity of the PEO *versus* PEO weight fraction in the blend: unfilled (○) and filled samples containing fumed silica A150 (◊), containing hydrophobic silica R202 (△), and containing Cloisite®25A (□).\
[116], Copyright 2011. Reproduced with permission from John Wiley and Sons.

is developed. On the other hand, further increasing of FMWCNTs concentration (10 wt%) induces the phase inversion. The functionalization of MWCNTs with either 30% of random methyl methacrylate and styrene copolymers (P(MMA-*co*-S)) having a $\bar{M}_n = 29.5$ kg/mol or with 80% of a P(MMA-co-S) having a $\bar{M}_n = 74.7$ kg/mol modifies the phase inversion region of a PPE/SAN blend [68]. This is mainly explained by a change in viscosity ratio between the two components.

5.3. Effect of the nature of the NPs on the compatibilization

5.3.1. Types of NPs

Several aspects of the NPs govern their localization, and their compatibilizing role in a polymer blend. In this section we are discussing of the influence of the type, the shape, the size and the surface chemistry of NPs. Molecular dynamics simulation was extensively used to study the influence of the shape, volume fraction and size of nanoparticles (anisotropic for platelets and rods and isotropic for spheres) on viscoelastic properties (such as melt shear viscosity or tensile strength) [138] or phase separation of

binary mixtures [19,139,140]. Allen et al. [141] showed that the phase behavior of anisotropic colloidal particles is different from that of spherical colloidal particles. Laradji et al. simulated the phase separation of several systems containing immiscible fluids and nanoparticles with different shapes (rods [142] and spheres [139,140,143]) but which interact preferentially with one of the two fluids. Concerning the nanorods, they showed that the morphology of the system depends strongly on the aspect ratio ν and the volume fraction ψ of the nanorods. Indeed, full phase separation occurs if $2\psi\nu < 3$. However, microphase separation occurs if $2\psi\nu > 3.29$ [142]. They also showed that contrary to nanorods, nanospheres in immiscible fluids do not lead to microphase separation. Laradji and Hore [140] extended this investigation to large-scale dissipative particle dynamics in three dimensions.

As in immiscible block copolymers, in polymer blends, several fillers have been used as compatibilizing agent. Different natures of fillers can induce different morphologies and properties. Added fillers can mainly differentiate by their shape, their size and their surface chemistry.

Table 3 lists the different fillers (layered double hydroxides (LDH), silica, layered silicate: montmorillonite (MMT), and organically modified MMT (noted OMMT), TiO_2, $CaCO_3$, carbon black, and carbon nanotubes found in the literature as mineral or organic additives in polymer systems.

5.3.2. *Influence of the shape*

Different shapes of fillers were introduced in polymer blends: spheres, rods and platelets. There are two main effects of the shape on the final properties of the system: (i) the specific surface area of the filler (and hence its aspect ratio) and (ii) the matrix/droplet interface saturation. When polymers are adsorbed at the surface of the inorganic filler, a large surface area per unit weight would lead to a large stabilizing energy gain [155].

Cassagnau et al. [144,156] schematically represent the complex shear modulus *versus* shear deformation for elastomers filled with different types of fillers (silica, organo-clays and carbon nanotubes), at two levels of dispersion (Fig. 17).

They noticed a paradox between spherical nanoparticles (fumed silica) and platelets (organo-clay). Indeed, increasing the exfoliation in the case of organo-clays lead to a decrease in the percolation threshold (identified by an increase of the shear modulus) and a decrease in the limit of viscoelastic linearity. This is due to an increase of the frictional interactions between layers. Whereas, increasing the dispersion in the case of the fumed silica by functionalization (surface grafting of end-tethered chains) leads to the opposite behavior (increase in the percolation threshold and in the limit of viscoelastic linearity). These schematic results on rheological behavior of elastomeric filled systems based on different fillers' shape points out the importance of the shape of the nanoparticles on the morphology of the system.

Very recently, Göldel et al. [56,97,157] reveal that the aspect ratio of solid fillers plays a major role in the transfer dynamics and stability at the blend interface in melt mixed multiphase polymer blends. They proved that high aspect ratio objects were transferred faster and with more

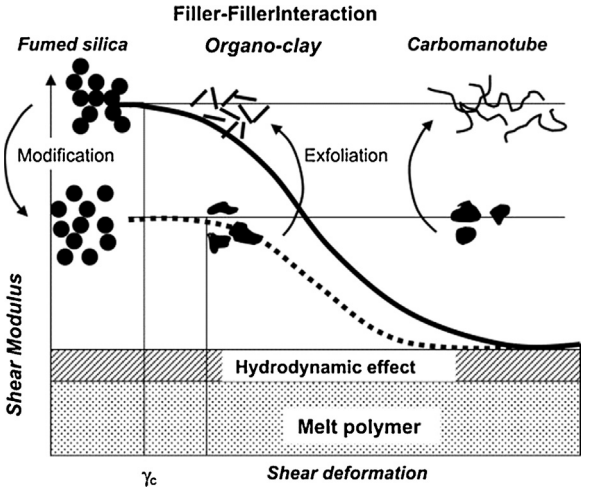

Fig. 17. Contribution to the complex shear modulus *versus* strain for elastomeric filled with different types of fillers (spheres = SiO_2 and platelets = MMT) at two levels of dispersion.
[156], Copyright 2010. Reproduced with permission from Elsevier Ltd.

efficiency as compared to low aspect ratio fillers. This is due to the change of blend interface curvature during the transfer process and it explains the fast and complete transfer of CNTs from a less favorable into a more favorable wetting blend phase. They called this difference "Slim-Fast Mechanism". They verified experimentally by comparing PC/SAN blends filled with either MWCNTs or CB that after 5 min of melt mixing, CNTs were mainly localized in the PC phase whereas the amount of CB at the blend interface was not negligible.

Zhang et al. [158] made films based on 50/50 PS/PMMA (prepared by solution in toluene) with 5 vol% of three different nanoparticles: Cloisite®6A (that is an organically modified montmorillonite), tungsten disulfide nanotubes and tungsten disulfide multi-layered "onion" shaped particles. They showed that W_2S onion shaped nanoparticles do not affect the phase segregation morphology, whereas the other two do. Moreover, Cloisite®6A is more efficient in reducing the PMMA domain size. The authors explained that since platelets have a high aspect ratio and can deform and follow the interface, they can cover a large surface domain whereas nanotubes and spheres cannot. Hence, to saturate the interface between matrix and droplets of an immiscible polymer blends, platelets are the best candidate. There are numerous articles dealing with immiscible polymer blends containing platelets fillers (more often, layered silicates) and Table 4 summarizes the polymers and layered silicate used in the literature.

To be efficient as compatibilizing agents, layered silicates in polymer blend composites must be well dispersed, *i.e.* intercalated or exfoliated. And the most crucial factor in controlling dispersion (and hence morphology) is the extent of interaction between the modified platelets and the polymer matrix [59] (see Section 5.3.4). Moreover, the well dispersed nanoclays resulted in improved thermal, mechanical [201] and fire properties. Fang et al. [170] showed how the interface between two polymers may be stabilized by clay platelets depending on the

Table 3
Different NPs fillers (their shape, average particle size, specific surface area, treatment surface and the corresponding reference).

Nanoparticles	Shape	Average particle size (nm)	Specific surface area (m^2/g)	Treatment surface	Ref.
Fumed silica	Spheres	3–250	50–400	Hydrophilic (naturally) or hydrophobic (after modification)	[144]
MMT and O-MMT	Platelets	–	–	Organically modified to adjust the affinity with the polymer	cf. Table 4
LDH (magnesium aluminum)	Platelets	D_{50} < 10 μm	–	Modified with a $RCOO^-$; modified with interstitial OH^-	[145]
$CaCO_3$	Unknown	80	12	No treatment	[146]
Carbon black	Spheres	12; 18	1487; 180–250	No treatment	[147,148,89]
Carbon nanotube (MWCNT)	Rods	Outer: 20–30: inner: 5–10 Length: 10–50 μm	–	Often functionalized to render the surface more organophilic	[149,72,150]
Graphite oxide	Isometric, irregular spheroids	D_{90} < 5 μm Thickness = 100 nm	26	Oxidized	[151]
Graphene	Platelets	–	–	Oxidized	[78,152,153]
Gold nanorods (CdSe)	Rods	18*48 nm; 8*30 nm	–	Poly(ethylene glycol)-thiol modified; coated with trioctylphosphine oxide	[154,125]
TiO_2	Spheres	300; 15	–	–	[62,77]

strength of interaction between the two polymers (Fig. 18). Fig. 18a represents the exfoliated structure obtained when both polymers have a strong interaction with the silicate platelets (the case of PA6/PEAA/*o*-clay). Fig. 18b represents intercalated structure when there are no interactions between polymers A and B and silicates external surface. Finally, Fig. 18c is representative of a strong interaction between polymer A and the silicates with no interaction between polymer B and silicates external surface (case of PA6/HDPE/o-clay) leading to partially exfoliated structures.

In a rapid communication, Wang et al. [192] showed that PP and PS macromolecules of a 70PP/30PS/O-MMT system are only partially intercalated into the galleries of O-MMT with parts of the chains being located outside the gallery (Fig. 19). Then, they hypothesized that the outside parts of PP and PS chains serve as a compatibilizer just like a block copolymer.

To achieve this exfoliated structure in which clay platelets are independently dispersed in the polymer blend matrix, layered silicates are often organically modified by surfactants. Indeed, the degree of exfoliation is predominantly determined by the interactions between the polymer matrix and the surfactant at the surface of the organoclay. Moreover, these surfactants can play an important role to compatibilize the polymer blend system. Gelfer et al. [174] added 10% of Cloisite®6A in PS/PMMA blends. This Cloisite®6A (O-MMT) contained 45% of a dimethyl dihydro ditallow ammonium (DMDTA) surfactant; they considered that 15% of the surfactant in the MMT was loosely bounded or unbounded to the clay surface. This 1.5% (in the composite) free surfactant would improve the miscibility between PS and PMMA leading to droplet size reduction. An interesting study used online measured electrical conductance (OMEC) to characterize morphology development and kinetics of clay distribution in a rubber blend during mixing process [215]. It was found that the release of the ionic surfactant from the clay galleries during the mixing is the main reason for the electrical conductance of rubber organoclay composites. Hence, both NR and HNBR molecules can intercalate the clay tactoids that act as compatibilizer.

Sinha Ray et al. [155] calculated the volume fraction of clay (φ_c) needed to saturate the PS particles surface in a 20PS/80PP blend, assuming that all platelets are located at the interface:

$$\varphi_c = \frac{3e}{R}\varphi_{PS} \quad (7)$$

where e is the thickness of clay platelets, R is the PS average droplet radius and φ_{PS} is the volume fraction of PS. They showed then that the saturation concentration is very small when clay is fully exfoliated (almost $\varphi_c = 0.001\%$ assuming $\varphi_{PS} = 20\%$, $R = 8$ μm and $e = 1$ nm).

Huitric et al. [103] also evaluated the weight fraction of Cloisite®30B platelets present at the interphase between LDPE and PA12 or in the PA12 phase. They prepared 80/20 and 20/80 PE/PA systems with varying amounts of O-MMT (0–6%). Using the number average diameter of the dispersed phase (D_n), the average thickness of the interphase (e), the inter-reticular distance between platelets (d_{ir}), and the thickness of a clay particle, they determined that for the 80/20 PE/PA composition, all the clay platelets are located at the interphase, whereas for the 20/80 PE/PA, one part of the platelets are situated in the PA matrix, even for 1 wt% of C30B. Obviously, the fraction of clays at the interphase reaches a saturation amount (between 1 and 2 wt% of C30B) and beyond 2% the clay platelets accumulated in the PA matrix. Hence, 2% is known to be the fraction needed to cover the nodules with a quasi-continuous interphase.

5.3.3. *Influence of the size*

We demonstrated previously that the addition of fillers to a polymer blend can stabilize the morphology. This effect is dependent on the surface area of the filler and its ability to disperse in the polymer melt. Dispersion/aggregation of particles is a key factor for final morphologies of

Table 4
Non-exhaustive list of the publications dealing with thermoplastic polymer blends systems comprising layered silicates fillers.

Matrices	Clays	Remarks	Ref.
EPDM/EVA (50/50)	Hexadecyl ammonium-MMT	Competitive adsorption of EPDM and EVA on the layered silicate reduces the interfacial tension and results to a co-continuous structure	[159]
PA6/ABS (50/50)	Nanofil2 (stearylbenzyldimathyl ammonium-MMT)	Induced solid-like behavior by incorporation of organoclay in a co-continuous morphology	[160]
EOC-*g*-MA/PP (70/30) EPR-*g*-MA/PP (70/30)	Nanomer® I.44	Improvement of the thermal degradation	[161]
HDPE/PS + PE-*g*-MA	MMT modified with octadecylamine (1–7 wt%)	3% is the optimal content to achieve the best level of intercalation; 1% of PE-*g*-MA gives the best results in XRD	[162]
LDPE/POE + PE-*g*-MA	Nanomer® I.44	Wagener and Reisinger's method is used to evaluate the degree of exfoliation	[163]
LLDPE/EMA (60/40) + LLDPE-*g*-MA	Cloisite®30B et Cloisite®20A	Optimum dispersion and properties are obtained for 5 wt% of MMT	[79]
PS/ABS and HIPS/ABS (10/90; 80/20)	MMT-Na^+, Cloisite®20A, MMT treated dimethyl octadecyl-(3-trimethoxysilyl propyl) ammonium chloride	Higher tensile energy and impact strength are obtained with simultaneous mixing	[80]
PLLA/PBS (75/25)	Cloisite®25A and Twice Functionnalized Organoclay (TFC) with epoxy groups	Fully exfoliated TFC leads to the improvement of tensile modulus and elongation at break	[164]
PA6/PP + SEBS-*g*-MA	MMT-Na^+ modified to octadecyl-ammonium-MMT (O-MMT)	The formation of PA6-O-MMT clusters (when incorporating SEBS/SEBS-*g*-MA) improves the toughness/stiffness balance	[165]
PA6, 6/SEBS-*g*-MA (80/15 + 5%MMT)	Cloisite®30B	To optimize toughness and other mechanical properties the amount of exfoliated organoclay in the nylon 66 matrix as to be maximize	[166]
Plasticized starch (PLS)/PP-*g*-MA	MMT-Na^+ and Cloisite®30B (5%)	MMT-Na^+ locates in the PLS whereas C30B locates in the PLS and at the interface	[167]
PC/PBT (60/40)	Cloisite®15A, 20A, 25A and 30B	There is a transesterification between PC and PBT leading to the formation of block copolymers	[168]
PP/PA6 (10/90)	Cloisite®30B	Interfacial tension between PP and PA6 is reduced but MMT do not participate to the compatibilization	[58]
PC/PMMA (80/20)	MMT-Na^+	Low $\bar{M}_n$ PMMA are prepared by *in situ* suspension polymerization	[169]
PCL/PEO (20/80 and 80/20)	Cloisite®-Na^+ and C30B	Formation of a network structure	[98]
PA6/HDPE (or HDPE-*g*-acrylic acid) (70/30)	C18-bentonite (octadecyl trimethyl ammonium)	The clay platelets play the role of coupling species	[170]
PP/PA6 (70/30)	O-MMT (dioctadecyl dimethyl ammonium)	Blends are prepared by ribbon extrusion process	[171]
HDPE/PA6 (75/25)	Cloisite®15A	The presence of O-MMT leads to a co-continuous system	[172]
PP+PP-*g*-MA + SEBS-*g*-MA/PA6	Nanofil 15 and Nanofil 919	Adding nanoclays increases the modulus whereas it decreases the impact strength	[173]
PMMA/PS	Cloisite®6A and C20A	Clays increase the compatibility between PS and PMMA	[174]
PA6/SEBS-*g*-MA (0–40 wt% of SEBS-*g*-MA)	Nanomer I.30TC	A higher adhesion leads to a smaller critical interparticle distance	[175]
PLA/ε-PCL (95/5)	Dimethyl distearyl ammonium ions	ε-PCL with $\bar{M}_w$ = 10k is the best additive for PLA/clays	[176]
PBT/PE (99/1 to 1/99)	Nanofil 919	Platelets are localized at the interface, leading to an interfacial tension reduction (coalescence suppression)	[108,109]
LDPE/PA12 (90/10 to 10/90)	Cloisite®30B (1–6%)	For PA matrix with 2% of clay, the interphase thickness is 11 nm	[103]
PP + PP-*g*-MA/PTT (75/25)	C20A and C30B	Nanoclays incorporation increases crystallizability of polymers; compatibilizer is remarkably more influential than nanoclays regarding crystallization and melting characteristics	[177]
PVDF/EVA 70/30	Cloisite®30B, Nanomer I.30T	Hydrophilic organoclays in EVA with high contents of VAc lead to toughness enhancement whereas hydrophobic organoclays induce high modulus with lower content of VAc EVA	[178]
PA6/EPR	Cloisite®15A, 20A, 25A, 93A and 30B	Formation of "core-shell" particles that increase the toughness	[179]

Table 4 (*Continued*)

Matrices	Clays	Remarks	Ref.
PA6/EPR (80/20, 20/80, 99.5/0.5)	Cloisite®20A	As long as the clay becomes exfoliated in the matrix, it effectively prevents the coalescence of the dispersed domains	[100]
PP/EPR-*g*-MA 30/70	Nanomer I.44PA	Coalescence is suppressed when clay are localized into the EPR-*g*-MA phase exclusively	[112]
PMMA/SAN 50/50	Cloisite®25A and C15A	Platelets are localized at the interface even after three times extrusion	[180]
PP/SBS (92/5)	Kaolinite clay treated with dimethyl sulfoxide (3 wt%)	SBS rubber helps to finely disperse clay particles in PP matrix improving the toughness	[181]
LDPE/PA6 + PE-*g*-MA (20/80)	Cloisite®30B	Rheology is sensitive to clay dispersion, its localization and phase morphology	[182]
PP/SEBS 80/15	Cloisite®20A (5%)	Clays surrounded by elastomer caused the SEBS particles to become elongated in shape and retarded the its coalescence	[183]
PP/EVA/PP-*g*-MA (55/40/5)	Cloisite®30B and C20A (5%)	Blending sequence effects on the morphology and properties of the mixtures are dependent on the organoclay used	[85]
PA6/HDPE (20/80)	Nanomer I.30TC	Clay enhances the crystallization of the γ-form of PA-6	[184]
PA6/ABS (80/15 to 60/35) + EnBACO-MAH	Cloisite®30B	A Gramespacher and Meissner method is used to investigate the rheological behavior	[185]
HDPE/PA6 75/25	Cloisite®15A	Compatibilizer is used (EAA/PBO, HDAA/PBO and EGMA*). A possible thermo-oxidative degradation of the organic modifier of MMT and the subsequent interaction between the degradation products and the compatibilizer leads to poor properties	[186]
PP/PS (80/20 and 50/50)	Cloisite®20A and 2M2ODA	Clays located at the interface reduce the interfacial tension and the dispersed phase size and increase in mechanical properties	[155]
PC/PMMA (30/70)	Cloisite®20A, C30B, C25A and C15A	Effect of the initial interlayer spacing of the organoclay on the overall morphology and properties	[110,187,188]
PP+PP-*g*-MA/PA6 (70/30/0 to 55/25/15)	O-MMT (hexadecyl trimethyl ammonium bromide)	Crystallization is modified by the presence of OMMT; there is a remarkably reduction of pHRR due to a 'ring' structure	[189]
PVDF/PA6 30/70	Cloisite®30B, C20A	PVDF crystallization modification	[190]
PS/PEMA 25/75	Dimethyldioctadecyl ammonium hectorite	Organoclays adsorb the PEMA chains and PS chains are shaped into separate domains. Organoclays exhibit an emulsifying effect	[104]
PP/PA6 (10/90)	Nanomer I30TC, Cloisite® 20A and C30B	Nanoclay compared to kaolin clay. Nanoclay decreases water absorption of PA6	[191]
PP/PS (70/30)	O-MMT (dioctadecyldimethyl ammonium)	It is possible that PP or PS exhibit parts of the chains being located outside the galleries acting as compatibilizer	[192]
PC/ABS (57/38) + 5%O-MMT PA6/ABS	O-MMT (hexadecyl trimethyl ammonium)	By choosing the proper polymer, self-organization of clays from one phase to another could be performed	[193]
PA6/EPDM-*g*-MA	MMT modified with dioctadecyl dimethyl ammonium	The interparticle distance of a PA6/EPDM-*g*-MA filled with O-MMT has a dramatic influence on impact strength	[194]
PBT/ABS (65/30) + EMG terpolymer	MMT modified with cetyl pyridium chloride	Order of mixing has influence on the preferential crystal growing direction of PBT owing to the antagonistic effect of ABS and OMT	[195]
PA6/PS (70/30)	MMT modified with non polar ammonium salts	*In situ* bulk polymerization is employed to synthesis the PS/O-MMT	[196]
PA6/LLDPE	Cloisite®25A	The size of the separated domains decreases with increasing content of organoclay	[197]
a-PA/EOR	Cloisite®30B, C93A, C20A, trimethyl hydrogenated-tallow ammonium MMT	The presence of organoclay causes the elastomer particles to become elongated and irregular in shape	[198]
a-PA/EOR (or EOR-*g*-MA) (80/20)	MMT Na^+ modified with trimethyl hydrogenated tallow ammonium chloride	Clay for elastomer particle size reduction. Beneficial balance of toughness *versus* stiffness with maleated elastomer	[199]
LDPE/PET	Cloisite®10A, C15A, C30B	The key factor for organoclay compatibilization efficiency (for PE/PET) is the surfactant	[200]
PS/PVME	Laponite MMT (both modified dimethyl dioctadecylammonium) Fluorohectorite (modified trimethyl octadecylammonium)	Layered silicates with large disk diameters (10 μm) do not affect the morphology of the phase separated structure and only accelerate the phase separation kinetics	[36]

Table 4 (*Continued*)

Matrices	Clays	Remarks	Ref.
PS/PMMA (50/50)	Cloisite®6A (tungsten disulfide nanotubes and tungsten disulfide multi-layered onion shaped particles)	The aspect ratio and bending energy play a major role in the compatibilization process; sample is prepared in solution	[158]
PLA/PBSA (70/30)	6% of Cloisite®-Na^+, C15A, C20A, C25A and C30B; 0–9% of C20A	Effect of different surfactants used to modify the surface of MMT	[201–203]
Biodegradable aliphatic polyester (APES)/TPS	Cloisite®30B	Mechanical properties are evaluated	[204]
PS/PMMA; PC/SAN24; PMMA/EVA (70/30; 50/50; 30/70)	Cloisite®20A, C6A	*In situ* grafts formation induces reduction in domains size and localization of clay platelets along the interfaces	[205]
PEO/PMMA (50/50)	Cloisite®25A	The nanocomposites are prepared *via* solvent casting	[206]
PA/SAN (80/20 to 20/80)	2% of exfoliated nanoclay	PA/clay nanocomposite is a commercially available grade (obtained from Ube Inc.)	[207]
PP (PP-*g*-MA)/PBSA	Cloisite®-NA^+; C20A	Organoclay acts simultaneously as nanofiller and compatibilizer when two chemically different polymers have strong interactions with organoclay surface	[208]
EPDM-g-MA/PA6 (20/80)	4% of Nanomer I.30TC	Having maximum percentage of OMMT platelets in the PA6 matrix and keeping good interfacial adhesion between PA6 and EPDM-g-MA are beneficial to impact strength	[74]
PA6/PP (70/30)	0–10% of 1.30TC Nanomer	Highest strength values are observed at an organoclay content of 4 wt% for the blends	[209]
PP (PP-g-MA and SEBS-*g*-MA)/PA6	Nanofil 919; Nanofil 15	Adding nanoclays improve the modulus, whereas the impact level was below that of the pure polymers	[210]
PA6/ABS (SANMA as compatibilizer)	Nanofil 2	OMMT refines the co-continuous structures and leads to mechanical stiffening as indicated by the DMA results	[59]
PA6/ABS (POE-*g*-MA) (80/20)	4% of nanoclay	PA6/clay nanocomposite is a commercially available grade M1030D (obtained from Unitika Co.)	[211]
LDPE (PE-*g*-MA)/APES	Cloisite®30B, C20A	Dispersibility and properties of nanocomposites C30B are better than those containing C20A	[212]
PA11/PS	Cloisite®30B	After PS extraction, a porous PA11 material was obtained and clays increase the volume porosity and modified the pore size distribution	[213]
PC/PBT (30/70; 50/50)	Cloisite®30B, 15A and 20A	Wetting coefficient and DMTA were used to evaluate the location of the nanoparticles	[67]
PP/PA6 (70/30)	$[(C_{18}H_{37})_2(CH_3)_2N^+Cl^-]$ modified clay	The presence of the organoclay leads to a strong interaction among PP, PA6 and the organoclay	[214]
HNBR/NR (50/50)	Nanofil 9 (5%)	On Line Measured Electrical Conductance (OMEC) was used to monitor the dispersion of nanoclay in polymer blend and the kinetics of distribution	[215]
PPR/SEBS/SEBS-*g*-MA (or POE-*g*-MA or PPB-*g*-MA) and PPR/SEBS-*g*-MA (or POE-*g*-MA or PPB-*g*-MA)	Nanomer I31PS	POE-*g*-MA facilitate the exfoliation and toughen the nanocomposite without marked degradation in rigidity	[216]
HDPE/PP (80/20 to 20/80)	Cloisite®15A (0–5%)	Nanocomposites were prepared as high strength fibers for automotive and engineering applications	[217]
HDPE/LLDPE/(HDPE-*g*-MA or LLDPE-*g*-MA) (72/25)	Cloisite®20A	Maleic anhydride grafted polyethylene facilitates both, the exfoliation and/or intercalation of the clays and its adhesion to HDPE/LLDPE blend	[218]
Epoxy resin/CTBN	Nanomer I.28E	The CTBN interpenetrates into the clay galleries leading to a domain size reduction of phase separated CTBN	[219]
PLA/PHBV '85/15 and 70/30)	Cloisite®30B	The melt viscosity and elasticity of the PLA/PHBV/clay nanocomposites were significantly enhanced which was helpful for improving the foamed structure of microcellular injection molded components	[220]

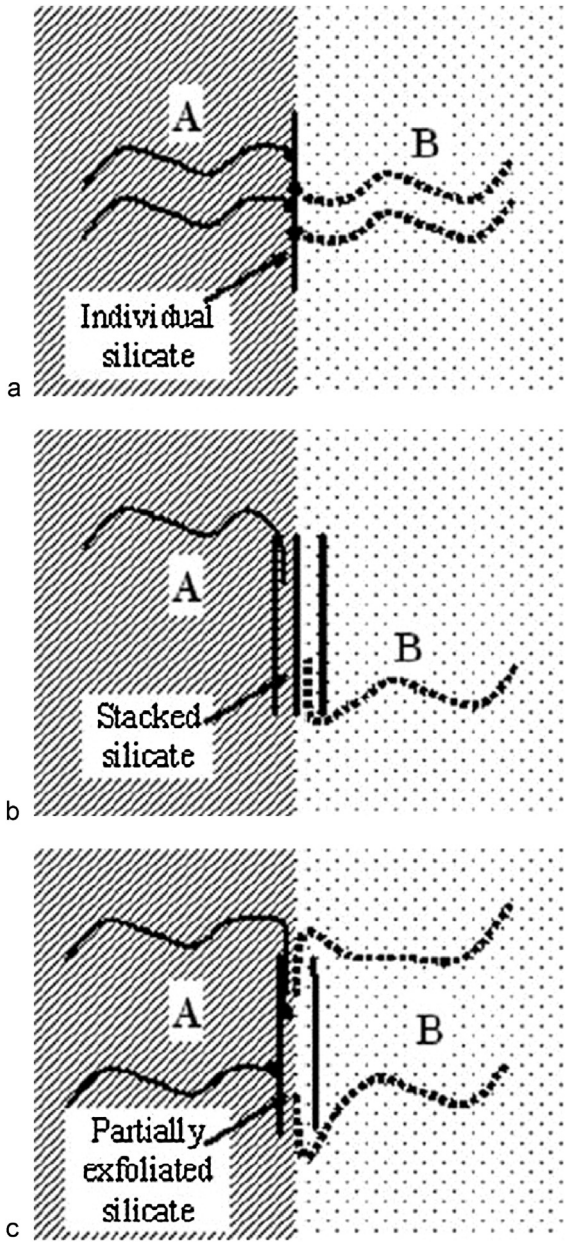

Fig. 18. Schematic representation of the compatibilization of two immiscible polymers by layered silicates: (a) both polymers A and B have strong interaction with silicate, (b) neither polymer A nor polymer B have interaction with silicates surface, and (c) polymer A has strong interaction with silicates while polymer B has no.
[170], Copyright 2007. Reproduced with permission from John Wiley and Sons.

particle/polymer systems. And it is well-known that polymer chains are depleted at the surface of a solid because the number of possible conformations is decreased (decreasing the configurational entropy). The particle size influences the dispersion/aggregation phenomenon and in systems where only entropic forces are considered, if $R_p/R_g < 1$, particles disperse uniformly; whereas if $R_p/R_g > 1$, particles aggregate [221]. Concerning spherical nanoparticles in polymer blends, as mentioned previously and

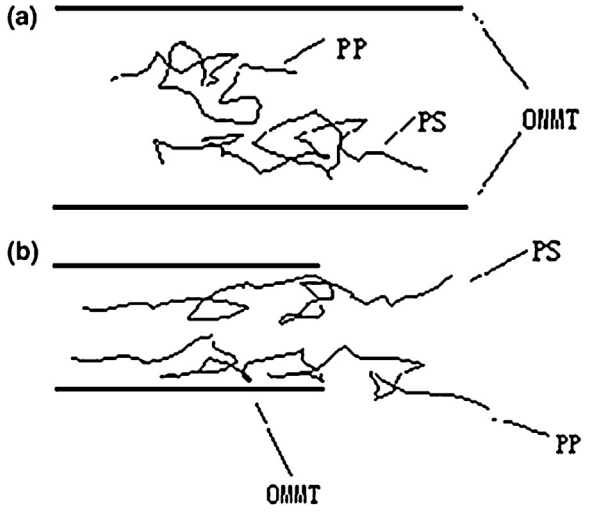

Fig. 19. Schematic representation of the structure in PP/PS/OMMT blend where parts of the PP and PS molecules located outside the gallery serving as a compatibilizer.
[192], Copyright 2003. Reproduced with permission from John Wiley and Sons.

demonstrated by Ginzburg, the size of the particle has an influence on the phase behavior of a blend. Hence, depending on the size (R_p) of the particle compared to the gyration radius (R_g) of macromolecules, particle can either play the role of a compatibilizer or not (cf. Section 2.2 and Fig. 3). Fenouillot et al. [41] summarized the influence of the R_p/R_g ratio on the compatibilizing effect as follows:

- If $R_p/R_g < 1$, then the addition of the nanoparticle reduces the enthalpy of the system because it decreases the polymer/polymer interaction. Then the system is stabilized.
- If $R_p/R_g > 1$, the particle-rich phase segregates from the blend even at low concentration.

Many authors proved this compatibilizing effect by the identification of the shift of the phase separation temperature in the presence of nanoparticles with a size (R_p) comparable to the radius of gyration (R_g) of the polymer matrix [38,222,223].

There are few articles dealing with the influence of the size of tactoids on the compatibilizing effect. Yurekli et al. [36] work on the influence of the lateral dimensions of three organically modified layered silicates on the phase separation of polystyrene/poly(vinyl methyl ether) blend in solution. They revealed that the presence of short lateral platelets (30 nm and 0.5–1.0 μm) slowed the phase separation kinetics, whereas at 5 μm lateral size, clay had no noticeable effect.

5.3.4. Influence of surface chemistries

The chemistry of the filler can affect its dispersion in the polymer blend system. Hence, different dispersion would lead to different final properties. Moreover, the chemistry of organically modified clays can change mechanical properties (stiffness) either in polymer blends with different polarities [178] or when dispersed in the same polymer. For example, Borah et al. [79] incorporated

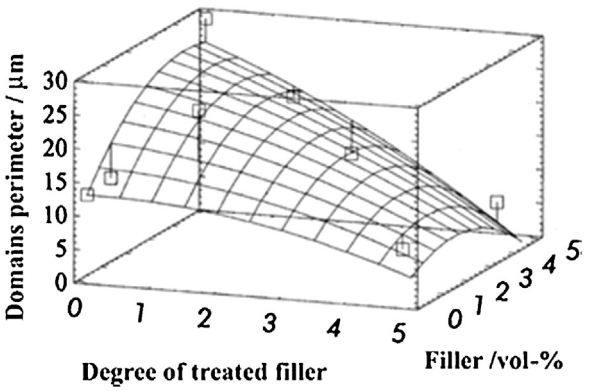

Fig. 20. Size of the EPDM domains (dispersed in a 90SAN/10EPDM) with various degrees of treated $CaCO_3$ (0–5 assigned to 0–100% stearate coverage, respectively) and with different volume fraction of added $CaCO_3$ in the blend.
[146], Copyright 2002. Reproduced with permission from John Wiley and Sons.

two different organically modified MMT (Cloisite®30B and Cloisite®20A) in LLDPE/EMA (60/40) polymer blends. The Cloisite®30B is modified with a polar methyl, tallow, bis-2-hydroxyethyl quaternary ammonium chloride, whereas the Cloisite®20A is modified by an apolar dimethyl dehydrogenated tallow quaternary ammonium chloride. Hence the affinity of each O-MMT with LLDPE or EMA is not the same. They demonstrated by performing dynamic mechanical analysis on their systems that a better affinity of Cloisite®20A with LLDPE matrix lead to a better dispersion and hence to a higher storage modulus. In the case of Kelarakis et al. [178], they also proved that the degree of chemical affinity between binary polymer matrices and embedded nanoparticles has an effect on macroscopic properties. They dispersed either 5% of an hydrophobic MMT (I.30T) or an hydrophilic MMT (Cloisite®30B) in 70PVDF/30EVA blends with two different amounts of vinyl acetate (VAc) (15 and 32 wt%). They observed good correlation between rheological (viscosity), mechanical (tensile) and microscopic (SEM) results. Hydrophilic MMT (Cloisite®30B) tends to reduce the size of EVAc32 minor phase, increase the storage modulus and improve the elongation at break of the PVDF/EVAc32 blend; whereas, the hydrophobic MMT (I.30T) has the same effect on the less polar EVAc15 group content system. On the contrary, Paul et al. [198] obtained slight differences in EOR dispersed phase size and shape when varying the structure of the quaternary ammonium salt of the organoclay in a MMT-filled amorphous PA/EOR blend. Hence the mechanical properties were not significantly affected.

It was shown that the surface coverage of nanoparticles by apolar molecules (and also the polarity) has an influence on the size of the dispersed phase in a polymer matrix and on the final mechanical properties. Hrnjak-Murgić et al. [146] incorporated stearate-modified nano-calcium carbonate (precipitated $CaCO_3$) in 90/10 SAN/EPDM. They first studied both the influence of stearate coverage (0, 16, 47, 78 and 100%) and $CaCO_3$ content (0–5 vol%) on the EPDM phase size (Fig. 20). The smallest EPDM dispersed phase size was obtained for 5 vol% of fully stearate covered $CaCO_3$ particles. The mechanical performances of the filled blends were consistent with their morphology; *i.e.* the most satisfied mechanical properties were obtained for the smallest EPDM phase size composite. This is probably due to a better adhesion at the interface with fully modified nanoparticles. However, Tong et al. [224] from studies on the morphology of PDMS/PIB blends filled with hydrophobic and hydrophilic silica showed that the discrepancy in the morphology evolution of the blend upon the addition of silica nanoparticles is controlled not only by the surface chemistry of particles but also by their concentration in the blends.

Recently, MWCNTs were functionalized by ATRP with random copolymers of methyl methacrylate and styrene (P(MMA-*co*-S) copolymers) having different molecular weights. There is an influence of the molecular weight of grafted copolymers on the localization of the nanotubes in a SAN/PPE blends [68]. Low molecular weight P(MMA-co-S) grafted CNTs are localized at the interface whereas, by increasing the molecular weight, more MWCNTs are confined in the PPE phase. The surface chemistry of nanoparticles also has an effect on the phase diagram of polymer blends. Karim et al. [225] showed that the addition of untreated fumed silica destabilized the upper critical solution phase boundary of PS/PB polymer blend. Whereas surface modified fumed silica stabilizes the system. Moreover, the molecular mass of a polymer coated or grafted on CNTs has a dramatic influence on the migration behavior of the nanotubes [226]. PMMA-coated and PMMA-grafted CNTs do not migrate necessarily into the same phase of a polymer blend when PMMA molecular weights are low. Indeed, the grafted CNTs are guided by thermodynamic reasons, whereas coated CNTs (with a low molecular weigt PMMA) behave like pristine CNTs.

Graphene oxide (GO) with a single atomic layer thickness can be viewed as an amphiphilic molecule or a colloidal surfactant, which can be stabilized at air–water, liquid–liquid or solid–liquid interfaces. Very recently, a few authors demonstrated the compatibilizing effect of a GO in PMMA/PS or PA/PPO or PA6/PVDF blends [227–229]. Moreover, Ye et al. [229] demonstrated that this effect was affected by the processing temperature. Its efficiency decreases when temperature increases because of a thermal chemical reduction leading to an increase in hydrophobicity of GO.

As demonstrated, the compatibilizing effect of nanoparticles is mostly influenced by their localization in the polymer blend and hence by their surface chemistry. In all examples from the literature cited up to now, the localization of nanoparticles at the interface is not really accurate and the size and surface chemistry are not well-controlled parameters. This is only very recently, that authors started to develop new nanoparticles with highly controlled surface properties and structure and to control their localization and dispersion in polymer blends. It must be noted that many authors studied the control of nanoparticle dispersion in block copolymer leading to various morphologies [230–235] but not in blends of homopolymers, that are most commonly used in industrial applications. In 2008, Walther [236] was the first to study the effect of the incorporation of Janus nanoparticles on

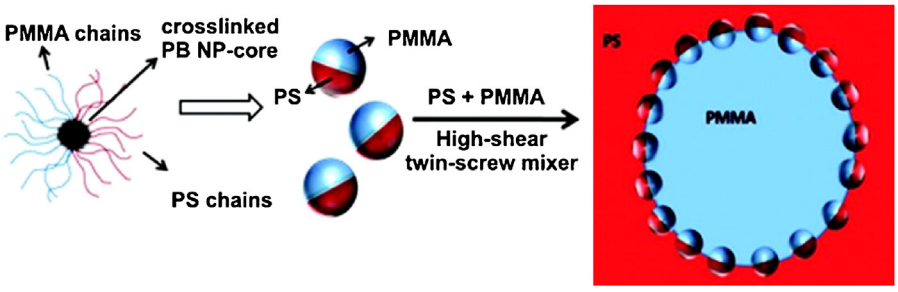

Fig. 21. Schematic representation of Janus NPs and their adsorption at the blend interface of a PS/PMMA blend. [236], Copyright 2008. Reproduced with permission from the American Chemical Society.

the morphology of a PS/PMMA blends (at compositions of 60/40 and 80/20). The whole-organic Janus NPs were composed of a crosslinked polybutadiene core grafted with two PS and PMMA half-sphere (Fig. 21).

An energy balance calculation based on the desorption energy of the particle from the interface permitted to conclude that the biphasic nature of the Janus NPs is the reason for a complete adsorption and a firm attachment at the interface of the PS/PMMA system. They observed a dramatic decrease of the droplet domain diameter (D_n) when adding 1–20 wt% of Janus NPs (Fig. 22). For 20 wt% of Janus NPs in 60/40 and 80/20 PS/PMMA, they measured very interesting PMMA dispersed phase size with D_n = 140 and 80 nm, respectively. TEM images showed fully covered PMMA droplets with Janus NPs (for 10 and 6 wt% of NPs in 60/40 blends) and a NPs center-to-NPs center distance of 30–35 nm. They compared the compatibilizing effect (D_n) of the Janus NPs with that of a SBM triblock copolymer (PS-*b*-PB-*b*-PMMA) both with the same R_g, and concluded on a tremendous superior stabilization effect of the Janus NPs compared to the triblock (Fig. 23). Moreover, as the D_n *versus* compatibilizer content levels off for the block copolymer, it continues to decrease with the percentage of Janus NPs. Indeed, the adsorption of biphasic particles at the interface of the blend pursues even at high loading rate.

Kwon et al. [237] coated gold-NPs (Au NPs) of two different sizes (5.9 and 20.7 nm) with PS-*b*-PSN_3 (polystyrene-*block*-poly(4-azidostyrene)) block copolymers and compared their compatibilizing effect on PS/PTPA (polytriphenylamine) polymer blends with that of PS-*b*-PTPA block copolymer. Fig. 24 reproduces the schematic representation of the three systems. They incorporated from 0.1 to 1.0 vol% and 0.1 to 5.0 vol% of Au NP-1 and Au NP-2, respectively in a 80PS/20PTPA blend and measured the number average diameter (D_n) of PTPA droplets. All Au NPs were segregated along the PS/PTPA interface, leading to a compatibilizing effect and D_n decreases and levels off when the volume fraction of Au NP-1 or Au NP-2 increase, as expected. Contrary to Walther, here, the leveling off of D_n *versus* volume fraction of Au NPs was observed from 1 and around 3 vol% of Au NP-1 and -2, respectively (Fig. 25a). This corresponds to the saturation of the interface [238]. In Fig. 25a, the D_n evolution is compared with that of PS/PTPA/PS-*b*-PTPA system. It is evident that Au NP-1 is the most efficient compatibilizing agent. In Fig. 25b,

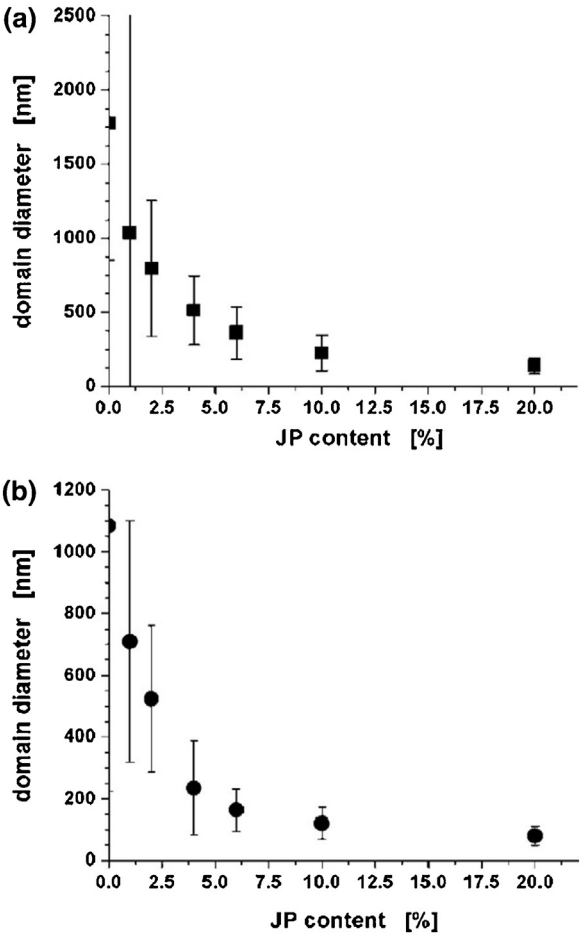

Fig. 22. Number average diameter of the PMMA droplets *versus* the content of Janus NPs at PS/PMMA ratios of 60/40 (a) and 80/20 (b). [236], Copyright 2008. Reproduced with permission from the American Chemical Society.

the interfacial area coverage (Ac) is plotted *versus* vol% of compatibilizer. The hypothesis and details for the estimation of Ac are given in the corresponding article. This plot permits to evaluate the volume fraction of compatibilizer (Au NPs or block copolymer) needed to fully cover the PS/PTPA interface. The values are given in Fig. 25b: ϕ_p = 0.98, 3.38 and 3.90 vol% for Au NP-1, Au NP-2 and

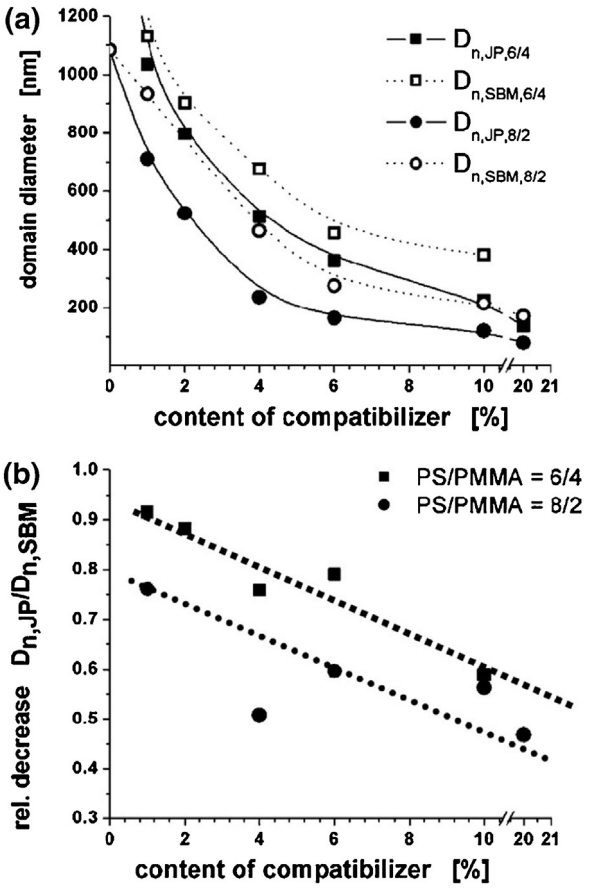

Fig. 23. (a) Number average diameter of PMMA droplets as a function of the content of compatibilizer (being Janus NPs or SBM triblock copolymer) for 60/40 and 80/20 PS/PMMA blends. (b) $D_{n,JP}/D_{n,SBM}$ ratio as a function of the content of compatibilizer for 60/40 and 80/20 PS/PMMA blends. [236], Copyright 2008. Reproduced with permission from the American Chemical Society.

PS-*b*-PTPA copolymer, respectively. At higher amounts of Au NP-1 (>1), nanoparticles continue to accumulate at the interface but forming multilayers as proved by TEM. In the case of larger Au NP-2, they segregate at the interface as a monolayer even at 5 vol%. The authors wisely pointed out the great advantage of Au-functionalized nanoparticles regarding to block copolymers as compatibilizing agent as Au NPs exhibit quasi-irreversible adsorption to the interface, whereas block copolymers would forms micelles and/or free chains.

Very recently, Huang et al. [34] modified silica NPs with polystyrene *via* surface-initiated atom transfer radical polymerization and incorporated them into a PMMA/SAN blend. They clearly identified that SiO_2 grafted with low molecular weight PS macromolecules ($M \leq 2000$ g/mol) migrated at the interface of the PMMA/SAN blend, whereas hydrophilic SiO_2 (SiO_2–OH) and SiO_2 modified with high molecular weight PS chains ($M = 46{,}000$ g/mol) migrated to the PMMA phase due to a lower interfacial tension. This selective localization of modified silica NPs has an effect on the phase separation of the blend. In the same manner, Chung et al. [35] incorporated chloride terminated PMMA brushes modified silica NPs in deuterated poly (methyl methacrylate)/poly(styrene-*ran*-acrylonitrile) 50/50 blend. They demonstrated that, as the brush length was low (1800 g/mol) the NPs segregated to the dPMMA/SAN interface. Whereas when the brush length increased (from 21,000 to 160,000 g/mol), the NPs migrated from the interface to the dPMMA phase. Contact angles measurements showed that the material became more hydrophilic as the PMMA brush length increased.

To our knowledge, there are only two articles dealing [236,237] with the effect of the incorporation of bi-functionalized nanoparticles on the nanostructuration of a polymer blend system. Nevertheless, there is nothing on blending conditions optimization and evaluation of the final performances.

6. Properties and applications

There is a huge literature dealing with general concerns on the influence of the nanoparticles localization on the properties of immiscible polymer blends [74,203,209,210]. Actually, the influence of fillers on blend morphologies and properties has been already reported far before the nanocomposites based on organoclay. In 1992, Maiti et al. [239] studied the distribution of carbon black and silica in nitrile rubber/epoxidized natural rubber (ENR) blends. The interest for the obtaining of specific morphologies is often guided by the motivation to obtain specific properties. The aim of this part is to explain how the particular morphology obtained for ternary systems can impact properties.

6.1. Mechanical properties

Elastomeric components are often added to rigid polymers to improve the impact strength or toughness of the final system. Mineral fillers can also be incorporated to those binary systems and their localization will have an influence on the mechanical properties. This was demonstrated by Dasari et al. [86] who incorporated organoclay in PA66/SEBS-*g*-MA blends and showed that the highest impact strength was obtained when the maximum percentage of exfoliated Cloisite®30B was in the PA66 matrix rather than in the SEBS-*g*-MA dispersed phase. Indeed, Cloisite dispersed in the SEBS-*g*-MA phase reduced the cavitation ability of the elastomeric particles, reducing the toughening efficiency [166]. More recently, Borah et al. [79] added different organically modified Cloisite (Cloisite®20A and 30B) into LLDPE/EMA blends; when Cloisite is located in the dispersed EMA phase, the impact strength is high and the tension set is low, whereas Cloisite located at the interface lead to low impact strength.

The incorporation of fillers such as clay platelets can also affect both the size and structure of the dispersed elastomeric phase leading to the modification of the properties. When clay is suitably organically modified in order to localize at the interface of a PA6/EPR blend, a "core-shell" structure of the elastomeric particle is obtained leading to toughness enhancement [240]. This effect -leading to favorable size and structure of the dispersed EPR phase- combined with high PA6 matrix reinforcement obtained by adding exfoliated clay platelets in the matrix can give

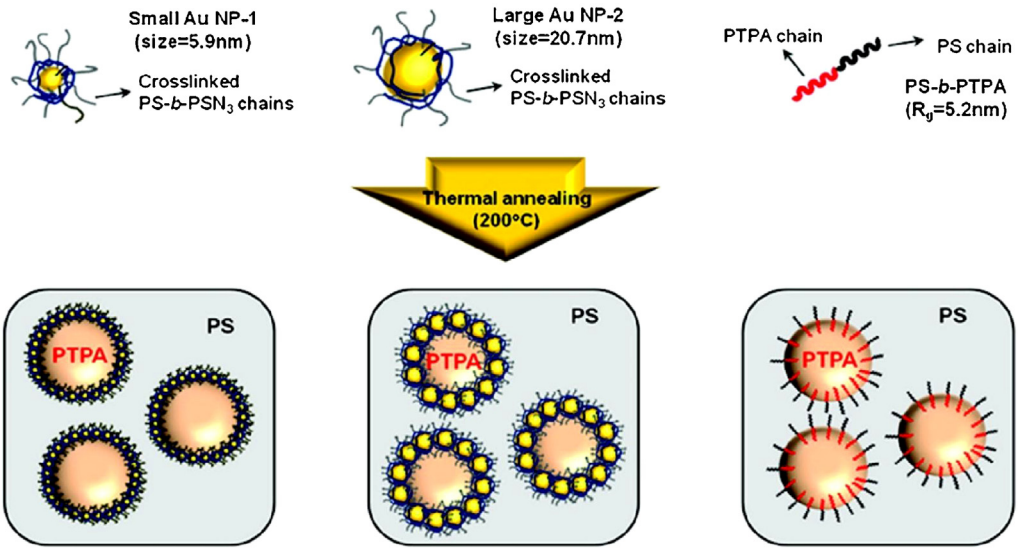

Fig. 24. Schematic representation of small (5.9 nm) Au NP-1, large (20.7 nm) Au NP-2 and PS-*b*-PTPA compatibilizer in PTPA/PS blend. [237], Copyright 2011. Reproduced with permission from the American Chemical Society.

the best balance mechanical behavior [179]. The major toughening mechanisms in elastomer reinforced polymer matrix are rubber particle cavitation, crazing and shear yielding. PP/SBS/clay systems (in which all clay platelets are coated by SBS rubber) exhibit higher crack initiation and propagation resistance than PP/SBS blend (measured by *J*-integral tests) [181]. While no crazing is found for these two systems, rubber cavitation occurs that promotes shear yielding in the PP matrix. Moreover the shear plastic deformation zone is more intense in the case of PP/SBS/clay system.

It was demonstrated by Wu [241,242] that the interparticle distance between the elastomeric dispersed droplets as a dramatic influence on mechanical properties. There is a critical interparticle distance (τ_c) below which the behavior of the material becomes ductile. As shown by Wang et al. [194], the interparticle distance of a PA6/EPDM-*g*-MA filled with O-MMT has a dramatic influence on impact strength (Fig. 26). The brittle-ductile transition – identifying the critical interparticle distance, τ_c – is clearly visible. The lowest value of impact strength (when $\tau < \tau_c$) obtained for the 4 wt% MMT filled blend is explained by the fact that at this relatively high amount of clay, the formation of the clay network will block the overlap of the stress volume between elastomeric particles in a large extent (contrarily to the 1 wt% MMT where this blocking effect is weak). Hence, by adding clay platelets, the elastomer particle size and the interparticle distance can be varied and optimized to obtain a super-toughened nanocomposite [105,243,244]. Paul et al. [199] obtained

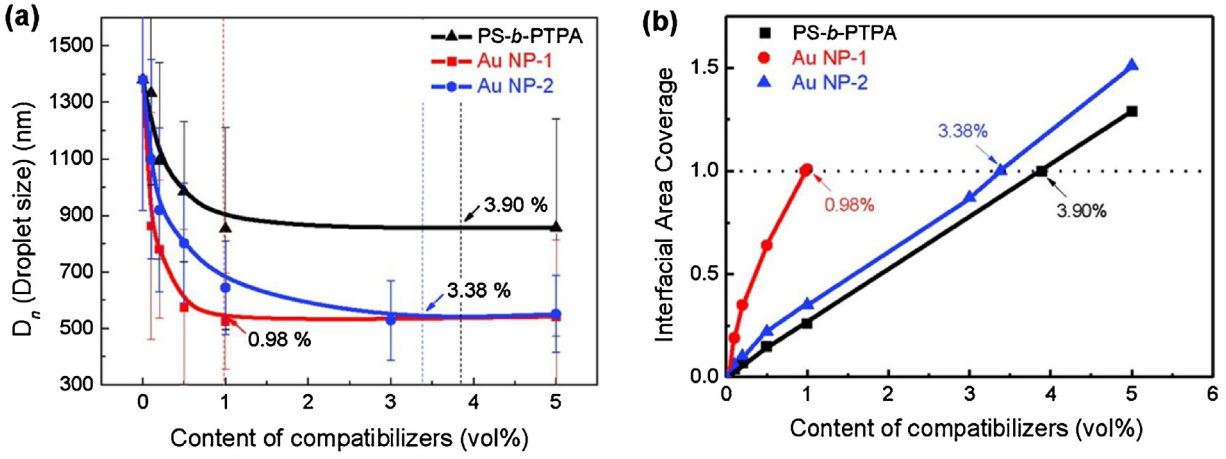

Fig. 25. (a) Evolution of the number average diameter of the PTPA droplets *versus* the volume content of compatibilizers. (b) Interfacial area coverage (Ac) by the compatibilizer at the PS/PTPA interface *versus* vol% of compatibilizer. The compatibilizers are PS-*b*-PTPA block copolymer in black, Au NP-1 in red and AU NP-2 in blue. (For interpretation of the references to color in this figure legend, the reader is referred to the web version of the article.) [237], Copyright 2011. Reproduced with permission from the American Chemical Society.

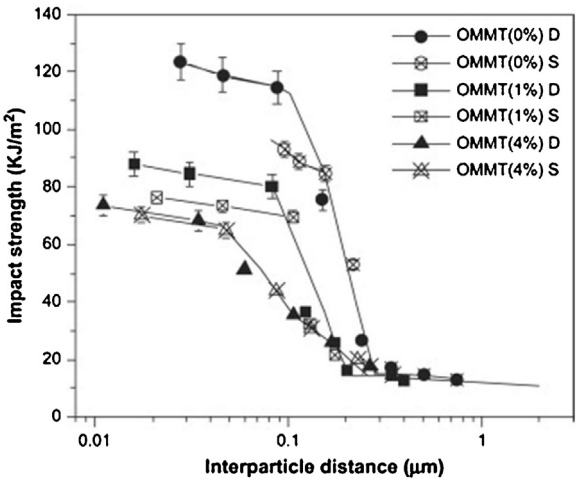

Fig. 26. Impact strength as a function of interparticle distance for PA6/EPDM-*g*-MA blends filled with 1 and 4 wt% of organoclay. D and S represent dynamic (specimen were obtained by a unique processing method, called dynamic packing injection molding (DPIM)) and static (specimens are obtained by a traditional injection molding) specimens, respectively. [194], Copyright 2007. Reproduced with permission from Elsevier Ltd.

a better balance of toughness *versus* stiffness for amorphous PA/ethylene-1-octene-*g*-MA blend filled with clay than for the corresponding unmaleated elastomer based system.

Yang et al. [245,246] performed almost the same study on PP/EPDM/SiO_2 nanocomposites. They varied the amount of elastomeric compound (10–30 wt%) and of the silica (1–5 wt%) and showed that PP/EPDM/SiO_2 systems exhibit the formation of a filler network structure that lead to a super toughened ternary composite with Izod impact strength 2–3 times higher than PP/EPDM binary blend. The temporary accumulation of SiO_2 NPs around EPDM particles increases the effective volume of rubber particles, thus decreasing the interparticle distance τ. Finally, a percolated network is formed at relatively low amounts of EPDM (20%) and silica. By comparing Wang and Yang results [194,245] concerning O-MMT and SiO_2, respectively, we plotted figures gathered all values (Fig. 27). Concerning Fig. 27 (up), the addition of MMT to PA6/EPDM firstly dramatically increases the EPDM percentage at which the brittle to ductile transition occurs (as explained above); secondly decreases the impact strength. On the contrary, for PP/EPDM/SiO_2 systems, the influence is less pronounced and the addition of SiO_2 decreases the EPDM percentage for which a brittle-ductile transition is observed and increases the impact strength. These tendencies to decrease or increase the impact strength when adding MMT and SiO_2, respectively, are shown in Fig. 27 (down).

Lately, Bitinis et al. [247] showed that the addition of natural rubber and clays to a PLA matrix allowed a straightforward production of toughened nanocomposites with tunable properties by melt blending. These results proved that both C15A and C30B organoclays act as compatibilizers for the PLA/NR blend because of their preferential location at the polymer interface, acting as a solid barrier and preventing the coalescence of NR droplets. Furthermore, different properties were obtained depending on

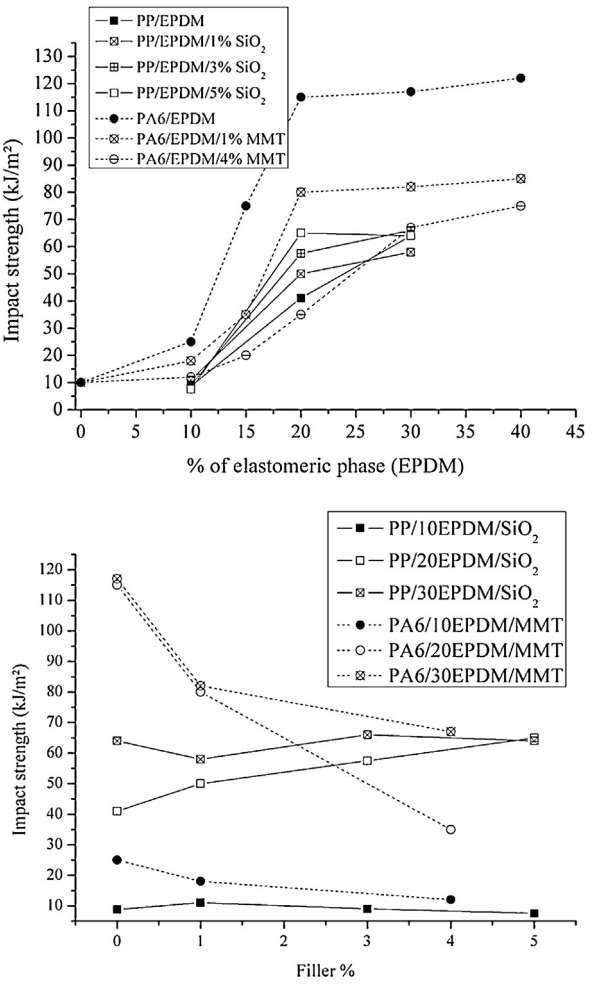

Fig. 27. Impact strength *versus* percentage of EPDM (up) and filler (down) for PA6/EPDM/MMT [245] and PP/EPDM/SiO_2 [194].

the used nanoclays. While C15A allowed a further increase of the elongation at break of the PLA/NR blend, the addition of C30B produced stiffer materials. This behavior was attributed to the different interactions of the nanoclays with the two polymers.

Carbon nanotubes are known to act as toughened agent in polymer blends [150,248]. More recently, interfacial adhesion was shown to be improved by adding carboxyl and hydroxyl functionalized multiwalled carbon nanotubes (FMWCNT) in HDPE (and HDPE-*g*-MA)/PA6 blends [72]. Peel adhesion strength was measured by peel adhesion tests and the effect of selectively distributed FMWCNTs at the interface on the initiation and propagation of crack are illustrated in Fig. 28. It was suggested that the presence of HDPE-*g*-MA prevented and/or delayed the migration of FMWCNTs, leading to more FMWCNTs at the interface of the immiscible blend during the processing.

6.2. Conductive and magnetic properties

There are different ways to render a polymer conductive and one of the most classical one is the addition of

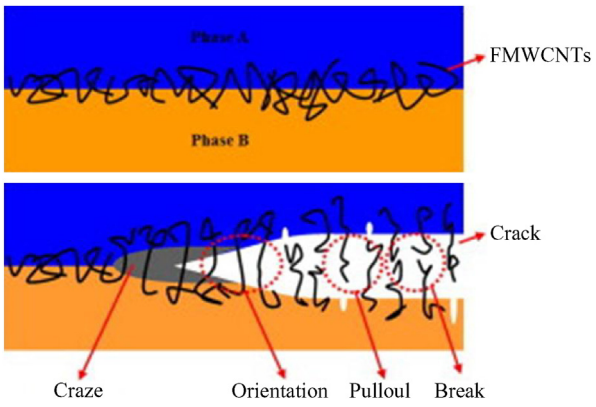

Fig. 28. Schematic representation of the selective distribution of FMWCNTs at the interface between phases A and B (a) and the crack propagation along the interface plane (b).
[72], Copyright 2013. Reproduced with permission from Elsevier Ltd.

conductive fillers in a polymer system. Carbon blacks are often added to reach a percolation threshold and make the polymer conductive [249]. The volume fraction of CB added to achieve percolation depends on CB structure, dispersion state and thermodynamic interactions between CB and the matrix, but also on the viscosity of the polymer matrix [250]. The selective distribution of CB into one continuous phase of a multiphase polymer material can produce conducting material at a lower filler content [148]. Another way to minimize the CB content to obtain percolation is to localize preferentially CB at the interface of a co-continuous multiphase material [40]. Gubbels et al. [89,99,251] reported a dramatic decreased in percolation threshold with a PE/PS/CB system. They varied the sequence of mixing during the process to pass the conductive CB particles from the less thermodynamically favorable phase to the more favorable and quenched the morphology at a non-equilibrium state. An extremely small percolation threshold was achieved when CB selectively localized at the interface of a co-continuous PE/PS blend. This is called double conductive percolation system [90]. As explained previously in the present article, the selective dispersion of CB at the interface is guided by three different factors: thermodynamics (lowest interfacial energy) [252], kinetics (sequence of mixing) [89] and polymer viscosity [252]. Percolation threshold can then decrease to a 2 wt% of CB for a 45:55 PE/PS blend [99]. After annealing (260 °C, 40 min), percolation could be observed at a concentration as low as 0.4 wt% CB.

More recently, research teams are interested in conductive thermoplastic polymer blends with carbon nanotubes (CNTs) [55,93,129,130]. For example, Zonder et al. [253] linked the rheological behavior (G'_r) of a polyamide 12/high density polyethylene/carbon nanotubes (PA12/HDPE/CNT) system with its electrical resistivity (ρ). By premixing CNT in the PE phase, the highest reinforcement effect is achieved together with the lowest resistivity for the different CNT contents (0.5, 1.75 and 2 wt%). For these samples, CNT are located at the interface.

Hwang et al. [254] confirmed this result with a PP/PS/MWCNT system.

Concerning magnetic materials, a new way to obtain composite magnetic microspheres is to melt-mix magnetic nanoparticles with a binary polymer blend and then selectively extract the dispersed polymer domains in which the magnetic particles are preferentially localized. To obtained PA6/Fe_3O_4 microspheres with regular shape and size, Wu et al. [255] incorporated magnetic Fe_3O_4 nanoparticles in FPS/PA6 blends where FPS stands for polystyrene with terminal maleic anhydride groups on the PS chain. FPS plays the role of a compatibilizer, reducing the PA6 droplet size in the blend (as explained previously) before extraction. Moreover, to remain a maximum Fe_3O_4 NPs in the PA6 phase, they were added after the complete reaction of the anhydride of FPS with the terminal amine of PA6 chains.

6.3. Thermal and fire behavior

This is well known that the addition of organo-modified MMT in polymer can prevent heat transfer and improve thermal stability of the system thanks to their barrier effect. In polymer blends this effect was enhanced by replacing a polyolefin by its corresponding maleic anhydride grafted polymer. The use of a more polar polymer improved the intercalated structure and hence provided a higher barrier effect [162]. Layered silicates also reduce the flammability of the polymer based nanocomposite [256]. This was also explained by the barrier effect, that reduced the diffusion of volatile products of thermo-oxidation to the gas phase, and oxygen from the gas phase to the polymer [257]. The three different formulations of Tang et al. [189] (comprising the same amounts of PA6, PP, PP-*g*-MA and O-MMT but different preparations) exhibited different cone calorimeter curves. In formulations called PP5 and PP7, clay platelets intercalated into the *in situ* formed PP-*g*-MA-*co*-PA6 copolymer at the interface between PP matrix and PA6 dispersed phase, leading to the formation of a "ring". Moreover, they demonstrated that this "ring" could lead to lower pHRR (the maximum value of the heat release rate (HRR), expressed as function of time) when in addition to inward labyrinth effect on volatile emission, there may be an outward one. Hence, the localization of the platelets in a polymer blend system can change the fire behavior.

A fire retardant (FR) system can be added to a layered silicate filled polymer blend system. Up to now different synergistic systems were studied and are reported below. The preferred localization of FR close to the platelets permits the adsorption of FR onto the clay platelets. The high aspect ratio of the platelets operates as dispersants for the FR particles and brings a synergy that can lead to improved thermal and fire behavior [258]. Hence the blend containing PS, PMMA, decabromodiphenylether (DB), antimony trioxide (AO) and Cloisite®20A was able to pass the UL-94-V0 test [258].

Other FR such as ammonium polyphosphate (APP) was added to layered silicate filled polymer blends to improve fire behavior. APP/clay system can play the role of a flame retardant system, and the polymer forming the dispersed phase, the carbonization agent. And there is an influence

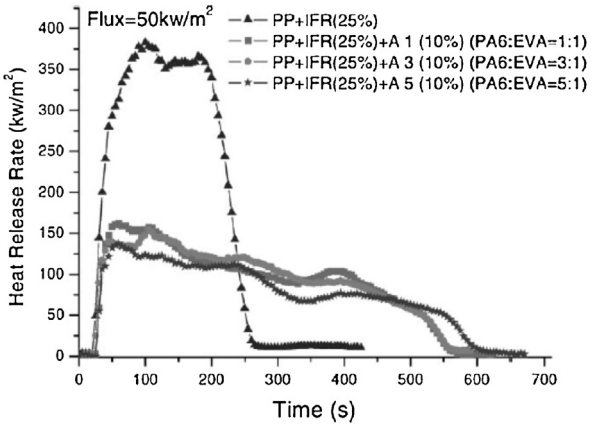

Fig. 29. Heat release rate *versus* time (obtained by cone calorimeter) for different formulations containing PP, intumescent flame retardant (IFR) and PA6/EVA alloys.
[261], Copyright 2005. Reproduced with permission from John Wiley and Sons.

of the preparation of the quaternary system on the fire properties. For example, Bourbigot et al. showed that the HRR profile of an EVA/APP/O-MMT/PA6 system depend on the localization on the clay platelets, either in EVA or in PA6 [259]. Previously, the same authors prepared intumescent systems based on PP/APP/PA6 with EVA and APP/EBuAMA (ethylene-butyl acrylate-maleic anhydride) as interfacial agents to improve the fire behavior of PP [260]. During the combustion, the formation of a carbonaceous shield slowed down the degradation of the formulations and enabled the formation of stable residue. The interfacial agent gave additional improvement, thanks to a synergistic effect at 5 wt% of EBuAMA and thanks to the carboxylic acid species formed in the case of EVA. The same type of intumescent behavior was obtained for PA6/EVA alloy clay nanocomposites based PP materials by Tang et al. [261]. The investigation of fire (Fig. 29) and mechanical properties of such fire retarded (FR) PP showed that the weight ratio of PA6 (in the PA6/EVA alloy) has to be between 2.5 and 8 in order that the FR PP has better fire and mechanical performances.

Metal hydroxides (aluminum trihydroxide, ATH and magnesium oxide, MH) were also incorporated by Bourbigot et al. [262] in the presence of nanoclay in LDPE/EVA polymer blends to increase the time to ignition (at cone calorimeter) especially for low irradiation, decrease the pHRR.

Very recently, the importance of the localization of a flame retardant (FR) system composed of organoclay and a nitroxyl ether compound (Flamestab-NOR 116) in a PET/PP blend was pointed out [263]. It was shown that the FR effect was enhanced in the case of PET-rich system (relative to PP-rich system). Indeed, as organoclays are localized in the PET phase or at the interface, when PET forms the matrix, a clay network structure is formed and a subsequent coat-like char layer is formed during degradation that can improve thermal stability and flame retardancy of the PET-rich blend.

7. Conclusions

Nanoparticles have great influence on mechanical, barrier, thermal, fire properties of polymers mainly because of their size. Indeed, the small dimensions of NPs generate high surface area and high interfacial area with the polymer chains and the configurational entropy of the polymer chains at the surface of NPs is greatly decreased. This loss of configurational entropy increases with the particle radius. The particle radius and all characteristics determining the nature of NPs (size, shape, surface chemistry) have a great influence on the behavior of ternary blends (two immiscible polymers and a filler), and especially on the capability for the NP to compatibilize the polymer blend. To compatibilize a polymer blends, NPs have to migrate to the interface between matrix and droplets. And to saturate the interface between matrix and droplets of an immiscible polymer blends, platelets are the best candidate. The aspect ratio is a key factor for the interfacial stability and the speed of nanofiller transfer through a blend interface during melt mixing. Moreover, to orientate the NPs at the interface the most efficient way is to design specific NPs with specific surface chemistry. And the literature is fairly poor on this subject, particularly by studying the influence of this particular structure (localization at the interface) on the viscoelastic and mechanical properties. Graphenes and halloysites seem to be promising fillers for polymeric based materials as they can exhibit anisotropic surface chemistry. Graphene can be oxidized leading to graphene oxide amphiphilic sheets and the amphiphilic structure of GO sheets can be used to compatibilize immiscible polymer blends. Moreover graphene and its derivatives can be used for barrier applications [264]. Halloysites have already been used in many areas such as biotechnology, pharmacy, medicine and energy. They are used as flame retardant, for corrosion protection, and to improve optical and electronic properties. Halloysites exhibit different inner and outer surface chemistries. They have recently been used as compatibilizers [265] but their anisotropic property can potentially be exploited for a wide variety of applications.

References

[1] Baer M, Hankey EH. Compatible belnds of rigid vinyl chloride and alpha-olefin polymers containing compatibilizing amounts of a halogenated polyolefin. US Pat 3085082. Monsanto Chemical Co.; 1963. 5 p.
[2] Baer M, Hankey EH. Vinyl chloride polymers containing elastomers and graft copolymer as compatibilizer. US Pat 3316327. Monsanto Co.; 1967. 4 p.
[3] Duck EW, Milner PW. Blends of polybutadiene with vinyl polymers. In: Proc Int Rubber Conf 5th. 1968. p. 359–76.
[4] Noland JS, Hsu NNC, Saxon R, Schmitt JM. Compatible high polymers. Poly(vinylidene fluoride) blends with homopolymers of methyl and ethyl methacrylate. Adv Chem Ser 1971;99:15–28.
[5] Kwei TK, Nishi T, Roberts RF. A study of compatible polymer mixtures. Macromolecules 1974;7:667–74.
[6] Yu AJ. Concept of compatibility in polyblends. Adv Chem 1971;99:2–14.
[7] Gaylord NG. Compatibilization concepts in polymer applications. Adv Chem 1975;142:76–84.
[8] Lipatov YS. Interphase phenomena in polymer blends. J Polym Sci Polym Symp 1977;61:369–88.
[9] Krause S. Polymer-polymer compatibility. In: Paul DR, Newman S, editors. Polymer blends, vol. 1. New York: Academic Press; 1978. p. 15–13.

[10] Paul DR. Interfacial agents ("compatibilizers") for polymer blends. In: Paul DR, Newman S, editors. Polymer blends, vol. 2. New York: Academic Press; 1978. p. 35–62.
[11] Koning C, van Duin M, Pagnouille C, Jerome R. Strategies for compatibilization polymer blends. Prog Polym Sci 1998;23:707–57.
[12] Brown SB. Reactive compatibilization of polymer blends. In: Utracki LA, editor. Polymer blends handbook, vol 1. Dordecht: Klumer Academic; 2002. p. 339–416.
[13] Sonnier R, Taguet A, Rouif S. Modification of polymer blends by E-beam and Gamma-irradiation. In: Mital V, editor. Functional polymer blends. Boca Raton: CRC Press; 2012. p. 261–304.
[14] Lipatov Y. Polymer blends and interpenetrating polymer networks at the interface with solids. Prog Polym Sci 2002;27:1721–801.
[15] Alexandre M, Dubois P. Polyler-layered silicate nanocomposites: preparation, properties and uses of new class of materials. Mater Sci Eng 2000;28:1–63.
[16] Giannelis EP, Krishnamoorti R, Manias E. Polymer–silicate nanocomposites: model systems for confined polymers and polymer brushes. Adv Polym 1999;138:107–47.
[17] Pavlidou S, Papaspyrides CD. A review on polymer-layered silicate nanocomposites. Prog Polym Sci 2008;33:1119–98.
[18] Sinha Ray S, Okamoto M. Polymer/layered silicate nanocomposites: a review from preparation to processing. Prog Polym Sci 2003;28:1539–641.
[19] Ginzburg VV. Nanoparticles/polymer blends: theory and modeling. In: Isayev AI, editor. Encyclopedia of polymer blends. Weinheim: Wiley-VCH; 2007. p. 233–67.
[20] Utracki LA. Compatibilization of polymer blends. Can J Chem Eng 2002;80:1008–16.
[21] Nesterov AE, Lipatov YS. Compatibilizing effect of a filler in binary polymer mixtures. Polymer 1999;40:1347–9.
[22] Gritsenko OJ, Nesterov AE. Segmental adsorption energy and phase behaviour of filled polymer blends. Eur Polym J 1991;27:455–9.
[23] Lipatov IS, Nesterov AE. Effect of filler concentration on the phase separation poly(methyl methacrylate) mixtures. Polym Eng Sci 1992;32:1261–3.
[24] Nesterov A. Effect of an interface with solid on the component distribution in separated phases of binary polymer mixtures. Eur Polym J 2001;37:281–5.
[25] Lipatov Y. Effect of polymer–filler surface interactions on the phase separation in polymer blends. Polymer 2002;43:875–80.
[26] Lipatov Y. Phase separation in filled polymer blends. J Macromol Sci Part B 2006;45:871–88.
[27] Ginzburg VV. Influence of nanoparticles on miscibility of polymer blends. A simple theory. Macromolecules 2005;38:2362–7.
[28] He G, Ginzburg VV, Balazs AC. Determining the phase behavior of nanoparticle-filled binary blends. J Polym Sci Part B: Polym Phys 2006;44:2389–403.
[29] Huang Y, Jiang S, Li G, Chen D. Effect of fillers on the phase stability of binary polymer blends: a dynamic shear rheology study. Acta Mater 2005;53:5117–24.
[30] Du M, Wu Q, Zuo M, Zheng Q. Filler effects on the phase separation behavior of poly (methyl methacrylate)/poly (styrene-co-acrylonitrile) binary polymer blends. Eur Polym J 2013;49:2721–9.
[31] Shumsky VF, Getmanchuk I, Ignatova T, Maslak Y, Cassagnau P, Boiteux G, Melis F. Effect of nanofillers on the phase separation and rheological properties of poly(methyl methacrylate)/poly(styrene-co-acrylonitrile) blends. Rheol Acta 2010;49:827–36.
[32] Gao J, Huang C, Wang N, Yu W, Zhou C. Phase separation of poly (methyl methacrylate)/poly (styrene-co-acrylonitrile) blends in the presence of silica nanoparticles. Polymer 2012;53:1772–82.
[33] Li W, l'Abee RMA, Goossens JGP. The control of silica nanoparticles on the phase separation of poly(methyl methacrylate)/poly(styrene-*co*-acrylonitrile) blends. Macromol Chem Phys 2013;214:2705–15.
[34] Huang C, Gao J, Yu W, Zhou C. Phase separation of poly(methyl methacrylate)/poly(styrene-co-acrylonitrile) blends with controlled distribution of silica nanoparticles. Macromolecules 2012;45:8420–9.
[35] Chung HJ, Kim J, Ohno K, Composto RJ. Controlling the location of nanoparticles in polymer blends by tuning the length and end group of polymer brushes. ACS Macro Lett 2012;1:252–6.
[36] Yurekli K, Karim A, Amis EJ, Krishnamoorti R. Influence of layered silicates on the phase-separated morphology of PS–PVME blends. Macromolecules 2003;36:7256–67.
[37] Yurekli K, Karim A, Amis EJ, Krishnamoorti R. Phase behavior of PS–PVME nanocomposites. Macromolecules 2004;37:507–15.
[38] Gharachorlou A, Goharpey F. Rheologically determined phase behavior of LCST blends in the presence of spherical nanoparticles. Macromolecules 2008;41:3276–83.
[39] Xia T, Huang Y, Peng X, Li G. Morphological transition induced by nanoparticles in dynamically asymmetric PS/PVME blends. Macromol Chem Phys 2010;211:2240–7.
[40] Sumita M, Sakata K, Asai S, Miyasaka K, Nakagawa H. Dispersion of fillers and the electrical conductivity of polymer blends filled with carbon black. Polym Test 1991;25:265–71.
[41] Fenouillot F, Cassagnau P, Majesté JC. Uneven distribution of nanoparticles in immiscible fluids: morphology development in polymer blends. Polymer 2009;50:1333–50.
[42] Wu S. Polymer interface and adhesion. New York/Basel: Marcel Dekker Inc.; 1982. p. 630pp.
[43] Wu S. Formation of dispersed phase in incompatible polymer interfacial and rheological effects. Polym Eng Sci 1987;27:335–43.
[44] Owens DK, Wendt RC. Estimation of the surface free energy of polymers. J Appl Polym Sci 1969;13:1741–7.
[45] Adamson AW, Gast AP. Physical chemistry of surfaces. New York: John Wiley & Sons; 1997, 808 p.
[46] Ross S, Morrison ID. Colloidal systems and interfaces. New York: John Wiley & Sons; 1988, 448 p.
[47] Kamal MR, Calderon JU, Lennox BR. Surface energy of modified nanoclays and its effect on polymer/clay nanocomposites. J Adhes Sci Technol 2009;23:663–88.
[48] Xing P, Bousmina M, Rodrigue D, Kamal MR. Critical experimental comparison between five techniques for the determination of interfacial tension in polymer blends: model system of polystyrene/polyamide-6. Macromolecules 2000;33:8020–34.
[49] Nuriel S, Liu L, Barber AH, Wagner HD. Direct measurement of multiwall nanotube surface tension. Chem Phys Lett 2005;404:263–6.
[50] Barber A, Cohen S, Wagner H. Static and dynamic wetting measurements of single carbon nanotubes. Phys Rev Lett 2004;92,186103/1-4.
[51] Nakae H, Inui R, Hirata Y, Saito H. Effects of surface roundness on wettability. Acta Mater 1998;46:2313–8.
[52] Ponsonnet L, Reybier K, Jaffrezic N, Comte V, Lagneau C, Lissac M, Martelet C. Relationship between surface properties (roughness, wettability) of titanium and titanium alloys and cell behaviour. Mater Sci Eng C 2003;23:551–60.
[53] Zhang X, Yu S, He Z, Miao Y. Wetting of rough surfaces. Surf Rev Lett 2004;11:7–13.
[54] Elias L, Fenouillot F, Majeste JC, Cassagnau P. Morphology and rheology of immiscible polymer blends filled with silica nanoparticles. Polymer 2007;48:6029–40.
[55] Cardinaud R, McNally T. Localization of MWCNTs in PET/LDPE blends. Eur Polym J 2013;49:1287–97.
[56] Göldel A, Kasaliwal GR, Pötschke P, Heinrich G. The kinetics of CNT transfer between immiscible blend phases during melt mixing. Polymer 2012;53:411–21.
[57] Wu S. Surface and interfacial tensions of polymers, oligomers, plasticizers, and organic pigments. In: Brandrup JIE, Grulke EA, Abe A, Bloch DR, editors. Polymer handbook, Part VI. New York: Wiley-Interscience/John Wiley & Sons; 1999. p. VI-521–569.
[58] Dharaiya DP, Jana SC. Nanoclay-induced morphology development in chaotic mixing of immiscible polymers. J Polym Sci Part B: Polym Phys 2005;43:3638–51.
[59] As'habi L, Jafari SH, Baghaei B, Khonakdar HA, Pötschke P, Böhme F. Structural analysis of multicomponent nanoclay-containing polymer blends through simple model systems. Polymer 2008;49:2119–26.
[60] Pour SAH, Pourabbas B, Salami Hosseini M. Electrical and rheological properties of PMMA/LDPE blends filled with carbon black. Mater Chem Phys 2013;143:830–7.
[61] Li P, Huang Y, Kong M, Lv Y, Luo Y, Yang Q, Li G. Fractionated crystallization and morphology of PP/PS blends in the presence of silica nanoparticles with different surface chemistries. Colloid Polym Sci 2013;291:1693–704.
[62] Li W, Karger-Kocsis J, Schlarb AK. Dispersion of TiO_2 particles in PET/PP/TiO_2 and PET/PP/PP-g-MA/TiO_2 composites prepared with different blending procedures. Macromol Mater Eng 2009;294:582–9.
[63] Baudouin A-C, Devaux J, Bailly C. Localization of carbon nanotubes at the interface in blends of polyamide and ethylene–acrylate copolymer. Polymer 2010;51:1341–54.
[64] Baudouin A-C, Bailly C, Devaux J. Interface localization of carbon nanotubes in blends of two copolymers. Polym Deg Stab 2010;95:389–98.

[65] Elias L, Fenouillot F, Majesté JC, Martin G, Cassagnau P. Migration of nanosilica particles in polymer blends. J Polym Sci Part B: Polym Phys 2008;46:1976–83.
[66] Katada A, Buys YF, Tominaga Y, Asai S, Sumita M. Relationship between electrical resistivity and particle dispersion state for carbon black filled poly (ethylene-*co*-vinyl acetate)/poly (L-lactic acid) blend. Colloid Polym Sci 2005;284:134–41.
[67] Kooshki RM, Ghasemi I, Karrabi M, Azizi H. Nanocomposites based on polycarbonate/poly (butylene terephthalate) blends effects of distribution and type of nanoclay on morphological behavior. J Vinyl Addit Techol 2013;19:203–12.
[68] Du B, Handge Ua, Wambach M, Abetz C, Rangou S, Abetz V. Functionalization of MWCNT with P(MMA-*co*-S) copolymers via ATRP: influence on localization of MWCNT in SAN/PPE 40/60 blends and on rheological and dielectric properties of the composites. Polymer 2013;54:6165–76.
[69] Wu D, Lin D, Zhang J, Zhou W, Zhang M, Zhang Y, Wang D, Lin B. Selective localization of nanofillers: effect on morphology and crystallization of PLA/PCL blends. Macromol Chem Phys 2011;212:613–26.
[70] Taghizadeh A, Favis BD. Carbon nanotubes in blends of polycaprolactone/thermoplastic starch. Carbohydr Polym 2013;98:189–98.
[71] Dharaiya D, Jana SC. Thermal decomposition of alkyl ammonium ions and its effects on surface polarity of organically treated nanoclay. Polymer 2005;46:10139–47.
[72] Chen J, Shi YY, Yang JH, Zhang N, Huang T, Wang Y. Improving interfacial adhesion between immiscible polymers by carbon nanotubes. Polymer 2013;54:464–71.
[73] Shi Y, Li Y, Xiang F, Huang T, Chen C, Peng Y, Wang Y. Carbon nanotubes induced microstructure and mechanical properties changes in cocontinuous poly(L-lactide)/ethylene-*co*-vinyl acetate blends. Polym Adv Technol 2012;23:783–90.
[74] Zhang L, Wan C, Zhang Y. Investigation on morphology and mechanical properties of polyamide 6/maleated ethylene-propylene-diene rubber/organoclay composites. Polym Eng Sci 2009;49:209–16.
[75] Elias L, Fenouillot F, Majesté JC, Alcouffe P, Cassagnau P. Immiscible polymer blends stabilized with nano-silica particles: rheology and effective interfacial tension. Polymer 2008;49:4378–85.
[76] Médéric P, Ville J, Huitric J, Moan M, Aubry T. Effect of processing procedures and conditions on structural, morphological, and rheological properties of polyethylene/polyamide/nanoclay blends. Polym Eng Sci 2011;51:969–78.
[77] Li W, Karger-kocsis Z, Thomann R. Compatibilization effect of TiO_2 nanoparticles on the phase structure of PET/PP/TiO_2 nanocomposites. J Polym Sci Part B: Polym Phys 2009;47:1616–24.
[78] Liebscher M, Blais M-O, Pötschke P, Heinrich G. A morphological study on the dispersion and selective localization behavior of graphene nanoplatelets in immiscible polymer blends of PC and SAN. Polymer 2013;54:5875–82.
[79] Borah JS, Karak N, Chaki TK. Effect of organoclay platelets on morphology and properties of LLDPE/EMA blends. Mater Sci Eng A 2011;528:2820–30.
[80] Chen B, Evans JRG. Mechanical properties of polymer-blend nanocomposites with organoclays: polystyrene/ABS and high impact polystyrene/ABS. J Polym Sci Part B: Polym Phys 2011;49:443–54.
[81] Hui S, Chaki TK, Chattopadhyay S. Effect of silica-based nanofillers on the properties of a low-density polyethylene/ethylene vinyl acetate copolymer based thermoplastic elastomer. J Appl Polym Sci 2008;110:825–36.
[82] Hui S, Chaki TK, Chattopadhyay S. Dynamic and capillary rheology of LDPE-EVA-based thermoplastic elastomer: effect of silica nanofiller. Polym Compos 2010;31:377–91.
[83] Lee KY, Goettler LA. Structure-property relationships in polymer blend nanocomposites. Polym Eng Sci 2004;44:1103–11.
[84] Li X, Park HM, Lee JO, Ha CS. Effect of blending sequence on the microstructure and properties of PBT/EVA-g-MAH/organoclay ternary nanocomposites. Polym Eng Sci 2002;42:2156–64.
[85] Martins CG, Larocca NM, Paul DR, Pessan LA. Nanocomposites formed from polypropylene/EVA blends. Polymer 2009;50:1743–54.
[86] Dasari A, Yu ZZ, Mai YW. Effect of blending sequence on microstructure of ternary nanocomposites. Polymer 2005;46:5986–91.
[87] Zaikin AE, Karimov RR, Arkhireev VP. A study of the redistribution conditions of carbon black particles from the bulk to the interface in heterogeneous polymer blends. Colloid J 2001;63:57–9.
[88] Zaikin AE, Zharinova EA, Bikmullin RS. Specifics of localization of carbon black at the interface between polymeric phases. Polym Sci Ser A 2007;49:328–36.
[89] Gubbels F, Jerome R, Vanlathem E, Deltour R, Blacher S, Brouers F. Kinetic and thermodynamic control of the selective localization of carbon black at the interface of immiscible polymer blends. Chem Mater 1998;10:1227–35.
[90] Sumita M, Sakata K, Hayakawa Y, Asai S, Miyasaka K, Tanemura M. Double percolation effect on the electrical conductivity of conductive particles filled polymer blends. Colloid Polym Sci 1992;270:134–9.
[91] Levon K, Margolina A, Patashinsky AZ. Multiple percolation in conducting polymer blends. Macromolecules 1993;26:4061–3.
[92] Feng J, Chan CM, Li JX. A method to control the dispersion of carbon black in an immiscible polymer blend. Polym Eng Sci 2003;43:1058–63.
[93] Liebscher M, Tzounis L, Pötschke P, Heinrich G. Influence of the viscosity ratio in PC/SAN blends filled with MWCNTs on the morphological, electrical, and melt rheological properties. Polymer 2013;54:6801–8.
[94] Zhou P, Yu W, Zhou C, Liu F, Hou L, Wang J. Morphology and electrical properties of carbon black filled LLDPE/EMA composites. J Appl Polym Sci 2007;103:497–502.
[95] Persson AL, Bertilsson H. Viscosity difference as distributing factor in selective absorption of aluminium borate whiskers in immiscible polymer blends. Polymer 1998;39:5633–42.
[96] Doan VA, Nobukawa S, Ohtsubo S, Tada T, Yamaguchi M. Selective migration of silica particles between rubbers. J Polym Res 2013;20:145–6.
[97] Göldel A, Kasaliwal G, Pötschke P. Selective localization and migration of multiwalled carbon nanotubes in blends of polycarbonate and poly(styrene-acrylonitrile). Macromol Rapid Commun 2009;30:423–9.
[98] Fang Z, Harrats C, Moussaif N, Groeninckx G. Location of a nanoclay at the interface in an immiscible poly(e-caprolactone)/poly(ethylene oxide) blend and its effect on the compatibility of the components. J Appl Polym Sci 2007;106:3125–35.
[99] Gubbels F, Blacher E, Vanlathem R, Jérôme R, Deltour R, Brouers F, Teyssié Ph. Design of electrical conductive composites: key role of the morphology on the electrical properties of carbon black filled polymer blends. Macromolecules 1995;28:1559–66.
[100] Khatua BB, Lee DJ, Kim HY, Kim JK. Effect of organoclay platelets on morphology of nylon-6 and poly(ethylene-ran-propylene) rubber blends. Macromolecules 2004;37:2454–9.
[101] Baudouin AC, Auhl D, Tao F, Devaux J, Bailly C. Polymer blend emulsion stabilization using carbon nanotubes interfacial confinement. Polymer 2011;52:149–56.
[102] Paul DR, Bucknall CB, editors. Polymer blends, vol. 2. New York: John Wiley & Sons; 2000, 589 p.
[103] Huitric J, Ville J, Médéric P, Moan M, Aubry T. Rheological, morphological and structural properties of PE/PA/nanoclay ternary blends: effect of clay weight fraction. J Rheol 2009;53:1101–19.
[104] Voulgaris D. Emulsifying effect of dimethyldioctadecylammonium-hectorite in polystyrene/poly(ethyl methacrylate) blends. Polymer 2002;43:2213–8.
[105] Lee H, Fasulo P, Rodgers W, Paul D. TPO based nanocomposites. Part 1. Morphology and mechanical properties. Polymer 2005;46:11673–89.
[106] Vermant J, Vandebril S, Dewitte C, Moldenaers P. Particle-stabilized polymer blends. Rheol Acta 2008;47:835–9.
[107] Serpe G, Jarrin J, Dawans F. Polyethylene–polyamide blends. Polym Eng Sci 1990;30:553–65.
[108] Hong JS, Kim YK, Ahn KH, Lee SJ, Kim C. Interfacial tension reduction in PBT/PE/clay nanocomposite. Rheol Acta 2007;46:469–78.
[109] Hong JS, Namkung H, Ahn KH, Lee SJ, Kim C. The role of organically modified layered silicate in the breakup and coalescence of droplets in PBT/PE blends. Polymer 2006;47:3967–75.
[110] Sinha Ray S, Bousmina M, Maazouz A. Morphology and properties of organoclay modified polycarbonate/poly(methyl methacrylate) blend. Polym Eng Sci 2006;46:1121–9.
[111] Palierne JE. Linear rheology of viscoelastic emulsions with interfacial tension. Rheol Acta 1990;214:204–14.
[112] Kontopoulou M, Liu Y, Austin JR, Parent JS. The dynamics of montmorillonite clay dispersion and morphology development in immiscible ethylene–propylene rubber/polypropylene blends. Polymer 2007;48:4520–8.
[113] Vermant J, Cioccolo G, Golapan Nair K, Moldenaers P. Coalescence suppression in model immiscible polymer blends by nano-sized colloidal particles. Rheol Acta 2004;43:529–38.

[114] Vandebril S, Vermant J, Moldenaers P. Efficiently suppressing coalescence in polymer blends using nanoparticles: role of interfacial rheology. Soft Matter 2010;6:3353–62.
[115] Kong M, Huang Y, Chen G, Yang Q, Li G. Retarded relaxation and breakup of deformed PA6 droplets filled with nanosilica in PS matrix during annealing. Polymer 2011;52:5231–6.
[116] Filippone G, Romeo G, Acierno D. Role of interface rheology in altering the onset of co-continuity in nanoparticle-filled polymer blends. Macromol Mater Eng 2011;296:658–65.
[117] Ville J, Médéric P, Huitric J, Aubry T. Structural and rheological investigation of interphase in polyethylene/polyamide/nanoclay ternary blends. Polymer 2012;53:1733–40.
[118] Entezam M, Khonakdar HA, Yousefi AA, Jafari SH, Wagenknecht U, Heinrich G. Dynamic and transient shear start-up flow experiments for analyzing nanoclay localization in PP/PET blends: correlation with microstructure. Macromol Mater Eng 2012;298:113–26.
[119] Pötschke P, Paul DR. Formation of co-continuous structures in melt-mixed immiscible polymer blends. J Macromol Sci Polym Rev 2003;43:87–141.
[120] Ho RM, Wu CH, Su AC. Morphology of plastic/rubber blends. Polym Eng Sci 1990;30:511–8.
[121] Kitayama N, Keskkula H, Paul DR. Reactive compatibilization of nylon 6/styrene–acrylonitrile copolymer blends. Part 1. Phase inversion behavior. Polymer 2000;41:8041–52.
[122] Omonov TS, Harrats C, Moldenaers P, Groeninckx G. Phase continuity detection and phase inversion phenomena in immiscible polypropylene/polystyrene blends with different viscosity ratios. Polymer 2007;48:5917–27.
[123] Paul D, Barlow J. Polymer blends. J Macromol Sci: Rev Macromol Chem Phys 1980;18:109–68.
[124] Utracki LA. On the viscosity–concentration dependence of immiscible polymer blends. J Rheol 1991;35:1615–37.
[125] Li L, Miesch C, Sudeep PK, Balazs AC, Emrick T, Russell TP, Hayward RC. Kinetically trapped co-continuous polymer morphologies through intraphase gelation of nanoparticles. Nano Lett 2011;11:1997–2003.
[126] Steinmann S, Gronski W, Friedrich C. Influence of selective filling on rheological properties and phase inversion of two-phase polymer blends. Polymer 2002;43:4467–77.
[127] Li Y, Shimizu H. Novel morphologies of poly(phenylene oxide) (PPO)/polyamide 6 (PA6) blend nanocomposites. Polymer 2004;45:7381–8.
[128] Wu G, Li B, Jiang J. Carbon black self-networking induced co-continuity of immiscible polymer blends. Polymer 2010;51:2077–83.
[129] Al-Saleh MH, Al-Anid HK, Hussain YA. Electrical double percolation and carbon nanotubes distribution in solution processed immiscible polymer blend. Synth Met 2013;175:75–80.
[130] Monemian S, Jafari SH, Khonakdar HA, Goodarzi V, Reuter U, Pötschke P. MWNT-filled PC/ABS blends: correlation of morphology with rheological and electrical response. J Appl Polym Sci 2013;130:739–48.
[131] Yuan JK, Yao SH, Sylvestre A, Bai J. Biphasic polymer blends containing carbon nanotubes: heterogeneous nanotube distribution and its influence on the dielectric properties. J Phys Chem C 2012;116:2051–8.
[132] Martin G, Barres C, Sonntag P, Garois N, Cassagnau P. Co-continuous morphology and stress relaxation behaviour of unfilled and silica filled PP/EPDM blends. Mater Chem Phys 2009;113:889–98.
[133] Bhadane PA, Champagne MF, Huneault MA, Tofan F, Favis BD. Continuity development in polymer blends of very low interfacial tension. Polymer 2006;47:2760–71.
[134] Lee SH, Kontopoulou M, Park CB. Effect of nanosilica on the co-continuous morphology of polypropylene/polyolefin elastomer blends. Polymer 2010;51:1147–55.
[135] Liu X, Bao R, Liu Z, Yang W, Xie B, Yang M. Effect of nano-silica on the phase inversion behavior of immiscible PA6/ABS blends. Polym Test 2013;32:141–9.
[136] Zhang M, Huang Y, Kong M, Zhu H, Chen G, Yang Q. Morphology and rheology of poly(L-lactide)/polystyrene blends filled with silica nanoparticles. J Mater Sci 2012;47:1339–47.
[137] Xiang F, Shi Y, Li X, Huang T, Chen C, Peng Y, Wang Y. Cocontinuous morphology of immiscible high density polyethylene/polyamide 6 blend induced by multiwalled carbon nanotubes network. Eur Polym J 2012;48:350–61.
[138] Knauert ST, Douglas JF, Starr FW. The effect of nanoparticle shape on polymer-nanocomposite rheology and tensile strength. J Polym Sci Part B: Polym Phys 2007;45:1882–97.
[139] Laradji M. A Langevin dynamics study of mobile filler particles in phase-separating binary systems. J Chem Phys 2004;120:9330–4.
[140] Laradji M, Hore MJA. Nanospheres in phase-separating multicomponent fluids: a three-dimensional dissipative particle dynamics simulation. J Chem Phys 2004;121:10641–8.
[141] Allen MP, Evans GT, Frenkel D, Mulder BM. Hard convex body fluids. Adv Chem Phys 1993;86:1–166.
[142] Hore MJA, Laradji M. Prospects of nanorods as an emulsifying agent of immiscible blends. J Chem Phys 2008;128:054901–54908.
[143] Laradji M, Macnevin G. Phase separation dynamics in binary fluids containing quenched or mobile filler particles. J Chem Phys 2003;119:2275–83.
[144] Cassagnau P. Melt rheology of organoclay and fumed silica nanocomposites. Polymer 2008;49:2183–96.
[145] Pérez Amaro L, Coiai S, Conzatti L, Manariti A, Ciardelli F, Passaglia E. The effect of layered double hydroxides dispersion on thermal and mechanical properties of poly(vinyl chloride)/poly(methyl methacrylate) blends. Polym Int 2013;62:554–65.
[146] Hrnjak-Murgić Z, Jelčić Ž, Kovačević V, Mlinac-Mišak M, Jelenčić J. Molecular and morphological characterization of immiscible SAN/EPDM blends filled by nano filler. Macromol Mater Eng 2002;287:684–92.
[147] Alsaleh M, Sundararaj U. Nanostructured carbon black filled polypropylene/polystyrene blends containing styrene–butadiene–styrene copolymer: influence of morphology on electrical resistivity. Eur Polym J 2008;44:1931–9.
[148] Feng J, Chan QCM. Carbon black-filled immiscible blends of poly(viny1idene fluoride) and high density polyethylene: electrical properties and morphology. Polym Eng Sci 1998;38:1649–57.
[149] Andrews R, Weisenberger MC. Carbon nanotube polymer composites. Curr Opin Solid State Mater Sci 2004;8:31–7.
[150] Liu L, Wang Y, Li Y, Wu J, Zhou Z, Jiang C. Improved fracture toughness of immiscible polypropylene/ethylene-co-vinyl acetate blends with multiwalled carbon nanotubes. Polymer 2009;50:3072–8.
[151] Fina A, Han Z, Saracco G, Gross U, Mainil M. Morphology and conduction properties of graphite-filled immiscible PVDF/PPgMA blends. Polym Adv Technol 2012;23:1572–9.
[152] Ma F, Yuan N, Ding J. The conductive network made up by the reduced graphene nanosheet/polyaniline/polyvinyl chloride. J Appl Polym Sci 2013;128:3870–5.
[153] Yan N, Xia H, Wu J, Zhan Y, Fei G, Chen C. Compatibilization of natural rubber/high density polyethylene thermoplastic vulcanizate with graphene oxide through ultrasonically assisted latex mixing. J Appl Polym Sci 2013;127:933–41.
[154] Deshmukh RD, Liu Y, Composto RJ. Two-dimensional confinement of nanorods in block copolymer domains. Nano Lett 2007;7:3662–8.
[155] Sinha Ray S, Pouliot S, Bousmina M, Utracki LA. Role of organically modified layered silicate as an active interfacial modifier in immiscible polystyrene/polypropylene blends. Polymer 2004;45:8403–13.
[156] Jancar J, Douglas JF, Starr FW, Kumar SK, Cassagnau P, Lesser AJ, Sternstein SS, Buehler MJ. Current issues in research on structure–property relationships in polymer nanocomposites. Polymer 2010;51:3321–43.
[157] Göldel A, Marmur A, Kasaliwal GR, Pötschke P, Heinrich G. Shape-dependent localization of carbon nanotubes and carbon black in an immiscible polymer blend during melt mixing. Macromolecules 2011;44:6094–102.
[158] Zhang W, Lin M, Winesett A, Dhez O, Kilcoyne AL, Ade H, Rubinstein M, Shafi KVPM, Ulman A, Gersappe D, Tenne R, Rafailovich M, Sokolov J, Frisch HL. The use of functionalized nanoparticles as non-specific compatibilizers for polymer blends. Polym Adv Technol 2011;22:65–71.
[159] Acharya H, Kuila T, Srivastava SK, Bhowmick AK. Effect of layered silicate on EPDM/EVA blend nanocomposite: dynamic mechanical, thermal, and swelling properties. Polym Compos 2008;29:443–50.
[160] As'habi L, Jafari SH, Khonakdar HA, Baghaei B. Morphological, rheological and thermal studies in melt processed compatibilized PA6/ABS/clay nanocomposites. J Polym Res 2010;18:197–205.
[161] Austin JR, Kontopoulou M. Effect of organoclay content on the rheology, morphology, and physical properties of polyolefin elastomers and their blends with polypropylene. Polym Eng Sci 2006;46:1491–501.
[162] Azizi S, Yunus WMZW, Ahmad M. Effect of polyethylene-grafted maleic anhydride on properties of high-density polyethylene and polystyrene blend/layered silicate nanocomposites. J Reinf Plast Compos 2011;30:1649–54.

[163] Baghaei B, Jafari SH, Khonakdar HS, Rezaeian I, As'habi L, Ahmadian S. Interfacially compatibilized LDPE/POE blends reinforced with nanoclay: investigation of morphology, rheology and dynamic mechanical properties. Polym Bull 2008;62:255–70.
[164] Chen GX, Kim HS, Kim ES, Yoon JS. Compatibilization-like effect of reactive organoclay on the poly(L-lactide)/poly(butylene succinate) blends. Polymer 2005;46:11829–36.
[165] Contreras V, Cafiero M, Silva SD, Rosales C, Perera R, Matos M. Characterization and tensile properties of ternary blends with PA-6 nanocomposites. Polym Eng Sci 2006;46:1111–20.
[166] Dasari A, Yu Z, Yang M, Zhang Q, Xie X, Mai Y. Micro- and nanoscale deformation behavior of nylon 66-based binary and ternary nanocomposites. Compos Sci Technol 2006;66:3097–114.
[167] DeLeo C, Pinotti CA, Carmo Gonçalves M, Velankar S. Preparation and characterization of clay nanocomposites of plasticized starch and polypropylene polymer blends. J Polym Environ 2011;19:689–97.
[168] Depolo WS, Baird DG. Particulate reinforced PC/PBT composites. II. Effect of nano-clay particles on dimensional stability and structure–property relationships. Polym Compos 2009;30:200–13.
[169] Dhibar S, Kar P, Khatua BB. Preparation of highly exfoliated and transparent polycarbonate/clay nanocomposites by melt blending of polycarbonate and poly(methyl methacrylate)/clay nanocomposites. J Appl Polym Sci 2012;125:E601–9.
[170] Fang Z, Xu Y, Tong L. Effect of clay on the morphology of binary blends of polyamide 6 with high density polyethylene and HDPE-graft-acrylic acid. Polym Eng Sci 2007;47:551–9.
[171] Feng M, Gong F, Zhao C, Chen G, Zhang S, Yang M. Effect of clay on the morphology of blends of poly(propylene) and polyamide 6/clay nanocomposites. Polym Int 2004;53:1529–37.
[172] Filippone G, Dintcheva NT, Acierno D, La Mantia FP. The role of organoclay in promoting co-continuous morphology in high-density poly(ethylene)/poly(amide) 6 blends. Polymer 2008;49:1312–22.
[173] Gahleitner M, Kretzschmar B, Vliet GV, Devaux J, Pospiech D, Bernreitner K, Ingolic E. Rheology/morphology interactions in polypropylene/polyamide-6 nanocomposites. Rheol Acta 2006;45:322–30.
[174] Gelfer MY, Song HH, Liu L, Hsiao BS, Chu B, Rafailovich M, Si M, Zaitsev V. Effects of organoclays on morphology and thermal and rheological properties of polystyrene and poly(methyl methacrylate) blends. J Polym Sci Part B: Polym Phys 2003;41:44–54.
[175] González I, Eguiazábal JI, Nazábal J. Compatibilization level effects on the structure and mechanical properties of rubber-modified polyamide-6/clay nanocomposites. J Polym Sci Part B: Polym Phys 2005;43:3611–20.
[176] Hasook A, Tanoue S, Iemoto Y. Characterization and mechanical properties of poly(lactic acid)/poly(ε-caprolactone)/organoclay nanocomposites prepared by melt compounding. Polym Eng Sci 2006;46:1001–7.
[177] Jafari SH, Khonakdar HA, Asadinezhad A, Wagenknecht U. Crystallization and melting behavior of nanoclay-containing polypropylene/poly(trimethylene terephthalate) blends. Express Polym Lett 2012;6:148–58.
[178] Kelarakis A, Giannelis EP, Yoon K. Structure–properties relationships in clay nanocomposites based on PVDF/(ethylene–vinyl acetate) copolymer blends. Polymer 2007;48:7567–72.
[179] Kelnar I, Khunová V, Kotek J, Kaprálková L. Effect of clay treatment on structure and mechanical behavior of elastomer-containing polyamide 6 nanocomposite. Polymer 2007;48:5332–9.
[180] Lee MH, Dan CH, Kim JH, Cha J, Kim S, Hwang Y, Lee CH. Effect of clay on the morphology and properties of PMMA/poly(styrene-co-acrylonitrile)/clay nanocomposites prepared by melt mixing. Polymer 2006;47:4359–69.
[181] Li Y, Wei GX, Sue HJ. Morphology and toughening mechanisms in clay-modified styrene-butadiene-styrene rubber-toughened polypropylene. J Mater Sci 2002;37:2447–59.
[182] Malmir S, Aghjeh MKR, Hemmati M, Tehrani RA. Relationship between morphology and rheology of PA/PE/clay blend nanocomposites. I. PA matrix. J Appl Polym Sci 2012;125:E503–16.
[183] Martí'n Z, Jiménez I, Gómez MA, Ade H, Kilcoyne DA. Interfacial interactions in PP/MMT/SEBS nanocomposites. Macromolecules 2010;43:448–53.
[184] Mehrabzadeh M, Kamal MR. Polymer-clay nanocomposites based on blends of polyamide-6 and polyethylene. Can J Chem Eng 2002;80:1083–92.
[185] Mojarrad A, Jahani Y, Barikani M. Influence of nanoclay on the rheological properties of polyamide 6/acrylonitrile butadiene styrene nanocomposites. J Appl Polym Sci 2012;125:E571–82.
[186] Scaffaro R, Botta L, Mistretta MC, La Mantia FP. Preparation and characterization of polyamide 6/polyethylene blend-clay nanocomposites in the presence of compatibilisers and stabilizing system. Polym Degrad Stab 2010;95:2547–54.
[187] Sinha Ray S, Bousmina M. Compatibilization efficiency of organoclay in an immiscible polycarbonate/poly(methyl methacrylate) blend. Macromol Rapid Commun 2005;26:450–5.
[188] Sinha Ray S, Bousmina M. Effect of organic modification on the compatibilization efficiency of clay in an immiscible polymer blend. Macromol Rapid Commun 2005;26:1639–46.
[189] Tang Y, Hu Y, Zhang R, Gui Z, Wang Z, Chen Z, Fan W. Investigation on polypropylene and polyamide-6 alloys/montmorillonite nanocomposites. Polymer 2004;45:5317–26.
[190] Vo LT, Giannelis EP. Compatibilizing poly(vinylidene fluoride)/nylon-6 blends with nanoclay. Macromolecules 2007;40:8271–6.
[191] Wang H, Zeng C, Elkovitch M, Lee LJ, Koelling KW. Processing and properties of polymeric nano-composites. Polym Eng Sci 2001;41:2036–46.
[192] Wang Y, Zhang Q, Fu Q. Compatibilization of immiscible poly(propylene)/polystyrene blends using clay. Macromol Rapid Commun 2003;24:231–5.
[193] Wang S, Hu Y, Song L, Liu J, Chen Z, Fan W. Study on the dynamic self-organization of montmorillonite in two phases. J Appl Polym Sci 2004;91:1457–62.
[194] Wang K, Wang C, Li J, Su J, Zhang Q, Du R, Fu Q. Effects of clay on phase morphology and mechanical properties in polyamide 6/EPDM-g-MA/organoclay ternary nanocomposites. Polymer 2007;48:2144–54.
[195] Xiao J, Hu Y, Lu H, Cai Y, Chen Z, Fan W. Effect of order of mixing on morphology and thermal properties of the compatibilized PBT and ABS alloys/OMT nanocomposites. J Appl Polym Sci 2007;104:2130–9.
[196] Yang J, Sun L, Xiang S, He J, Gu L, Zhong M. Influence of organoclay and preparation technique on the morphology of polyamide6/polystyrene/organoclay nanocomposites. J Appl Polym Sci 2008;110:276–82.
[197] Yoo Y, Park C, Lee SG, Choi KY, Kim DS, Lee JH. Influence of addition of organoclays on morphologies in nylon 6/LLDPE blends. Macromol Chem Phys 2005;206:878–84.
[198] Yoo Y, Tiwari RR, Yoo YT, Paul DR. Effect of organoclay structure and mixing protocol on the toughening of amorphous polyamide/elastomer blends. Polymer 2010;51:4907–15.
[199] Yoo Y, Cui L, Yoon PJ, Paul DR. Morphology and mechanical properties of rubber toughened amorphous polyamide/MMT nanocomposites. Macromolecules 2010;43:615–24.
[200] Yousfi M, Soulestin J, Vergnes B, Lacrampe MF, Krawczak P. Compatibilization of immiscible polymer blends by organoclay: effect of nanofiller or organo-modifier? Macromol Mater Eng 2013;298:757–70.
[201] Ojijo V, Cele H, Sinha Ray S. Morphology and properties of polymer composites based on biodegradable polylactide/poly[(butylene succinate)-*co*-adipate] blend and nanoclay. Macromol Mater Eng 2011;296:865–77.
[202] Ojijo V, Malwela T, Sinha Ray S, Sadiku R. Unique isothermal crystallization phenomenon in the ternary blends of biopolymers polylactide and poly[(butylene succinate)-co-adipate] nano-clay. Polymer 2012;53:505–18.
[203] Ojijo V, Sinha Ray S, Sadiku R. Effect of nanoclay loading on the thermal and mechanical properties of biodegradable polylactide/poly[(butylene succinate)-co-adipate] blend composites. ACS Appl Mater Interfaces 2012;4:2395–405.
[204] Park H-M, Kim G-H, Ha C-S. Preparation and characterization of biodegradable aliphatic polyester/thermoplastic starch/organoclay ternary hybrid nanocomposites. Compos Interfaces 2007;14:427–38.
[205] Si M, Araki T, Ade H, Kilcoyne ALD, Fisher R, Sokolov JC, Rafailovich MH. Compatibilizing bulk polymer blends by using organoclays. Macromolecules 2006;39:4793–801.
[206] Kim HB, Choi JS, Lee CH, Lim ST, Jhon MS, Choi HJ. Polymer blend/organoclay nanocomposite with poly(ethylene oxide) and poly(methyl methacrylate). Eur Polym J 2005;41:679–85.
[207] Moghbelli E, Sue H-J, Jain S. Stabilization and control of phase morphology of PA/SAN blends via incorporation of exfoliated clay. Polymer 2010;51:4231–7.
[208] Sinha Ray S, Bandyopadhyay J, Bousmina M. Effect of organoclay on the morphology and properties of poly(propylene)/poly[(butylene succinate)-co-adipate] blends. Macromol Mater Eng 2007;292:729–47.

[209] Chow WS, Ishak ZAM, Ishiaku US, Apostolov AA. The effect of organoclay on the mechanical properties and morphology of injection-molded polyamide 6/polypropylene nanocomposites. J Appl Polym Sci 2004;91:175–89.

[210] Gahleitner M, Kretzschmar B, Pospiech D, Ingolic E, Reichelt N, Bernreitner K. Morphology and mechanical properties of polypropylene/polyamide 6 nanocomposites prepared by a two-step melt-compounding process. J Appl Polym Sci 2006;100:283–91.

[211] Lai S-M, Liao Y-C, Chen T-W. Properties and preparation of compatibilized nylon 6 nanocomposites/ABS blends using functionalized metallocene polyolefin elastomer. I. Impact properties. J Appl Polym Sci 2006;100:1364–71.

[212] Hwang K-J, Park J-W, Kim I, Ha C-S, Kim G-H. Effect of a compatibilizer on the microstructure and properties of partially biodegradable LDPE/aliphatic polyester/organoclay nanocomposites. Macromol Res 2006;14:179–86.

[213] Deyrail Y, Mighri F, Bousmina M, Kaliaguine S. Polyamide/polystyrene blend compatibilisation by montmorillonite nanoclay and its effect on macroporosity of gas diffusion layers for proton exchange membrane fuel cells. Fuel Cells 2007;7:447–52.

[214] Su Q, Feng M, Zhang S, Jiang J, Yang M. Melt blending of polypropylene-*blend*-polyamide 6-*blend*-organoclay systems. Polym Int 2007;56:50–6.

[215] Ali Z, Le HH, Ilisch S, Thurn-Albrecht T, Radusch H-J. Morphology development and compatibilization effect in nanoclay filled rubber blends. Polymer 2010;51:4580–8.

[216] Liu B, Shangguan Y, Song Y, Zheng Q. Influences of compatibilizers on rheology and mechanical properties of propylene random copolymer/styrene-ethylene-butylene-styrene block copolymer/organic-montmorillonite nanocomposites. J Appl Polym Sci 2013;129:973–82.

[217] Mohan T, Kanny K. Melt blend studies of nanoclay-filled polypropylene (PP)–high-density polyethylene (HDPE) composites. J Mater Sci 2013;48:8292–301.

[218] Passador FR, Ruvolo-Filho AC, Pessan LA. Effects of different compatibilizers on the rheological, thermomechanical, and morphological properties of HDPE/LLDPE blend-based nanocomposites. J Appl Polym Sci 2013;130:1726–35.

[219] Vijayan P, Puglia D, Kenny J, Thomas S. Effect of organically modified nanoclay on the miscibility, rheology, morphology and properties of epoxy/carboxyl-terminated (butadiene-co-acrylonitrile) blend. Soft Matter 2013;9:2899–911.

[220] Zhao H, Cui Z, Wang X, Turng L-S, Peng X. Processing and characterization of solid and microcellular poly(lactic acid)/polyhydroxybutyrate-valerate (PLA/PHBV) blends and PLA/PHBV/clay nanocomposites. Composites Part A 2013;51:79–91.

[221] Mackay ME, Tuteja A, Duxbury PM, Hawker CJ, Van Horn B, Guan Z, Chen G, Krishnan RS. General strategies for nanoparticle dispersion. Science 2006;311:1740–3.

[222] Figueruelo JE, Gómez CM, Monzó IS, Abad C, Campos A. Modelling the influence of nanoparticles in the phase behaviour of an epoxy/polystyrene mixture, 2. Macromol Theory Simul 2007;16:458–75.

[223] Gomez C, Porcar I, Monzo I, Abad C, Campos A. Modelling the influence of nanoparticles in the phase behaviour of an epoxy/polystyrene mixture. Eur Polym J 2007;43:360–73.

[224] Tong W, Huang Y, Liu C, Chen X, Yang Q, Li G. The morphology of immiscible PDMS/PIB blends filled with silica nanoparticles under shear flow. Colloid Polym Sci 2010;288:753–60.

[225] Karim A, Liu DW, Douglas JF, Nakatani AI, Amis EJ. Modification of the phase stability of polymer blends by fillers. Polymer 2000;41:8455–8.

[226] Tao F, Nysten B, Baudouin A-C, Thomassin J-M, Vuluga D, Detrembleur C, Bailly C. Influence of nanoparticle–polymer interactions on the apparent migration behaviour of carbon nanotubes in an immiscible polymer blend. Polymer 2011;52:4798–805.

[227] Cao Y, Zhang J, Feng J, Wu P. Compatibilization of immiscible polymer blends using graphene oxide sheets. ACS Nano 2011;5:5920–7.

[228] Yang J, Feng C, Dai J, Zhang N, Huang T, Wang Y. Compatibilization of immiscible nylon 6/poly(vinylidene fluoride) blends using graphene oxides. Polym Int 2013;62:1085–93.

[229] Ye S, Cao Y, Feng J, Wu P. Temperature-dependent compatibilizing effect of graphene oxide as a compatibilizer for immiscible polymer blends. RSC Adv 2013;3:7987–95.

[230] Chiu JJ, Kim BJ, Kramer EJ, Pine DJ. Control of nanoparticle location in block copolymers. J Am Chem Soc 2005;127:5036–7.

[231] Kim BJ, Bang J, Hawker CJ, Chiu JJ, Pine DJ, Jang SG, Yang S-M, Kramer EJ. Creating surfactant nanoparticles for block copolymer composites through surface chemistry. Langmuir 2007;23:12693–703.

[232] Kim BJ, Bang J, Hawker CJ, Kramer EJ. Effect of areal chain density on the location of polymer-modified gold nanoparticles in a block copolymer template. Macromolecules 2006;39:4108–14.

[233] Kim BJ, Given-Beck S, Bang J, Hawker CJ, Kramer EJ. Importance of end-group structure in controlling the interfacial activity of polymer-coated nanoparticles. Macromolecules 2007;40:1796–8.

[234] Costanzo PJ, Beyer FL. Thermally driven assembly of nanoparticles in polymer matrices. Macromolecules 2007;40:3996–4001.

[235] Huang CM, Wei KH, Jeng US, Liang KS. Structural evolution of poly(styrene-b-4-vinylpyridine) diblock copolymer/gold nanoparticle mixtures from solution to solid state. Macromolecules 2007;40:5067–74.

[236] Walther A, Matussek K, Müller AHE. Engineering nanostructured polymer blends with controlled nanoparticle location using Janus particles. ACS Nano 2008;2:1167–78.

[237] Kwon T, Kim T, Ali FB, Kang DJ, Yoo M, Bang J, Lee W, Kim BJ. Size-controlled polymer-coated nanoparticles as efficient compatibilizers for polymer blends. Macromolecules 2011;44:9852–62.

[238] Willis JM, Caldas V, Favis BD. Processing-morphology relationships of compatibilized polyolefin/polyamide blends. Part II. The emulsifying effect of an ionomer compatibilizer as a function of blend composition and viscosity ratio. J Mater Sci 1991;26:4742–50.

[239] Maiti S, De SK, Bhowmick AK. Quantitative estimation of filler distribution in immiscible rubber blends by mechanical damping studies. Rubber Chem Technol 1992;65:293–302.

[240] Kelnar I, Kotek J, Kaprálková L, Hromádková J, Kratochvíl J. Effect of elastomer type and functionality on the behavior of toughened polyamide nanocomposites. J Appl Polym Sci 2006;100:1571–6.

[241] Wu S. Phase structure and adhesion in polymer blends: a criterion for rubber toughening. Polymer 1985;26:1855–63.

[242] Wu S. A generalized criterion for rubber toughening: the critical matrix ligament thickness. J Appl Polym Sci 1988;35:549–61.

[243] Kim DH, Fasulo PD, Rodgers WR, Paul DR. Effect of the ratio of maleated polypropylene to organoclay on the structure and properties of TPO-based nanocomposites. Part I. Morphology and mechanical properties. Polymer 2007;48:5960–78.

[244] González I, Eguiazábal JI, Nazábal J. Nanocomposites based on a polyamide 6/maleated styrene–butylene-co-ethylene–styrene blend: effects of clay loading on morphology and mechanical properties. Eur Polym J 2006;42:2905–13.

[245] Yang H, Zhang Q, Guo M, Wang C, Du R, Fu Q. Study on the phase structures and toughening mechanism in PP/EPDM/SiO_2 ternary composites. Polymer 2006;47:2106–15.

[246] Yang H, Zhang X, Qu C, Li B, Zhang L, Zhang Q, Fu Q. Largely improved toughness of PP/EPDM blends by adding nano-SiO_2 particles. Polymer 2007;48:860–9.

[247] Bitinis N, Verdejo R, Maya EM, Espuche E, Cassagnau P, Lopez-Manchado MA. Physicochemical properties of organoclay filled polylactic acid/natural rubber blend bionanocomposites. Compos Sci Technol 2012;72:305–13.

[248] Liu L, Wu H, Wang Y, Wu J, Peng Y, Xiang F, Zhang J. Selective distribution, reinforcement, and toughening roles of MWCNTs in immiscible polypropylene/ethylene-co-vinyl acetate blends. J Polym Sci Part B: Polym Phys 2010;48:1882–92.

[249] Huang JC. Carbon black filled conducting polymers and polymer blends. Adv Polym Techol 2002;21:299–313.

[250] Wu G, Asai S, Zhang C, Miura T, Sumita M. A delay of percolation time in carbon-black-filled conductive polymer composites. J Appl Phys 2000;88:1480–7.

[251] Gubbels F, Jérôme R, Teyssié P. selective localization of carbon black in immiscible polymer blends: a useful tool to design electrical conductive composites. Macromolecules 1994;27:1972–4.

[252] Ibarra-gómez R, Márquez A, Ramos-de Valle LF, Rodríguez-Fernández OS. Influence of the blend viscosity and interface energies on the preferential location of CB and conductivity of Br/EPDM blends. Rubber Chem Technol 2003;76:969–78.

[253] Zonder L, Ophir A, Kenig S, McCarthy S. The effect of carbon nanotubes on the rheology and electrical resistivity of polyamide 12/high density polyethylene blends. Polymer 2011;52:5085–91.

[254] Hwang TY, Yoo Y, Lee JW. Electrical conductivity, phase behavior, and rheology of polypropylene/polystyrene blends with multi-walled carbon nanotube. Rheol Acta 2012;51:623–36.

[255] Wu G, Cai X, Lin X, Yui H. Heterogeneous distribution of magnetic nanoparticles in reactive polymer blends. React Funct Polym 2010;70:732–7.

[256] Gilman JW. Flammability and thermal stability studies of polymer layered-silicate (clay) nanocomposites. Appl Clay Sci 1999;15:31–49.
[257] Zanetti M, Kashiwagi T, Falqui L, Camino G. Cone calorimeter combustion and gasification studies of polymer layered silicate nanocomposites. Chem Mater 2002;14:881–7.
[258] Pack S, Si M, Koo J, Sokolov JC, Koga T, Kashiwagi T, Rafailovich MH. Mode-of-action of self-extinguishing polymer blends containing organoclays. Polym Degrad Stab 2009;94:306–26.
[259] Bourbigot S, Duquesne S. Intumescence and nanocomposites: a novel route for flame-retardant polymeric materials. In: Morgan AB, Wilkie CA, editors. Flame retardant polymer nanocomposites. New York: Wiley & sons; 2007. p. 131–62.
[260] Almeras X, Dabrowski F, Bras ML, Poutch F, Bourbigot S. Using polyamide-6 as charring agent in intumescent polypropylene formulations. I. Effect of the compatibilising agent on the fire retardancy performance. Polym Degrad Stab 2002;77:305–13.
[261] Tang Y, Hu Y, Xiao J, Wang J, Song L, Fan W. PA-6 and EVA alloy/clay nanocomposites as char forming agents in poly(propylene) intumescent formulations. Polym Adv Technol 2005;16:338–43.
[262] Zhang J, Hereid J, Hagen M, Bakirtzis D, Delichatsios MA, Fina A, Castrovinci A, Camino G, Samyn F, Bourbigot S. Effects of nanoclay and fire retardants on fire retardancy of a polymer blend of EVA and LDPE. Fire Safe J 2009;44:504–13.
[263] Entezam M, Khonakdar HA, Yousefi AA. On the flame resistance behavior of PP/PET blends in the presence of nanoclay and a halogen-free flame retardant. Macromol Mater Eng 2013;298:1074–84.
[264] Yoo BM, Shin HJ, Yoon HW, Park HB. Graphene and graphene oxide and their uses in barrier polymers. J Appl Polym Sci 2014:131, http://dx.doi.org/10.1002/app.39628.
[265] Pal P, Kundu MK, Malas A, Das CK. Compatibilizing effect of halloysite nanotubes in polar–nonpolar hybrid system. J Appl Polym Sci 2014:131, http://dx.doi.org/10.1002/app.39587.